

NIST-GCR-95-665

**WATER DROPLET EVAPORATION FROM
RADIANTLY HEATED SOLIDS**

S. Tinker, M. di Marzo

**Mechanical Engineering Department
University of Maryland
College Park, MD 20742**

**September 1994
Issued December 1994**



**U.S. Department of Commerce
Ronald H. Brown, *Secretary*
Technology Administration
Mary L. Good, *Under Secretary for Technology*
National Institute of Standards and Technology
Arati Prabhakar, *Dirêctor***

Notice

This report was prepared for the Building and Fire Research Laboratory of the National Institute of Standards and Technology under grant number 70NANB1H1173. The statement and conclusions contained in this report are those of the authors and do not necessarily reflect the views of the National Institute of Standards and Technology or the Building and Fire Research Laboratory.

**WATER DROPLET EVAPORATION FROM
RADIANTLY HEATED SOLIDS**

Final Report

S. Tinker, M. di Marzo

**Prepared for the
Building and Fire Research Laboratory
National Institute of Standards and Technology
Gaithersburg, MD 20899**

**Mechanical Engineering Department
University of Maryland
College Park, MD 20742**

September 1994

ABSTRACT

A model describing the configuration of a water droplet evaporating on the surface of a radiantly heated semi-infinite solid is developed. A shape factor and the solid-liquid-vapor contact angle describe the transient droplet shape, though the initial value of the latter parameter is found to have a negligible effect on the droplet's evaporation. The droplet shape model and a modified radiation heat term are incorporated into a previously-developed computer model to predict the evaporation of a single droplet on a semi-infinite solid subjected to radiant heat input. The code predicts transient temperature profiles that agree well with experiment. A simplified, closed-form solution for the prediction of surface temperatures in the vicinity of an evaporating droplet is used to fit the data produced by the single droplet model. This closed-form solution facilitates calculations used in a model for the cooling of a surface by the evaporation of a sparse spray of water. The previously collected data base for sparse spray cooling using degassed water is expanded with a new set of experiments using water containing dissolved gases. Experimental results indicate that there is no significant difference in the sparse spray cooling when using either water containing dissolved gases or degassed water. Using superposition of effect, a computer code to model the sparse spray cooling of a solid surface subjected to radiant heat input from above is developed. The model agrees well with experimental data. The time constant governing the cooling of the surface is found to depend on the properties of the solid surface and is independent of the water mass flux. For both experimental and theoretical cases, the solid used is macor. Macor is a ceramic with a low thermal-conductivity. The surface temperatures of interest

range from 100 °C to the onset of the nucleate boiling condition for water. Radiant heat input is at relatively low temperatures (i.e., the radiant source is at less than 700 °C).

FOREWORD

This report describes the research performed during the period September 1992 - May 1994 under a joint research program between the Mechanical Engineering department of the University of Maryland at College Park and the Building and Fire Research Laboratory of the National Institute of Standards and Technology. The research was conducted in the laboratories of the BFRL by Ms. Susanne Tinker and Mr. Glenn White, Graduate Research Assistants of the ME Department, under the joint supervision of Dr. Marino di Marzo (ME Dept. - UMCP) and Dr. David D. Evans (BFRL - NIST). This report also constitutes the Master Thesis of Ms. Tinker, which has been completed and defended in the month of August 1994. Glenn White was responsible for the development of the single droplet evaporation computer model discussed in this report.

TABLE OF CONTENTS

<u>Section</u>	<u>Page</u>
List of Tables	v
List of Figures	vi
Nomenclature	ix
1. Introduction and Background	1
2. Model of the Transient Droplet Shape	4
2.1 Previous Geometric Model	4
2.2 Motivation for Developing New Droplet Shape Model	5
2.3 General Description of the Droplet Shape Model	6
2.4 Determination of Initial Contact Angle Bounds	6
2.5 Transient Droplet Shape	8
2.5.1 Stage 1 - Initial Configuration to Onset of Recession	8
2.5.2 Stage 2 - Onset of Recession to Complete Evaporation	10
2.6 Results Using the Proposed Droplet Shape Model	11
2.7 Summary	12
3. Modification of the Radiant Interfacial Heat Flux in the Single Droplet Evaporation Model	20
3.1 Experimental Radiant Panels Geometry	20
3.2 Previous Determination of the Radiant Interfacial Heat Flux	21
3.3 Modification to the Radiant Interfacial Heat Flux Term	22
4. Validation of the Single Droplet Computer Model	26
4.1 Brief Description of the Single Droplet Computer Model	26
4.2 Validation of the Single Droplet Computer Model	27
4.2.1 Inputs to the Computer Model	28
4.2.2 Validation Results	30
4.3 Closed-Form Solution	32
4.3.1 Description of the Closed-Form Solution	32
4.3.2 Determination of q_c and τ	33
4.3.3 Temperature Distribution Results	34
4.4 Summary	36
5. Effects of Dissolved Gases on the Sparse Spray Cooling of a Semi-Infinite Solid	48
5.1 Description of the Experiment	48

<u>Section</u>	<u>Page</u>
5.1.1 Experimental Setup	48
5.1.2 Experimental Procedure	50
5.1.3 Data Acquisition and Reduction	51
5.2 Results	52
5.2.1 Transient Average Surface Temperature	52
5.2.2 Surface Temperature Contours	56
5.3 Summary	58
6. Sparse Spray Cooling Model	83
6.1 Development of the Computer Model	83
6.1.1 Assumptions and Governing Equations	84
6.1.2 Superposition	86
6.1.3 Calculation Procedure	88
6.1.4 Droplet Distribution	91
6.2 Results and Analysis	95
6.2.1 Transient Average Surface Temperature	96
6.2.2 Surface Temperature Contours	100
6.3 Summary	101
7. Conclusions	130
Appendix A - Program MDEC	132
References	141

LIST OF TABLES

<u>Number</u>	<u>Page</u>
1. Raw Temperature Data for Figure 11	41
2. Raw Temperature Data for Figure 12	42
3. Raw Temperature Data for Figure 15	46
4. Raw Temperature Data for Figure 16	47
5. Time Constants for Sparse Spray Cooling Experiments	54
6. Raw Temperature Data: $G = 0.21 \text{ g/m}^2\text{s}$	76
7. Raw Temperature Data: $G = 0.5 \text{ g/m}^2\text{s}$	77
8. Raw Temperature Data: $G = 0.96 \text{ g/m}^2\text{s}$	78
9. Raw Temperature Data: $G = 1.3 \text{ g/m}^2\text{s}$	79
10. Raw Temperature Data: $G = 0.97 \text{ g/m}^2\text{s}$	80
11. Raw Temperature Data: $G = 1.5 \text{ g/m}^2\text{s}$	81
12. Raw Temperature Data: $G = 1.6 \text{ g/m}^2\text{s}$	82
13. Raw Temperature Data: $G = 0.5 \text{ g/m}^2\text{s}$	126
14. Raw Temperature Data: $G = 0.5 \text{ g/m}^2\text{s}$	127
15. Raw Temperature Data: $G = 0.96 \text{ g/m}^2\text{s}$	128
16. Raw Temperature Data: $G = 0.97 \text{ g/m}^2\text{s}$	129

LIST OF FIGURES

<u>Number</u>	<u>Page</u>
1. Droplet Configurations and Corresponding Maximum Contact Angles	14
2. Initial Droplet Configuration	15
3. Droplet Shape Transition	16
4. Droplet Volume v. Time	17
5. Effect of Contact Angle on Droplet Parameters	18
6. Transient Normalized Interfacial Heat Flux	19
7. Experimental Radiant Panels Geometry	24
8. Fractional Surface Area Coverage, f_{ϕ}	25
9. Experimental Setup	37
10. Panel Temperature v. Initial Surface Temperature	38
11. Surface Temperature Distributions: $T_{so} = 110\text{ }^{\circ}\text{C}$	39
12. Surface Temperature Distributions: $T_{so} = 130\text{ }^{\circ}\text{C}$	40
13. Evaporation Time v. Initial Surface Temperature	43
14. Average Conductive Flux v. Initial Surface Temperature	43
15. Surface Temperature Distributions: $T_{so} = 150\text{ }^{\circ}\text{C}$	44
16. Surface Temperature Distributions: $T_{so} = 100\text{ }^{\circ}\text{C}$	45
17. Droplet Dispenser	60
18. Comparison of Water Droplets	61
19. Transient Temperature Plot: $T_{so} = 111\text{ }^{\circ}\text{C}$	62
20. Transient Temperature Plot: $T_{so} = 131\text{ }^{\circ}\text{C}$	63

<u>Number</u>	<u>Page</u>
21. Transient Temperature Plot: $T_{so} = 151\text{ }^{\circ}\text{C}$	64
22. Transient Temperature Plot: $T_{so} = 162\text{ }^{\circ}\text{C}$	65
23. Transient Temperature Plot: $T_{so} = 182\text{ }^{\circ}\text{C}$	66
24. Contour Plot: $T_{so} = 111\text{ }^{\circ}\text{C}$, Time = 30 seconds	67
25. Contour Plot: $T_{so} = 111\text{ }^{\circ}\text{C}$, Time = 300 seconds	68
26. Contour Plot: $T_{so} = 111\text{ }^{\circ}\text{C}$, Time = 600 seconds	69
27. Contour Plot: $T_{so} = 151\text{ }^{\circ}\text{C}$, Time = 30 seconds	70
28. Contour Plot: $T_{so} = 151\text{ }^{\circ}\text{C}$, Time = 300 seconds	71
29. Contour Plot: $T_{so} = 151\text{ }^{\circ}\text{C}$, Time = 600 seconds	72
30. Contour Plot: $T_{so} = 162\text{ }^{\circ}\text{C}$, Time = 30 seconds	73
31. Contour Plot: $T_{so} = 162\text{ }^{\circ}\text{C}$, Time = 300 seconds	74
32. Contour Plot: $T_{so} = 162\text{ }^{\circ}\text{C}$, Time = 600 seconds	75
33. Simplified Program Flow Chart	103
34. Normalized Spatial Average Conductive Heat	104
35. Near and Far Field Solution Difference	105
36. Typical Experimental Droplet Distribution	106
37. Relationships Between D and Radial Position	107
38. Typical Calculated Droplet Distribution	108
39. Transient Temperature Plot: $T_{so} = 131\text{ }^{\circ}\text{C}$	109
40. Transient Temperature Plot: $T_{so} = 162\text{ }^{\circ}\text{C}$	110
41. Transient Temperature Plot: $T_{so} = 151\text{ }^{\circ}\text{C}$	111

<u>Number</u>	<u>Page</u>
42. Transient Temperature Plot: $T_{so} = 162\text{ }^{\circ}\text{C}$	112
43. Experimental and Calculated Transient Dimensionless Temperature Plot	113
44. Contour Plot: $T_{so} = 131\text{ }^{\circ}\text{C}$, Time = 50 seconds	114
45. Contour Plot: $T_{so} = 131\text{ }^{\circ}\text{C}$, Time = 300 seconds	115
46. Contour Plot: $T_{so} = 131\text{ }^{\circ}\text{C}$, Time = 600 seconds	116
47. Contour Plot: $T_{so} = 162\text{ }^{\circ}\text{C}$, Time = 50 seconds	117
48. Contour Plot: $T_{so} = 162\text{ }^{\circ}\text{C}$, Time = 300 seconds	118
49. Contour Plot: $T_{so} = 162\text{ }^{\circ}\text{C}$, Time = 600 seconds	119
50. Contour Plot: $T_{so} = 151\text{ }^{\circ}\text{C}$, Time = 50 seconds	120
51. Contour Plot: $T_{so} = 151\text{ }^{\circ}\text{C}$, Time = 300 seconds	121
52. Contour Plot: $T_{so} = 151\text{ }^{\circ}\text{C}$, Time = 600 seconds	122
53. Contour Plot: $T_{so} = 162\text{ }^{\circ}\text{C}$, Time = 50 seconds	123
54. Contour Plot: $T_{so} = 162\text{ }^{\circ}\text{C}$, Time = 300 seconds	124
55. Contour Plot: $T_{so} = 162\text{ }^{\circ}\text{C}$, Time = 600 seconds	125

NOMENCLATURE

a	radius of liquid droplet edge (see Figure 2)
A	area
c	specific heat
d	droplet distribution function (see Equation 37)
D	random droplet distribution factor (see Equation 39)
f	frequency (see Equation 13)
f_ϕ	fractional coverage at polar angle ϕ (see Figure 8)
F_s	interfacial radiative heat flux (see Equation 9)
F_e	radiative heater coils to droplet surface view factor (see Equation 10)
G	mass flux (see Equation 13)
h	convective heat transfer coefficient
J_0, J_1	Bessel functions
k	thermal conductivity
l	penetration depth (see Equation 15)
q	heat flux
q_c	average conductive heat flux (see Figure 14)
Q	total conductive heat energy term (see Equation 35)
Q^*	strength of point sink (see Equation 35)
r	radial spatial coordinate
R	radius of wetted region underneath the droplet
s	droplet apex (see Figure 2)

t time
T temperature
U temperature drop
V droplet volume
z axial spatial coordinate

GREEK

α thermal diffusivity
 β shape factor
 δ thickness of macor solid
 ε absorptivity
 θ solid-liquid-vapor contact angle (see Figure 1)
 Θ dimensionless temperature (see Equation 42)
 λ dummy variable
 ρ radius of curvature; density
 ρ_ϕ reflectivity (see Equation 10)
 σ Stefan-Boltzmann radiation constant
 τ evaporation time
 ϕ polar angle

SUBSCRIPTS

cp chill plate
d wetted region underneath the droplet (see Equation 45)
j generic droplet identifier

l	liquid
o	initial value
p	radiant panel
r	receding value
s	solid
sat	saturation
so	surface initial value
ss	steady state
t	total calculation area (see Equation 45)
w	total wetted area of droplet impingement (see Equation 13)
∞	ambient

1. INTRODUCTION AND BACKGROUND

The removal of heat from a semi-infinite solid is the desired outcome for a number of engineering applications. Applying a sparse spray of water to its surface allows for large amounts of heat to be removed due to the high latent heat associated with the evaporation of water. Evaporative cooling and spray cooling are the common terms found to describe this kind of heat removal.

Industrial uses for spray cooling include the quenching of molten metals during casting and the coating of surfaces to form protective finishes. Spray and mist cooling find a variety of uses in the power generation industry, such as the cooling of turbine blades and cooling tower applications.

Several researchers have focused their studies on the fundamentals of the evaporation of droplets and their cooling effects. Simon and Hsu [1] studied the wetting characteristics of evaporating droplets on various surfaces. They recorded droplet shape histories at room temperature on copper, lucite and teflon surfaces. Both Toda [2] and Bonacina [3] performed early investigations of spray-surface interactions and provided fundamental insight into the uses of mist cooling. Photographic techniques were employed by Zhang [4] to determine flow patterns in evaporating droplets on glass and copper plates. Using these techniques, Zhang was able to construct liquid-air interfacial flow maps.

In the area of fire suppression and protection, sparse spray cooling finds numerous uses. The current work represents the last phase in a research effort spanning several years to quantify and develop models for the spray cooling of hot

surfaces in a fire environment. The research has been developed and performed as a mutual effort between the Building and Fire Research Laboratory at the National Institute of Standards and Technology (NIST) in Gaithersburg, Maryland and the Mechanical Engineering Department of University of Maryland at College Park.

Beginning in 1987, diMarzo and Evans [5] studied a single droplet evaporating on a high thermal conductivity surface. A theoretical model using a boundary element method to predict the cooling experienced by a semi-infinite solid due to an evaporating droplet was developed in 1989 by diMarzo, Kavooosi, and Klassen [6]. In 1992, Liao [7] developed a computer model to predict the transient thermal behavior of a solid caused by the evaporation of a single droplet and proposed a model for the impingement of a sparse spray of droplets. Both a high and a low thermal-conductivity surface heated from below by conduction were studied. Experimental techniques based on infrared thermography to record the evaporation of a droplet on a radiantly heated semi-infinite solid were developed in 1992 by diMarzo and Kidder [8]. Dawson [9] extended this experimental work to record the effects of a random distribution of droplets (spray) on the surface. In both cases, the solid exhibited low thermal-conductivity. A computer model of the evaporation of a single droplet for radiative heat input conditions constitutes the work of White [10] in 1993.

With the progression as discussed above, the research described hereafter pertains to the development and validation of a computer model to predict the cooling of a semi-infinite solid subjected to a sparse spray of water where the heat

input is by radiation from above. Concurrently, a modification to the transient configuration of an evaporating droplet is proposed and an in-depth validation of the single droplet evaporation model for the case of radiant heat input against experimental data [9] is presented. Experimental work to determine the effects of dissolved gases in the water on the sparse spray cooling of a surface has also been performed and will be discussed.

2. MODEL OF THE TRANSIENT DROPLET SHAPE

The development of a computer model for the prediction of a single droplet evaporating on a hot solid surface requires consideration of the transient configuration of the droplet. The shape of the droplet can have a significant impact on its evaporation. A representation of the droplet geometry is determined for the case of a radiantly heated solid surface. This representation is incorporated into a computer model that predicts the evaporation of a single droplet on a semi-infinite solid subjected to radiant heat input [10].

2.1 Previous Geometric Model

Common to all previous studies concerning the dropwise evaporative cooling of hot, solid surfaces [6,7] is the assumption that the droplet configuration is a spherical cap throughout its evaporation. This droplet geometry is given as

$$z = \sqrt{\left(\frac{1+\gamma}{4}\right)^2 - r^2} - \frac{(1-\gamma)}{2} \quad (1)$$

where,

$$\gamma = R_0 * \left[\left[\frac{4}{\beta^3} + \sqrt{\left(1 + \frac{16}{\beta^6}\right)} \right]^{\frac{1}{3}} + \left[\frac{4}{\beta^3} - \sqrt{\left(1 + \frac{16}{\beta^6}\right)} \right]^{\frac{1}{3}} \right] \quad (2)$$

β is called the shape factor, or shape parameter, and is defined as the ratio of the radius of the wetted region under the deposited droplet to the radius of a spherical droplet of equivalent volume [3]. This early droplet model requires only a single parameter, namely the shape factor, to fully describe the droplet's shape as it evaporates. In this model, as the droplet evaporates, the radius of the wetted region under the droplet remains constant.

2.2 Motivation for Developing New Droplet Shape Model

A new model for the transient droplet shape is proposed in light of evidence found by both Chandra and Avedisian [11] and Zhang [4] which suggests that droplets take on a flattened configuration after deposition. The radiant heat field above the droplet is expected to affect the droplet shape in a manner similar to that suggested by Chandra and Avedisian. The increased temperature at the liquid-vapor interface caused by the radiant heat field above the droplet results in a relaxation of the droplet's surface tension. The relaxation causes the droplet to spread over a larger region of the solid surface and obtain a thinner, flatter configuration. Furthermore, the droplet model takes into account that upon reaching a given shape, the droplet's solid-liquid interface shrinks whereas it was previously assumed to remain constant throughout the droplet's evaporation.

The shape of the droplet can have a significant impact on the evaporation process. Due to the thinner shape, a larger conductive heat flux from the solid to the liquid may occur. Therefore, it is important to accurately model the transient shape

of the droplet in order to capture its effects on the evaporation phenomena.

2.3 General Description of the Droplet Shape Model

As previously mentioned, the earlier droplet shape model requires a single parameter, namely the shape factor, to fully characterize its shape throughout evaporation. The model proposed here requires two parameters to fully describe its shape at any time during evaporation. The first parameter is the shape factor, β , while the second parameter is the solid-liquid-vapor contact angle, θ .

The shape factor is determined from previous single droplet experiments [8]. The evaporation of the droplet basically occurs in two stages. The first stage is from the deposition of the droplet until the onset of the droplet's recession. Recession of the droplet is characterized by a shrinkage in the solid-liquid interface. The second stage is from the recession of the droplet until its complete evaporation. These two stages will be discussed in greater detail shortly. There are two values of the contact angle that need to be specified prior to using the droplet shape model. These are the initial value of the contact angle and the value of the contact angle upon the recession of the droplet. The initial value of the contact angle represents a maximum angle and the value of the angle at recession represents a minimum. The determination of these values are essential and will also be discussed.

2.4 Determination of Initial Contact Angle Bounds

The values of the initial and receding contact angles need to be specified prior to using the droplet model. The receding angle, θ_r , is the minimum solid-

liquid-vapor contact angle which results from a balance in surface tension and surface adhesion forces. The value of the receding angle was determined by Simon and Hsu using photographic experimental techniques [1] and confirmed by Kidder [8] to be 7°. The value for the initial contact angle is not as straightforward and in fact encompasses a range of possible values based on the initial shape of the droplet. In order to determine the range of initial contact angle values, the minimum and maximum limiting values of the range must be determined.

The minimum value for the initial contact angle is found by assuming the droplet has a spherical shape upon deposition. Therefore, knowing the value for β , the minimum initial contact angle can be found by the following relationship

$$\theta_{0,\min} = \arctan\left(\frac{\left(\frac{1}{\gamma} + \gamma\right)^2}{4} - 1\right) \quad (3)$$

where γ is given by Equation (2).

There are two possible values for the maximum initial contact angle corresponding to two situations which may occur upon deposition. First, a restriction is placed on the droplet shape such that the droplet has its maximum height upon deposition. This restriction requires that the initial height of the droplet be greater than or equal to the height of the droplet at recession. By setting the initial height of the droplet equal to the height of the droplet at the onset of recession, the corresponding maximum value for the initial contact angle can be determined. A second situation may arise, however, if the maximum initial contact angle

corresponding to the recession height is greater than 90°. In this situation, the maximum value for the initial contact angle is taken as 90°, which agrees with values given by Chandra and Avedisian [11] for the solid surface temperature range of interest here. Figure 1 shows pictorially the two situations governing the maximum initial contact angle value.

2.5 Transient Droplet Shape

As the droplet evaporates, the transient droplet shape must transition smoothly from the initial configuration to its complete evaporation. The droplet shape transient consists of two stages, both of which provide smooth, gradual transitions between consecutive droplet configurations.

2.5.1 Stage 1 - Initial Configuration to Onset of Recession

The first stage begins at the initial configuration and ends at the onset of recession. The initial configuration is determined uniquely by the initial contact angle, the droplet volume, and the radius of the wetted region underneath the droplet. This radius is a function of the shape factor and is given by

$$R_o = \beta * \left(\frac{3 V_0}{4 \pi} \right)^{\frac{1}{3}} \quad (4)$$

If the contact angle is equal to its minimum limiting value, the initial configuration is that of a spherical cap shown at the top of the page in Figure 2 and described by the following equation

In the model, s_0' is iterated on until the resulting volume equals the initial volume.

$$z = \sqrt{\rho^2 - r^2} - b \quad (5)$$

where,

$$b = \frac{R_o}{\tan(\theta_{0,\min})}$$

$$\rho = \frac{R_o}{\sin(\theta_{0,\min})} \quad (6)$$

If the initial contact angle is not equal to its minimum limiting value, the configuration of the droplet can be described as a disk with a round edge as shown at the bottom of Figure 2. The round edge is assumed to fit a circular shape. The equations describing this configuration are

$$z = s'_0, \quad r \leq R_o - a'$$

$$z = \sqrt{\rho'^2 - (R_o - a')^2} - b', \quad r > R_o - a' \quad (7)$$

where,

$$\rho' = \frac{s'_0}{\sin(\theta_0)} (1 + \cos(\theta_0))$$

$$a' = s'_0 \left(\frac{1}{\sin(\theta_0)} + \cos(\theta_0) \right) \quad (8)$$

$$b' = \frac{s'_0}{\sin(\theta_0)} (1 + \cos(\theta_0)) \tan\left(\frac{\pi}{2} - \theta_0\right)$$

The onset of recession is reached when the solid-liquid-vapor contact angle reaches the receding angle. At this point, the shape of the droplet is assumed to be a spherical cap and, replacing $\theta_{0,\min}$ with θ_r , is described by (5) and (6). A spherical cap shape is expected because a minimization in the liquid-vapor interface for a given volume of water must occur before the droplet can recede.

Once the initial configuration of the droplet and the configuration of the droplet at the onset of recession are known, a smooth transition between the two configurations can be determined. Referring to the top of Figure 3, two lines are drawn, one tangent to the droplet apex and one tangent to the solid-liquid-vapor contact point. The point of intersection of these two lines can be found for both the initial and receding configurations, labeled A and B in Figure 3. The line connecting points A and B represents the locus of intersection points for all intermediate droplet shapes. If the initial height of the droplet were equal to the height of the droplet at the onset of recession, the line connecting A and B would be horizontal.

2.5.2 Stage 2 - Onset of Recession to Complete Evaporation

Once the solid-liquid-vapor contact angle equals the receding angle, the droplet is assumed to have the shape of a spherical cap. Upon further volume reduction, the droplet radius and height decrease while the contact angle remains constant. As the droplet evaporates, the droplet aspect ratio remains constant. The

bottom drawing in Figure 3 illustrates this stage of the droplet's evaporation.

2.6 Results Using the Proposed Droplet Shape Model

The results of the droplet's evaporation using the new droplet model are shown in Figures 4 through 6. The figures presented here correspond to an initial surface temperature of 130 °C, an initial droplet volume of 9 microliters, and a shape factor equal to 2.3. Figure 4 contains curves of volume versus time using both the previous and the new droplet model, labelled A and B, respectively. For the new droplet model, various initial contact angles, ranging from a minimum value of 25° to a maximum value of 90°, are shown. The curves show that the droplet's evaporation time is lower for the previous model than for the new model. That is, the curve labelled A reaches a zero volume before those labelled B. Though the initial contact angle for the previous droplet model equals that of the minimum value for the new model, the recession of the solid-liquid interface that occurs in the new model affects the evaporation of the droplet. Therefore, it is found that the difference between the two models is seen after the droplet reaches its receding conditions. Figure 4 also shows that in the current model the value of the initial contact angle has very little effect on evaporation times.

Other transient quantities that reflect the sensitivity of the evaporation process to the initial solid-liquid-vapor contact angle are the shape factor, β , the normalized radius, R/R_0 , and the solid-liquid-vapor contact angle, θ . Figures 5 illustrates how these quantities behave for the minimum and maximum initial values of the contact

angle. Similar to evaporation time, the shape factor and the shrinkage of the wetted region (R/R_0) are relatively independent of initial contact angle. The shrinkage of the wetted region (R/R_0) does not display a smooth behavior due to the way in which the code redistributes the droplet volume after each time step, which will be discussed in more detail in Chapter 4. Another interesting result shown in Figure 5 is that the receding angle is reached at the same time for the two limiting cases shown, at approximately 55 percent of the evaporation time. This agrees with data from diMarzo and Kidder [8] that suggests receding conditions are reached at 55 to 85 percent of the evaporation time for initial surface temperatures between 130 and 160 °C.

A final aspect worth investigating is the behavior of the transient heat flux under the droplet. In Figure 6, the heat flux is normalized with respect to the average heat flux transferred to the droplet through the solid-liquid interface during the entire evaporation process. In this figure, it is important to note that the largest flux, and thus vaporization, occurs at the droplet's edge. The shrinkage of the wetted region under the droplet is apparent at $t/\tau = 0.9$, where the radius of the wetted region becomes approximately 40 percent of the initial value.

2.7 Summary

The modified transient droplet shape model presented consists of two parameters to fully describe its shape, as opposed to the single parameter characteristic of previous models. This new droplet shape model may take on a

Chandra and Zhang [11, 4]. Results show that the evaporation time is longer for the droplet described by the new model than for the droplet described by previous models. The longer evaporation times were found to be a result of the droplet's recession. It was also shown that the new parameter describing the droplet configuration, namely the solid-liquid-vapor contact angle, only has an effect on the droplet's evaporation through its value upon. The transient droplet shape model discussed here is incorporated in a code [10] to predict the evaporation of a single droplet on a radiantly-heated, semi-infinite, solid surface. This code utilizes a boundary element method for the solid thermal behavior and three one-dimensional solution schemes for the liquid droplet. A predictor-corrector scheme couples the solid and liquid behavior. A validation of the computer model against experimental data is presented in Chapter 4.

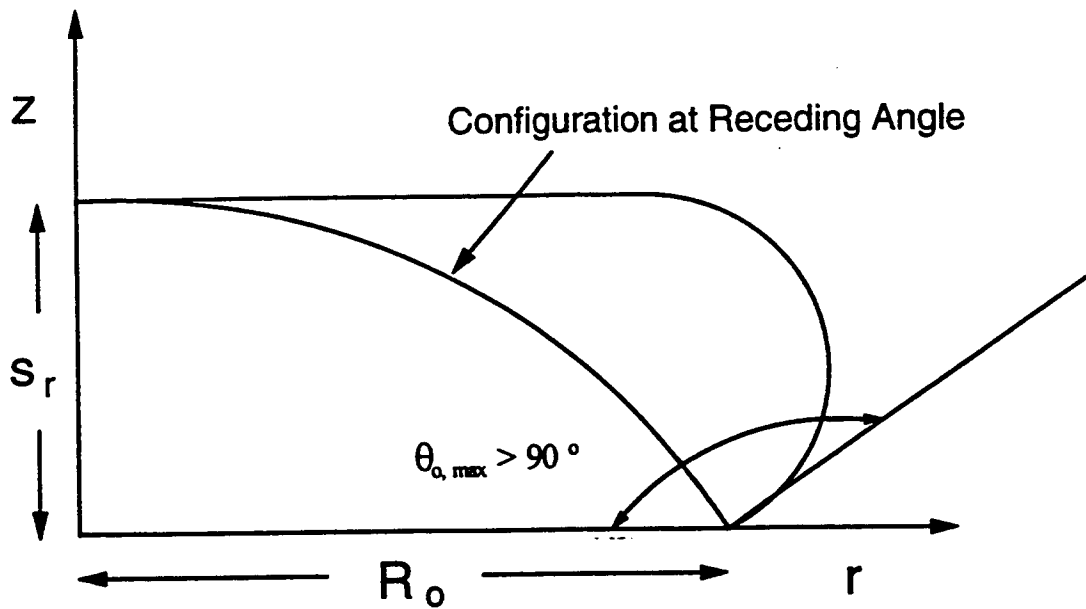
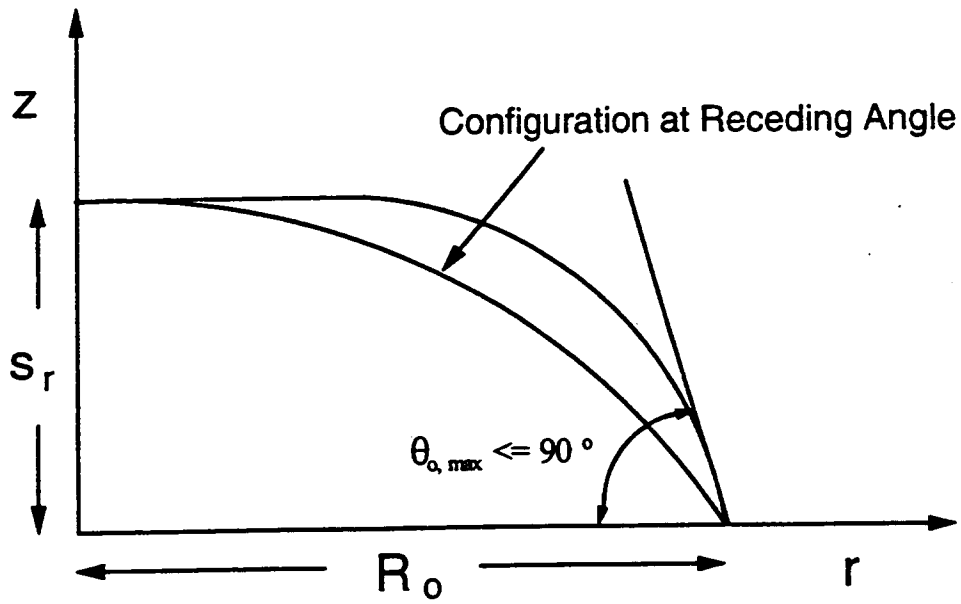


Figure 1 - Droplet Configurations and Corresponding Maximum Contact Angles

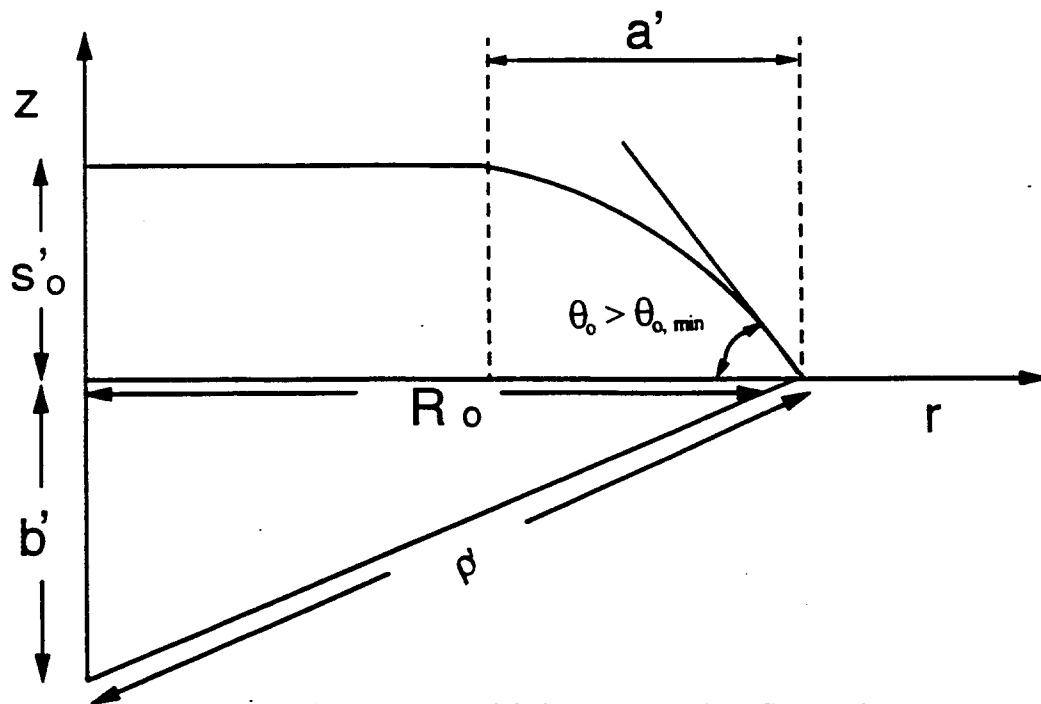
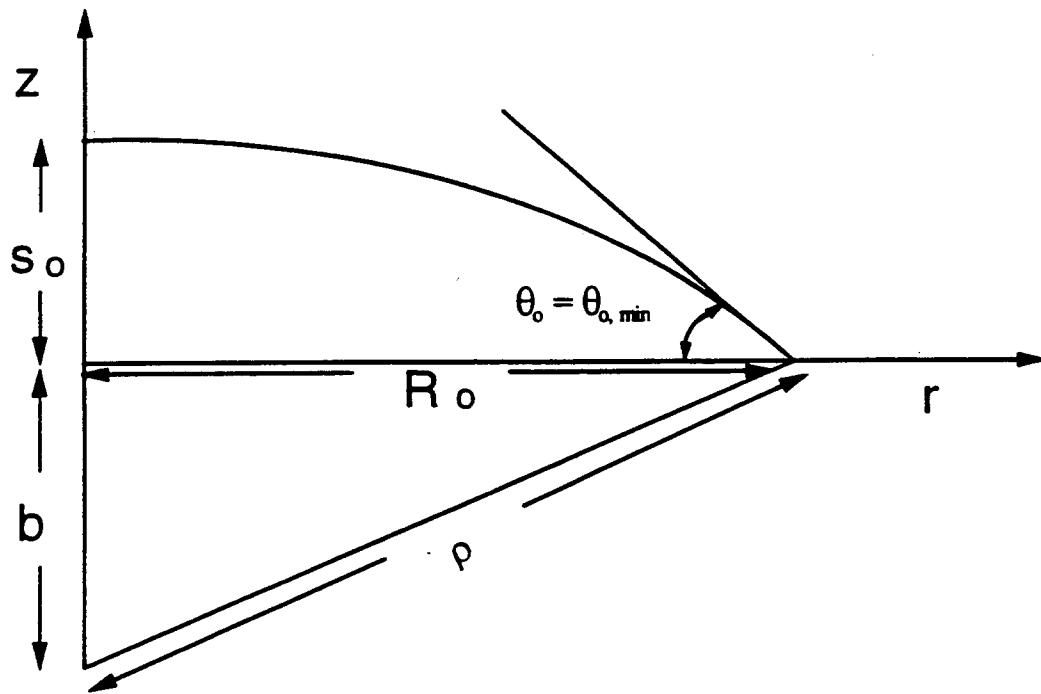


Figure 2 - Initial Droplet Configuration

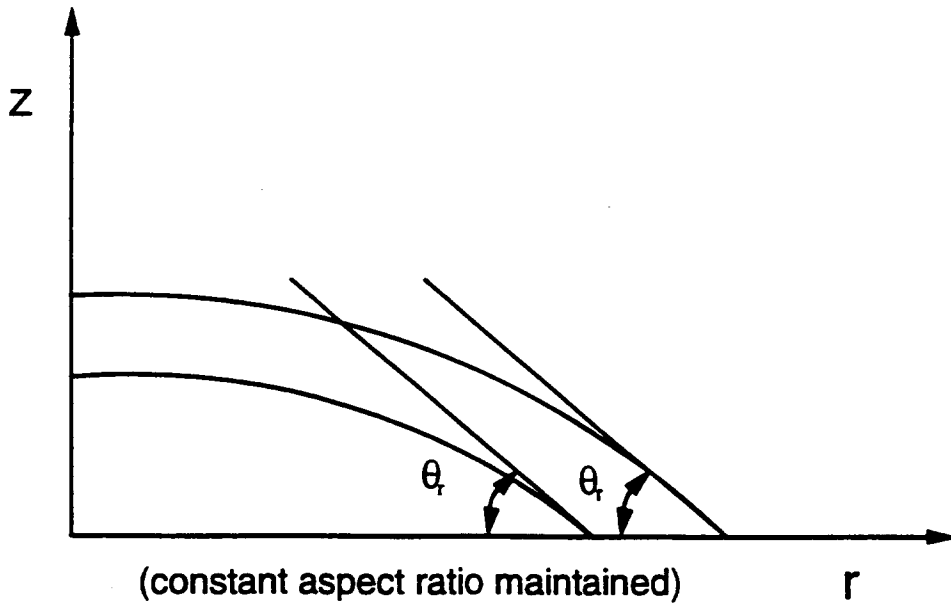
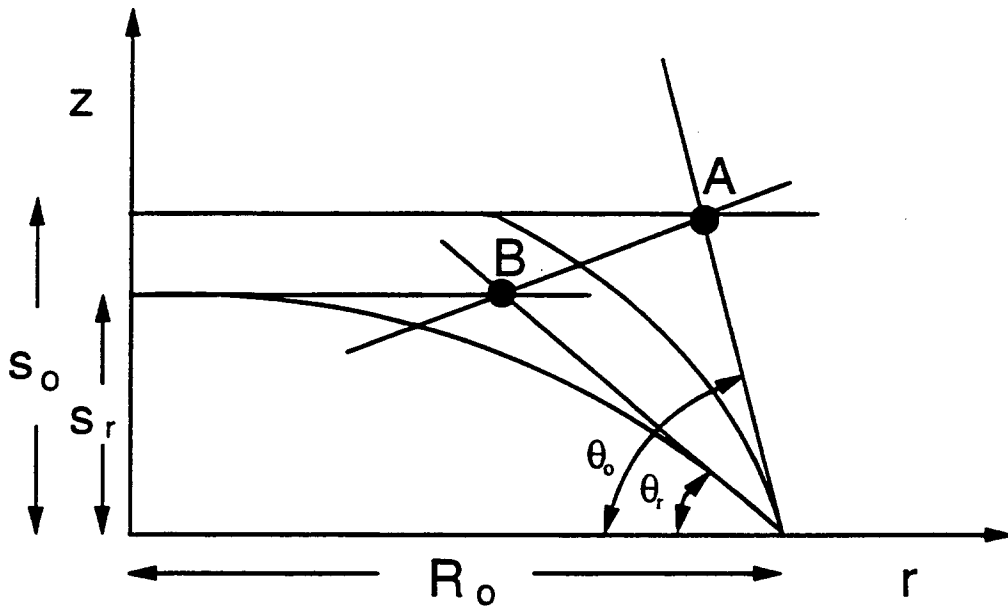


Figure 3 - Droplet Shape Transition

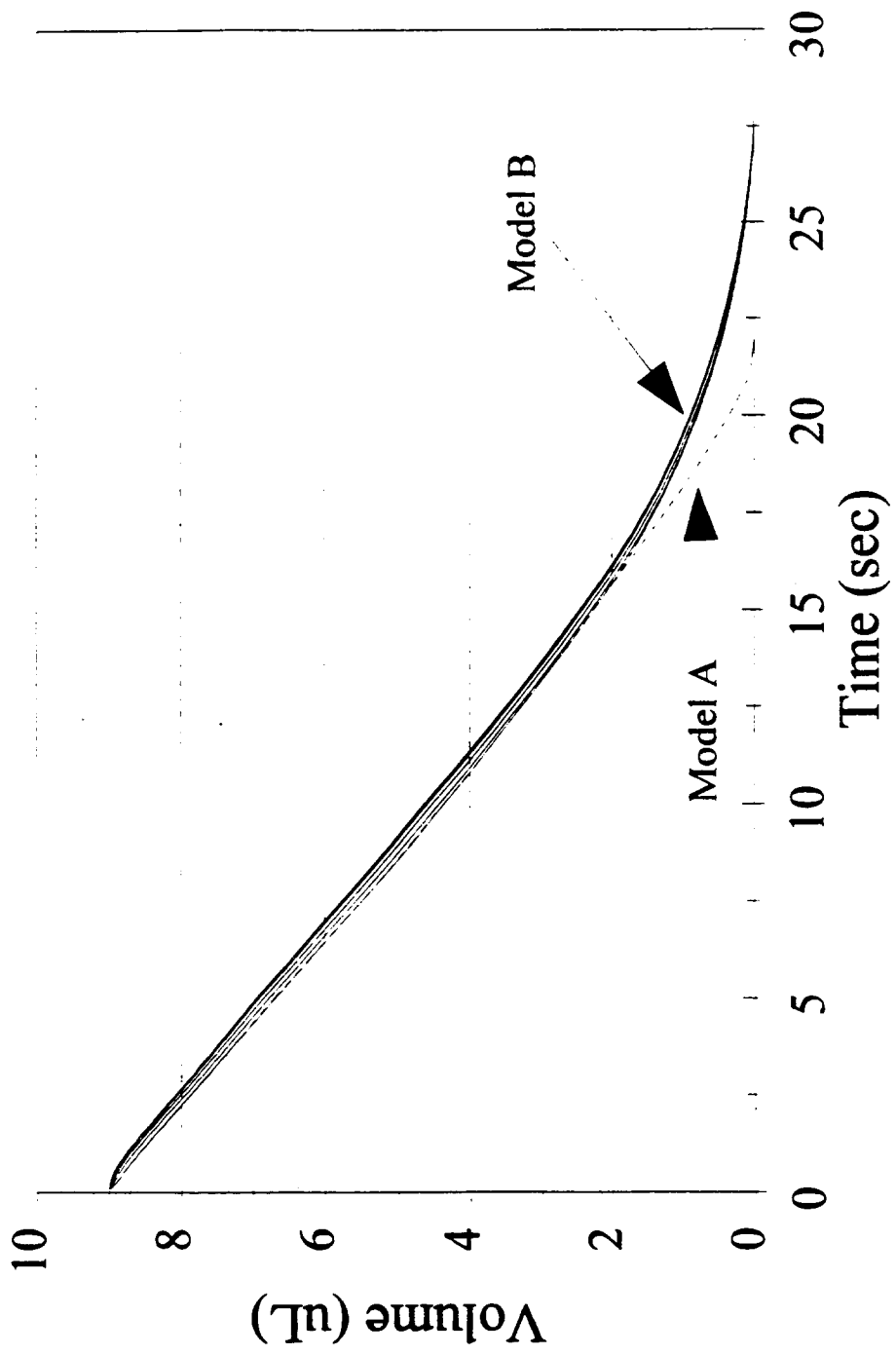


Figure 4 - Droplet Volume v. Time

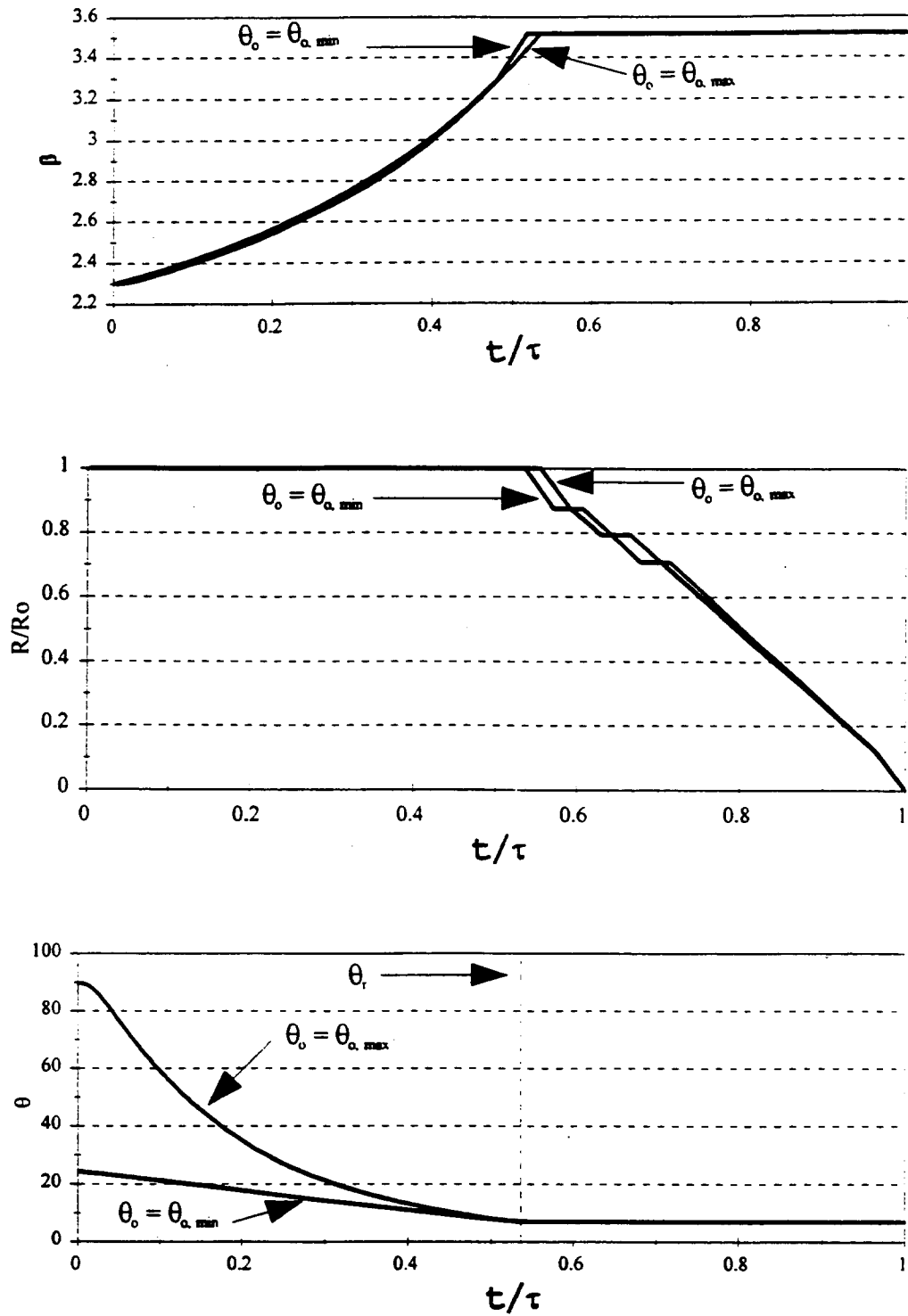


Figure 5 - Effect of Contact Angle on Droplet Parameters

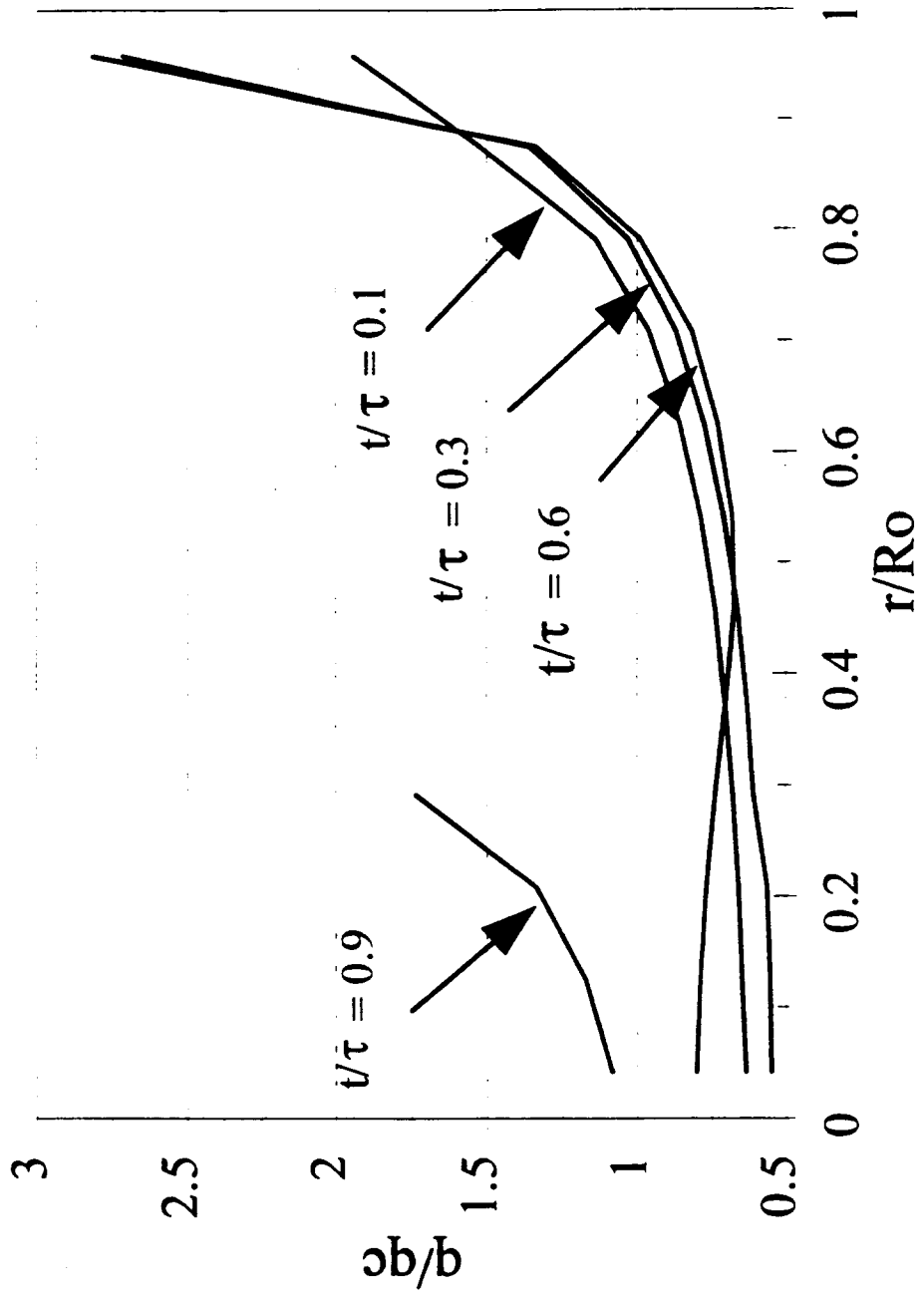


Figure 6 - Transient Normalized Interfacial Heat Flux

3. MODIFICATION OF THE RADIANT INTERFACIAL HEAT FLUX IN THE SINGLE DROPLET EVAPORATION MODEL

As mentioned earlier, a model was developed to predict the evaporation phenomena associated with a single droplet evaporating on a hot, low thermal conductivity surface where the heat input is by radiation from above [10]. A significant effort in developing this model centered around the quantification of the radiant heat input. While performing a recent validation of the code against experimental work, the author found that one of the parameters involved in the radiation portion of the model needed to be modified. The basis of that modification is discussed presently.

3.1 Experimental Radiant Panels Geometry

For the experimental work performed by Dawson [9] on the single droplet evaporation, heat input was by radiation from above the surface. The radiant heat input was provided by three, truncated conical radiant panels located above the surface. The geometry of the panels with respect to the surface is shown in Figure 7. The two panels that are the same size have external diameters of 0.2 meters and depths of 0.8 meters. The third panel has an external diameter of 0.3 meters and a depth of 0.07 meters and surrounds the perimeter of the surface. The panels can reach temperatures of 700 °C and are controlled by an Omega CN-7100 digital process controller.

3.2 Previous Determination of the Radiant Interfacial Heat Flux

In developing the single droplet model to include radiation effects, White [10] divided the radiation into two parts with respect to the liquid, an interfacial heat flux term and a residual term that can be applied as a volumetric heat generation. White defines this interfacial heat flux as

$$F_s = F_\epsilon \sigma T_p^4 \quad (9)$$

Viskanta and Toor [12] provide a general expression for F_ϵ which includes scattering within the liquid and bottom reflection. White has reduced this expression to

$$F_\epsilon = 2 \int_0^{\pi/2} f_\phi \cos(\phi) \sin(\phi) (1 - \rho_\phi) d\phi \quad (10)$$

The terms making up this expression have the following meanings

- (1) ϕ - polar angle of incident radiation with respect to the normal to the droplet surface
- (2) ρ_ϕ - reflectivity from the droplet's surface, a function of ϕ (less than 0.1 for ϕ less than 60 °)
- (3) f_ϕ - fractional surface area coverage by the radiant panels (found by White for the laboratory geometry and shown in Figure 8)

Several assumptions were made in determining a value for F_ϵ . These are

- (1) the liquid-vapor interface is horizontal and flat
- (2) scattering within the droplet is negligible
- (3) radiation reaching the liquid-solid interface is completely absorbed by the solid

- (4) the geometry is symmetric, including azimuthal symmetry of the droplet and symmetry of the radiant panels with respect to the droplet
- (5) reflection at the liquid-vapor interface obeys Fresnel's relations for electro-magnetic theory - water is considered as a dielectric

With these assumptions, Equation (10) was numerically integrated and a value of 0.226 was calculated for F_{ε} .

3.3 Modification to the Interfacial Radiant Heat Flux Term

Of the assumptions listed at the end of section 3.2, the first one is the most questionable. Considering the droplet shape that is discussed in Chapter 2, the shape of the droplet surface, especially near the edges, may not have a normal that is in the vertical direction. If this is the case, much of the radiation coming in at large polar angles would not be reflected away as is assumed.

To rectify the problem stemming from the curvature of the surface, ideally F_{ε} should be treated as a function of the droplet geometry. However, because evaluating F_{ε} in this way is cumbersome, a multiplier is instead introduced as an attempt to obtain an average value for F_{ε} that still includes the geometric effects.

With the droplet shape considered as flat and horizontal, the term inside the integral given in (10) ($f_{\phi} \cos(\phi) \sin(\phi) (1 - \rho_{\phi})$) is evaluated at discrete ϕ values. The term is then evaluated for the droplet having a contact angle of 25° which is the minimum value discussed in Section 2.4. The angle, ϕ , for this droplet geometry is actually the angle between the angle of incidence and the normal to the droplet surface, assuming the radiation passes through the center of the droplet. Taking a

ratio of the quantity obtained after summation for the curved droplet geometry to the same quantity obtained for the flat droplet geometry yields a value of approximately 1.9. Following the same procedure for a droplet having a contact angle equal to the receding angle yields a ratio of approximately 1. Therefore, the correction factor for F_{ϵ} should lie somewhere between 1 and 1.9.

A modification of F_{ϵ} by a factor of 1.75 was used in the validation effort that is presented in Chapter 4. The average value between 1 and 1.9 of 1.45 was increased in order to provide a single, simple correction that incorporates other effects in the code that are not easily accounted for. These other effects will be expanded upon in Chapter 4.

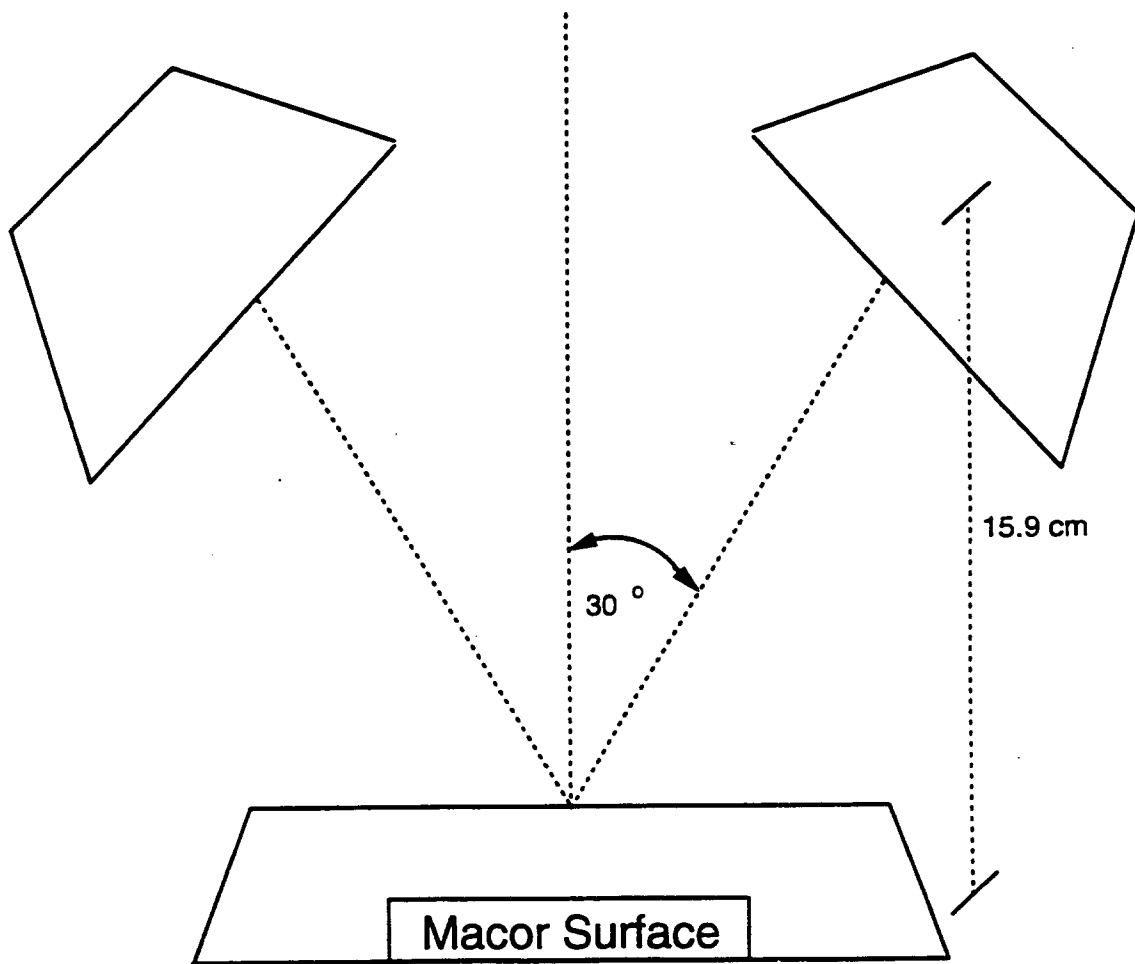


Figure 7 - Experimental Radiant Panels Geometry

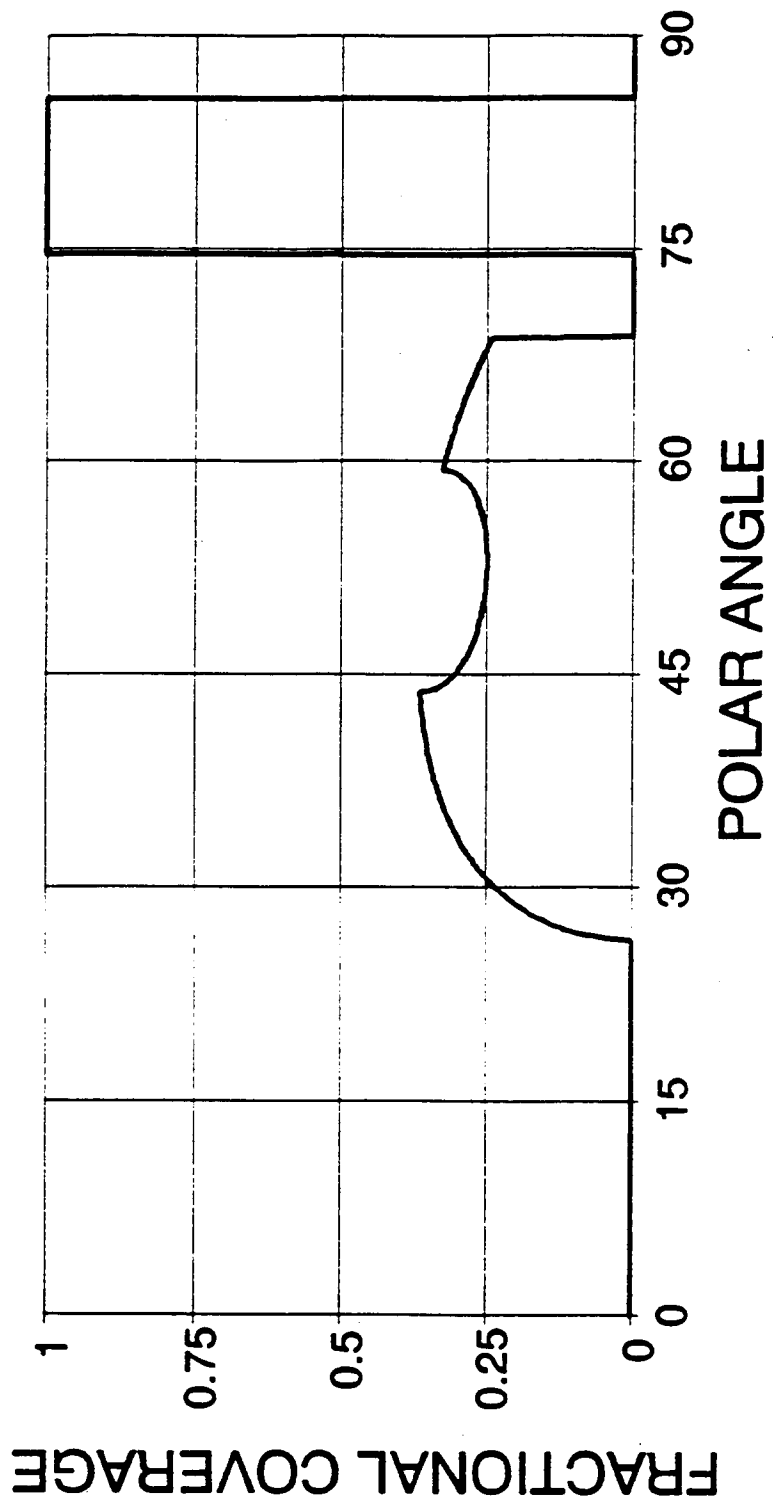


Figure 8 - Fractional Surface Area Coverage, f_{ϕ}

4. VALIDATION OF THE SINGLE DROPLET COMPUTER MODEL

In a previous model of the sparse spray cooling of semi-infinite solids [7], a database was used to provide the temperature distribution during the vaporization of a droplet. The parameters of the database consisted of various times during the evaporation of a single droplet, various initial surface temperatures, and the corresponding temperature drop. The information comprising the database was obtained from a single droplet computer model. Both the single droplet model and sparse spray model in the previous work focused on a solid that was heated by conduction from below.

The sparse spray cooling model of current concern is discussed in detail in the Chapter 6 and focuses on the cooling of a surface that is being heated from above by radiation. Again, in order to accurately model what is happening at a point on the surface relatively close to an evaporating droplet, the single droplet model mentioned in the two preceding chapters needed to be studied and quantified. Results of the validation of the single droplet model are now discussed. A closed-form solution that approximates the single droplet's effect on the surface will be presented in section 4.5.

4.1 Brief Description of the Single Droplet Computer Model

The computer code of White [10] models a single droplet evaporating on a surface that is under the experimental conditions shown in Figure 9. The results used as the basis for validation of the sparse spray cooling model were also obtained using this experimental setup. This section is intended to provide a general idea of

how the single droplet computer code works. Details of the development of the model can be found in reference [10].

The droplet shape is modelled using the geometry proposed in Chapter 2. Radiation effects are handled in the manner described in Chapter 3, with the largest portion of the radiation applied as an interfacial heat flux and the remaining distributed throughout the droplet as a heat generation term. The modification to the interfacial heat flux term discussed in Chapter 3 is used in the validation presented here.

The model assumes a one-dimensional conductive heat transfer with internal generation in the liquid layer. The one-dimensional assumption was justified previously from diMarzo's coupled model [13] and is reinforced by the thinner droplet geometry that results from the direct radiation. The thermal behavior of the solid is governed by a transient, two-dimensional (r,z) diffusion equation which is solved using a Boundary Element Method. Coupling of the liquid and the solid is accomplished using a predict-correct method.

4.2 Validation of the Single Droplet Computer Model

Experimental results obtained by Dawson [9] for the evaporation of a single droplet on a macor surface are used as the basis for validation of the single droplet computer model. Validation of the code is determined by two criteria. The first criterion is the total evaporation time of the droplet. The second criterion is the transient surface temperature profile predicted by the code.

4.2.1 Inputs to the Computer Model

Running the computer model requires several inputs. These inputs are used as a description of the conditions that occurred during an experiment. The first two parameters that are discussed relate to the initial heating conditions of the experiment, that is the initial surface temperature and the temperature of the radiant panels. The single droplet evaporation experiments run by Dawson were for initial surface temperatures of 110 °C and 130 °C. Therefore, these are the initial surface temperatures that are used for validation purposes. Various initial surface temperatures correspond to radiant panel temperatures when a temperature of the solid 0.0254 meters below the surface is held constant. The experimental surface bottom temperature ranged from 32 °C to 40 °C for the various initial surface temperatures and was maintained by a chill plate underneath the surface. A curve fit to the panel temperature versus initial surface temperature was obtained from experimental data and is shown in Figure 10. Using the curve fit, panel temperatures of 473 °C and 512 °C are used for initial surface temperatures of 110 °C and 130 °C, respectively.

Three remaining parameters are needed in order to use the model. These parameters pertain to the droplet itself and are the initial droplet volume, the initial shape factor, and the initial and receding contact angles. Dawson measured an initial droplet volume of 10 microliters for his single droplet experiments. For the validation of the code, an initial droplet volume of 9 microliters is used. This volume is selected to represent the average droplet volume that was used during the

experiments. A volume decrease is expected to occur because an experimental run consists of consecutive droplet evaporations and surface recoveries. In this way, while the surface recovers to its initial temperature, the water in the dispenser is being heated. Some of the water will evaporate, thereby causing less water to be dispensed for the following cycle.

The initial shape factor, β_0 , is the ratio of the diameter of the droplet immediately after impact to the diameter of the equivalent spherical droplet prior to impact. For initial surface temperatures ranging from 110 °C to 160 °C, Kidder found initial shape factor values in a range between 1.5 and 2.5 [8]. The initial surface temperatures of interest here are 110 °C and 130 °C, yielding shape factor values approximately equal to 2. A value of 2.3 is used for the code validation as an attempt to account for the difference in droplet release height between the experiments of Kidder and Dawson. Dawson's release height was 0.3 meters higher than Kidder's.

The geometric model presented in Chapter 2 requires a value for the initial contact angle in addition to a value for β_0 . Because the study of that model showed that the initial contact angle had no effect on the droplet's evaporation, a minimum value for the contact angle is selected for the validation purposes. The minimum contact angle corresponding to the values for β_0 and the initial droplet volume is found to be approximately 25 °. Therefore, the droplet shape model that is employed is that of a spherical cap with the recession of the solid-liquid interface.

4.2.2 Validation Results

Using the various input parameters stated in 4.2.1, evaporation times and surface temperature distributions were obtained. Evaporation times predicted by the computer model were 45 seconds for an initial surface temperature of 110 °C and 26 seconds for an initial surface temperature of 130 °C. The experiments selected for comparison had evaporation times of 40.2 seconds and 24 seconds, respectively.

The difference in evaporation times results from the discretization of both the time and the water droplet in the computer model. The water droplet is modeled as discrete annular columns in the code. During each time step, the amount of water that makes up a particular column is the maximum amount of water that can be vaporized in that column, even if the heat supplied to that column during a time step is more than is required to vaporize the column. For the next time step, the remaining droplet volume is redistributed and the columns are reconfigured. In reality, the time and droplet volume are continuous so that all of the heat that is supplied acts to vaporize the droplet. Part of the redistribution effect is corrected through the increase in the value of F_g . An error in the evaporation time on the order of 10% is acceptable in view of the arbitrary correction. Generally, errors are smaller than 10% except at low temperatures where the vaporization process is longer and redistribution effects are larger.

The predicted surface temperature distributions are compared to the experimental distributions in Figures 11 and 12. The raw data used in these figures are contained in Table 1 and Table 2. The figures are for initial surface temperatures

of 110 °C and 130 °C. Three times during the droplet's evaporation are displayed. The first time corresponds to the beginning of the droplet's evaporation, the second time is just prior to the complete evaporation of the droplet, and the last time is just after evaporation of the droplet when the surface is recovering.

A single line depicts the predicted temperature distribution, while the thicker, jagged line represents the experimental data. The appearance of the experimental results are due to the means of data acquisition. A line scan function on an infrared camera is used to display the temperature distribution. Using a PC and frame grabber software, the line is digitized in a pixel by pixel manner. Each pixel location in the vertical direction can be associated with a temperature and each pixel in the horizontal direction can be associated with a radial location. The thickness of the data arises because the line scan function produces a band of pixels when it is grabbed and digitized. Furthermore, note that during the droplet's evaporation, temperature distributions begin at the edge of the droplet. Using the thermographic technique, recorded surface temperatures underneath the droplet cannot be associated to infrared emissions.

From the comparisons made in Figures 11 and 12, it is evident that the computer model is able to predict reasonable transient surface temperature distributions caused by the evaporation of a single droplet. At early times, there is some deviation between the predicted and experimental temperatures at the droplet's edge. Again, this is a result of the inability of the infrared camera to record what is happening underneath the droplet and to the experimental uncertainties associated

with the position of the droplet's outer edge. As the surface recovers, the computer model lags the experimental data slightly for normalized radial location between 0 and 1. However, as time progresses, these differences are decreased.

4.3 Closed-Form Solution

A closed-form solution for the transient surface temperature distribution is now presented. The closed-form solution provides a simple, yet reasonable means of obtaining temperature differences at points on a surface near the droplet. It is useful for the model of sparse spray cooling because it eliminates the need for a database, which can take up significant amounts of computer memory and computation time.

4.3.1 Description of the Closed-Form Solution

A closed-form solution to the problem of a disk with constant and uniform heat flux on an insulated surface is given in reference [14]. The solution has the following form

$$T - T_{so} = \frac{-qR}{k_s} \int_0^{\infty} J_0\left(\frac{\lambda r}{R}\right) J_1(\lambda) \operatorname{erf}\left(\frac{\lambda\sqrt{\alpha_s t}}{R}\right) \frac{d\lambda}{\lambda} \quad (11)$$

where q is the constant and uniform heat flux acting over a disk of radius R . The temperature at various locations (r) and times (t) can be found using Equation (11).

Although the evaporation of a single droplet does not have a constant and uniform solid-liquid interfacial heat flux, the solution described by (11) models the phenomenon closely if minor modifications are made. Specifically, a modification to the radius, R , needs to be made in order to account for both the recession of the

solid-liquid interface and the fact that the conductive heat flux is neither constant nor uniform. The heat flux, q , is replaced by the term $(q_c + q_o)$, where q_c accounts for the conductive contribution to the vaporization of the droplet and q_o is the initial steady state heat flux through the solid. Equation (11) yields a solution for the surface temperature distribution during the evaporation of the droplet. An expression can also be found for the solid surface temperature distribution for times after the droplet has evaporated ($t > \tau$) by modifying (11) to obtain [10]

$$T(x, t) - T_{so} = \frac{-qR}{k_s} \int_0^\infty J_0\left(\frac{\lambda x}{R}\right) J_1(\lambda) \left[\operatorname{erf}\left(\frac{\lambda\sqrt{\alpha_s t}}{R}\right) - \operatorname{erf}\left(\frac{\lambda\sqrt{\alpha_s(t-\tau)}}{R}\right) \right] \frac{d\lambda}{\lambda} \quad (12)$$

Surface temperature distributions in the vicinity of a droplet can be obtained for the evaporation of the droplet as well as for the recovery of the surface using Equations (11) and (12). However, the conductive heat flux contribution to the droplet's evaporation (q_c) and the evaporation time (τ) must be known before the solutions can be used.

4.3.2 Determination of q_c and τ

In order to use the solutions given in Equations (11) and (12), the evaporation time (τ) and the conductive heat flux contribution (q_c) to the vaporization of the droplet must be known. The initial heat flux (q_o) is known from the initial surface temperature, the bottom surface temperature, and the thickness of the solid. The evaporation time can be obtained experimentally or by using the single droplet computer model. The conductive heat flux must be found using the computer model.

For a range of initial surface temperatures and their corresponding panel

temperatures, with the other inputs discussed in section 4.2.1, the computer model was run to obtain the resulting evaporation times and conductive heat fluxes. Results are plotted in Figure 13 and Figure 14, and curves are fit to the computed data points. The results are used in the comparison of the closed-form solution against the computer model.

4.3.3 Temperature Distribution Results

Surface temperature distributions given by the closed-form solution are compared against those obtained using the computer model in Figures 15 and 16 and raw data are in Tables 3 and 4. The distributions shown are for the same conditions used for the validation results of the single droplet model. Comparisons are made for two times during the droplet's evaporation and one time after the droplet has evaporated for initial surface temperatures of 150 °C and 100 °C. These initial surface temperatures represent a relatively high and a relatively low value for the range of surface temperatures that are found in the spray cooling database of concern to fire protection applications.

In order to compare the closed-form solution to the results of the single droplet model, the radial shrinkage of the droplet needs to be accounted for. Since the solution represents a fit to the data, a simple means to account for the shrinkage of the wetted region is to introduce a constant into the expression. The constant effectively decreases the temperature difference given by the closed-form solution. Such a decrease has the same effect of shrinking the radius. The effect of introducing this factor into the closed-form solution is most apparent in the first two

temperature distributions shown in Figure 15. The first distribution predicted by the closed-form solution lies slightly above that predicted by the code because of the modification to the radius. The next distribution, which corresponds to a time after the recession of the droplet has begun, predicted by the closed-form solution lies slightly below that predicted by the code. If the modification to the radius was not included, both of the closed-form distributions would lie below the code distributions with the latter one significantly lower.

Temperature distributions predicted using the single droplet computer model are shown by thick, solid lines and those obtained from the closed-form solution are shown by the thin, dashed lines. The closed-form solution for the temperature distribution agrees well with the predicted distributions with respect to both space and time. In these figures, distributions underneath the droplet are shown. The difference in character between the closed-form solution and the single droplet model underneath the droplet is a reflection of the boundary conditions that govern the two problems. The closed-form solution has a constant heat flux boundary condition underneath the droplet, while the computer model has a constant temperature underneath the droplet. The differences in temperature distribution underneath a droplet are not expected to cause significant error in the sparse spray cooling model. Since a radial temperature distribution corresponds to the droplet, the accuracy of predictions near the droplet is less important than the accuracy far from the droplet due to the area associated with each. Additionally, experimental data does not yield correct temperature distributions underneath a droplet.

At an early time during the droplet's evaporation, there is virtually no difference in the distributions except for the behavior underneath the droplet which was just discussed. The biggest difference between the distributions is found at a time just prior to the complete evaporation of the droplet. At this time, the shrinkage of the droplet has occurred and is apparent in the distribution predicted by the single droplet model. The effect of using the closed-form solution as opposed to the single droplet model to calculate the average surface temperature in the sparse spray cooling code will be quantified in Chapter 6. Immediately after the droplet has evaporated, again slight discrepancies are shown between the two curves underneath the droplet. However, these discrepancies die out quickly as time progresses.

4.4 Summary

The single droplet computer model of White was validated with respect to evaporation times and surface temperature distributions against experimental data. A relatively simple closed-form solution was shown to yield temperature distributions that agree with the model predictions. The closed-form solution requires the droplet evaporation time and the conductive heat flux contribution to the vaporization of the droplet. These two pieces of information can be obtained using the single droplet model. A model for the sparse spray cooling of a surface for the same experimental setup as described in this chapter utilizes the closed-form solution as a simple means of calculating temperature depressions at points in the vicinity of droplets. The sparse spray cooling model is the subject of Chapter 6.

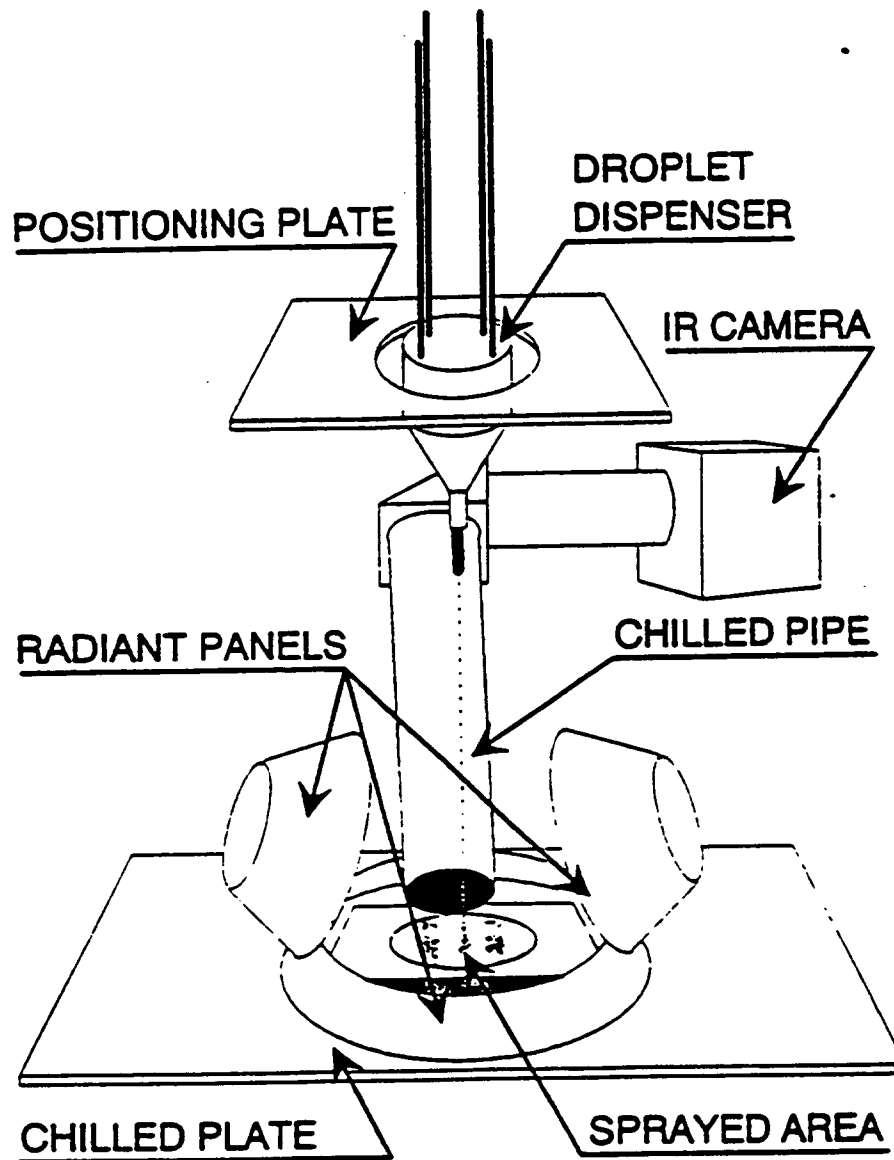


Figure 9 - Experimental Setup

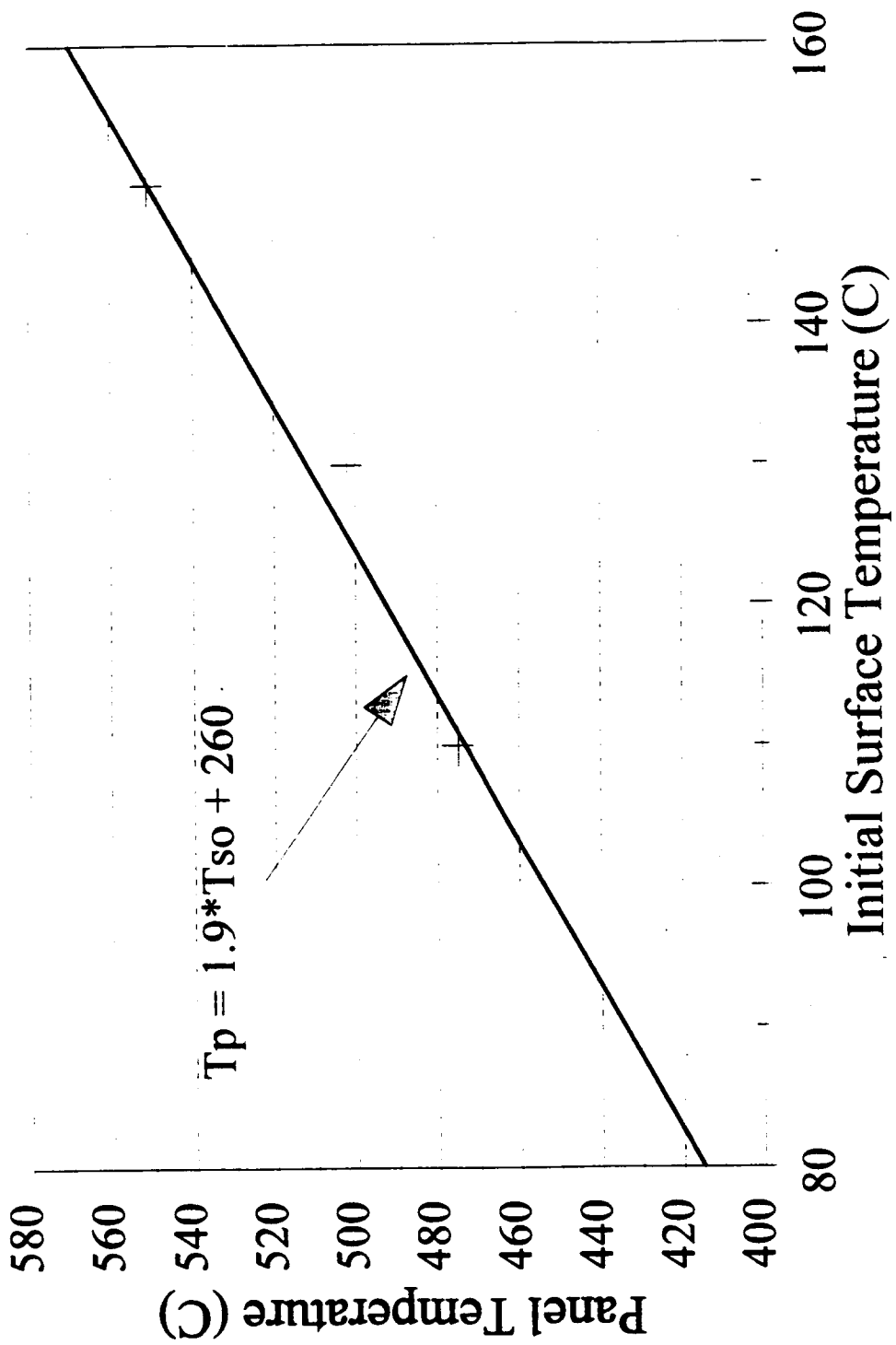


Figure 10 - Panel Temperature v. Initial Surface Temperature

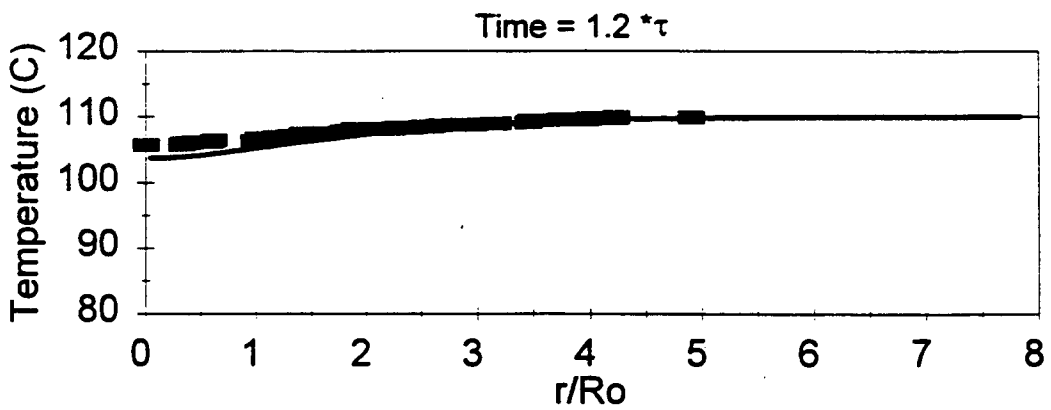
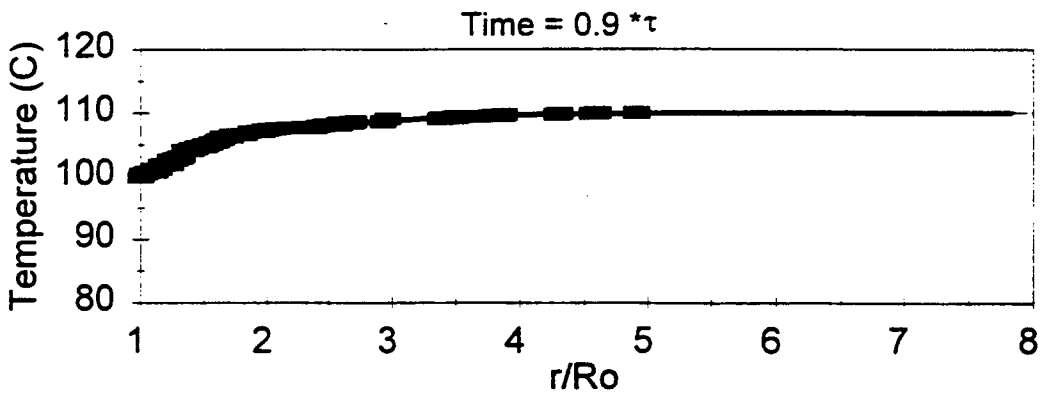
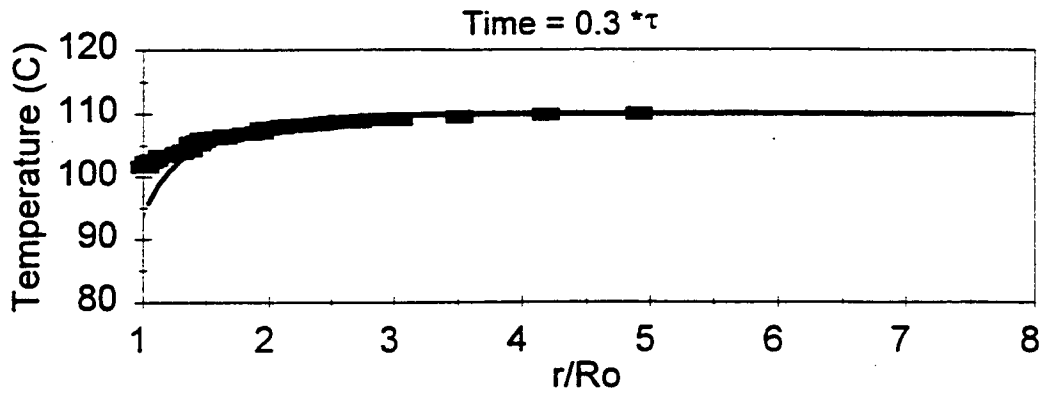


Figure 11 - Surface Temperature Distributions;
 $T_{so} = 110 \text{ } ^\circ\text{C}$

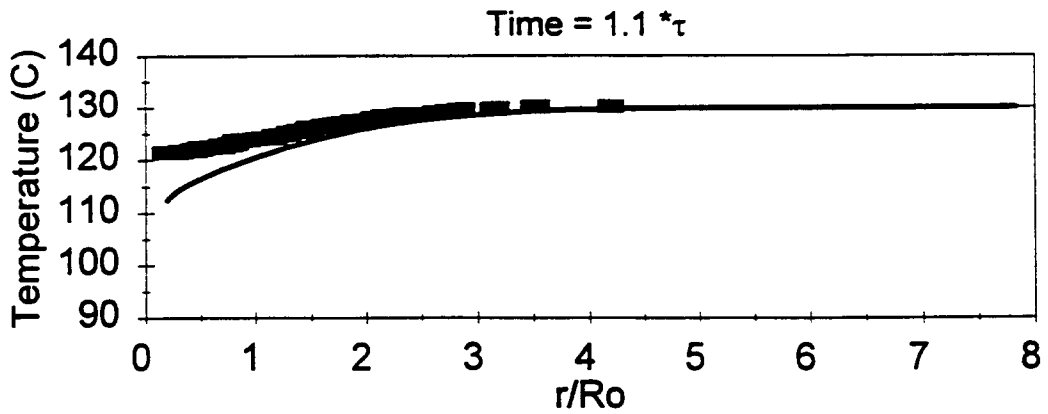
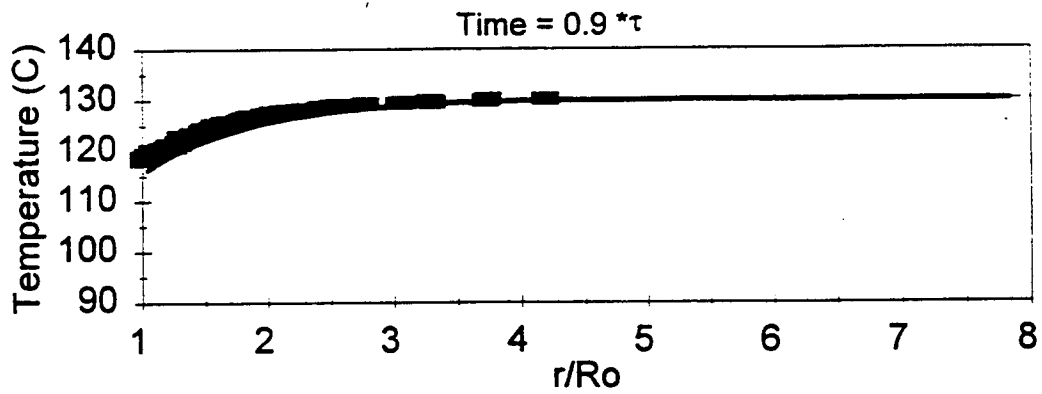
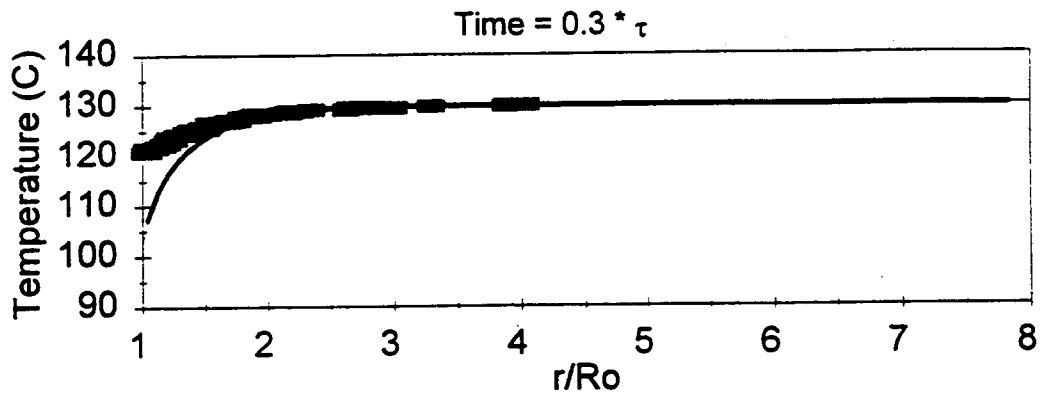


Figure 12 - Surface Temperature Distributions;
 $T_{so} = 130 \text{ } ^\circ\text{C}$

Time = 0.3 tau				Time = 0.9 tau				Time = 1.2 tau			
eRo	Experiment	eRo	Single Droplet Code	eRo	Experiment	eRo	Single Droplet Code	eRo	Experiment	eRo	Single Droplet Code
0.0000	85.1200	0.0417	86.4831	0.0000	84.86	0.0417	84.27	0.0000	105.86	0.0417	103.72
0.0727	85.1200	0.1250	86.5784	0.1435	84.86	0.1250	84.50	0.3273	105.86	0.1250	103.74
0.0600	85.2750	0.2083	86.6150	0.1836	85.12	0.2083	84.75	0.3455	105.87	0.2083	103.76
0.1435	85.2750	0.2917	86.6785	0.2545	85.12	0.2917	85.14	0.4000	105.87	0.2917	103.87
0.1818	85.7400	0.3750	86.7715	0.4000	85.43	0.3750	85.76	0.4384	106.13	0.3750	103.96
0.2545	85.7400	0.4583	86.8861	0.4545	85.43	0.4583	86.75	0.6000	106.13	0.4583	104.06
0.2600	86.0500	0.5417	87.0708	0.4727	85.74	0.5417	88.44	0.6182	106.44	0.5417	104.22
0.3455	86.0500	0.6250	87.3061	0.5455	85.74	0.6250	82.87	0.6618	106.28	0.6250	104.37
0.3818	86.5150	0.7083	87.6437	0.5636	86.21	0.7083	85.33	1.0182	106.75	0.7083	104.53
0.4182	86.5150	0.7917	88.1433	0.5836	86.21	0.7917	87.43	1.1455	106.75	0.7917	104.71
0.4384	86.9800	0.8750	88.5870	0.5818	86.52	0.8750	86.85	1.1818	106.90	0.8750	104.89
0.4545	86.9800	0.9583	89.7837	0.6182	86.52	0.9583	86.98	1.2384	106.90	0.9583	105.06
0.4727	87.2900	1.0417	85.7543	0.6182	86.83	1.0417	100.83	1.3091	107.06	1.0417	105.27
0.4727	87.2900	1.1250	86.8543	0.6727	86.83	1.1250	101.75	1.3818	107.06	1.1250	105.48
0.5455	87.7550	1.2083	100.8370	0.6727	87.45	1.2083	102.48	1.4182	107.37	1.2083	105.65
0.5455	87.7550	1.2917	102.4980	0.7091	87.45	1.2917	103.10	1.5091	107.37	1.2917	105.84
0.5818	88.2200	1.3750	103.7220	0.7273	87.80	1.3750	103.87	1.6000	107.52	1.3750	106.03
0.6384	88.2200	1.4583	104.7140	0.7636	87.80	1.4583	104.18	1.7818	107.88	1.4583	106.22
0.6545	88.5300	1.5417	105.5310	0.7818	87.91	1.5417	104.85	1.8000	107.83	1.5417	106.40
0.7091	88.5300	1.6250	106.2130	0.8000	87.91	1.6250	105.08	1.8608	108.14	1.6250	106.57
0.7273	88.8150	1.7083	106.7860	0.8182	88.22	1.7083	105.47	1.9091	107.80	1.7083	106.75
0.8000	88.8150	1.7917	107.2710	0.8182	88.22	1.7917	105.83	2.0545	108.14	1.7917	106.91
0.8182	100.0800	1.8750	107.8830	0.8384	88.38	1.8750	106.18	2.0545	108.14	1.8750	107.04
0.8384	100.0800	1.9583	108.6340	0.8545	88.38	1.9583	106.47	2.1836	108.14	1.9583	107.23
0.8545	100.3900	2.0417	108.3340	0.8727	88.00	2.0417	106.75	2.2384	108.14	2.0417	107.38
0.8727	100.3900	2.1250	108.5800	0.8608	88.00	2.1250	107.01	2.2727	108.30	2.1250	107.53
0.8900	100.7000	2.2083	108.8080	0.8273	88.15	2.2083	107.25	2.3455	108.30	2.2083	107.87
0.9091	100.7000	2.2917	108.9950	0.8455	88.15	2.2917	107.47	2.4000	108.30	2.2917	107.80
0.9273	100.8550	2.3750	108.1540	0.8636	88.48	2.3750	107.88	2.4000	108.30	2.3750	107.83
0.9455	100.8550	2.4583	108.2880	0.8836	88.48	2.4583	107.87	2.5091	108.45	2.4583	108.05
0.9636	101.3200	2.5417	108.4040	1.0000	88.83	2.5417	108.04	2.5818	108.45	2.5417	108.17
0.9818	101.3200	2.6250	108.5020	1.0000	88.83	2.6250	108.21	2.6545	108.61	2.6250	108.28
1.0000	101.8300	2.7083	108.5850	1.0182	100.38	2.7083	108.36	2.6545	108.61	2.7083	108.38
1.0182	101.8300	2.7917	108.6550	1.0384	100.38	2.7917	108.50	2.8182	108.76	2.7917	108.48
1.0384	102.4850	2.8750	108.7140	1.0545	100.70	2.8750	108.82	2.8836	108.76	2.8750	108.58
1.0545	102.4850	2.9583	108.7840	1.1091	100.70	2.9583	108.74	3.1455	108.82	2.9583	108.67
1.0727	102.7150	3.0417	108.8050	1.1091	101.17	3.0417	108.85	3.1818	108.82	3.0417	108.78
1.0900	102.7150	3.1250	108.8400	1.1455	101.17	3.1250	108.85	3.4545	108.07	3.1250	108.84
1.1455	103.3350	3.2083	108.8860	1.1836	101.78	3.2083	109.04	3.4727	108.38	3.2083	108.82
1.1818	103.3350	3.2917	108.8830	1.1818	101.78	3.2917	109.13	3.6545	108.38	3.2917	108.89
1.2727	103.8000	3.3750	108.8130	1.2000	101.84	3.3750	109.21	3.7455	108.54	3.3750	108.88
1.2600	103.8000	3.4583	108.8360	1.2384	101.84	3.4583	109.28	3.8818	108.54	3.4583	108.12
1.3273	104.2850	3.5417	108.8430	1.2384	102.56	3.5417	109.34	4.0000	108.60	3.5417	108.18
1.3636	104.2850	3.6250	108.8540	1.2727	102.56	3.6250	109.40	4.2182	108.88	3.6250	108.24
1.3818	105.3500	3.7083	108.8630	1.2727	102.87	3.7083	109.48	4.2384	108.85	3.7083	108.30
1.4000	105.1850	3.7917	108.8710	1.3091	102.87	3.7917	109.51	4.8091	109.85	3.7917	108.35
1.4384	105.1850	3.8750	108.8770	1.3091	103.18	3.8750	109.58				
1.4384	105.8600	3.9583	108.8820	1.3273	103.18	3.9583	109.60				
1.4727	105.8600	4.0833	108.8870	1.3455	104.11	4.0833	109.68				
1.4727	106.1250	4.2000	108.8820	1.4000	104.11	4.2000	109.72				
1.5636	106.1250	4.4182	108.8850	1.4000	104.42	4.4182	109.77				
1.5818	106.2800	4.5833	108.8870	1.4384	104.42	4.5833	109.82				
1.6384	106.2800	4.7500	108.8880	1.4545	104.75	4.7500	109.85				
1.6545	106.5800	4.8182	108.8880	1.5091	104.75	4.8182	109.88				
1.6800	106.5800	5.0833	108.8880	1.5091	105.04	5.0833	109.91				
1.8000	106.8000	5.2500	110.0000	1.5455	105.04	5.2500	109.93				
1.8545	106.8000	5.4182	110.0000	1.5836	105.35	5.4182	109.94				
1.9091	107.0550	5.5833	110.0000	1.5818	105.35	5.5833	109.95				
1.9273	107.0550	5.7500	110.0000	1.6000	105.31	5.7500	109.96				
1.9455	107.8750	5.9182	110.0000	1.6000	105.31	5.9182	109.97				
1.9818	107.8750	6.0833	110.0000	1.6182	105.82	6.0833	109.98				
2.0000	107.8300	6.2500	110.0000	1.6384	105.82	6.2500	109.98				
2.0600	107.8300	6.4182	110.0000	1.6545	106.28	6.4182	109.99				
2.1091	108.1400	6.5833	110.0000	1.7091	106.28	6.5833	109.99				
2.2545	108.1400	6.7500	110.0000	1.7273	106.59	6.7500	109.99				
2.2727	108.2950	6.9182	110.0000	1.8182	106.59	6.9182	109.99				
2.3818	108.2950	7.1887	110.0000	1.8727	107.08	7.1887	110.00				
2.4384	108.4500	7.3000	110.0000	1.9636	107.08	7.3000	110.00				
2.4900	108.8050	7.8333	110.0000	1.9818	107.37	7.8333	110.00				
2.5836	108.7800	8.1887	110.0000	2.0000	107.37	8.1887	110.00				
2.7091	108.7800	8.5000	110.0000	2.0384	107.82	8.5000	110.00				
2.8182	108.0700	8.8333	110.0000	2.0545	107.52	8.8333	110.00				
3.0384	108.2250	9.1887	110.0000	2.1818	107.88	9.1887	110.00				
3.9091	108.3350	9.5000	110.0000	2.3818	107.88	9.5000	110.00				
4.1818	108.8450	9.8333	110.0000	2.4182	107.99	9.8333	110.00				
4.8091	110.0000	10.5000	110.0000	2.4384	107.99	10.5000	110.00				
				11.5000	108.14	11.5000	110.00				
				12.5000	108.14	12.5000	110.00				
				2.5818	108.45						
				2.6727	108.45						
				2.8900	108.61						
				2.8273	108.61						
				2.9836	108.07						
				3.3818	108.07						
				3.4000	108.23						
				3.4900	108.23						
				3.5091	108.38						
				3.6545	108.38						
				3.7818	108.54						
				3.8545	108.54						
				3.8727	108.60						
				4.2900	108.60						
				4.3091	108.85						
				4.5836	108.85						
				4.8000	110.00						
				4.8091	110.00						

Table 1 - Raw Temperature Data for Figure 11

Time = 0.3 * tau				Time = 0.9 * tau				Time = 1.1 * tau			
r/Ro	Experiment	r/Ro	Sample Droplet Code	r/Ro	Experiment	r/Ro	Sample Droplet Code	r/Ro	Experiment	r/Ro	Sample Droplet Code
0.0000	110.01	0.0417	95.11	0.0000	109.23	0.0417	99.73	0.1818	121.48	0.0417	107.32
0.0727	110.01	0.1250	95.24	0.1887	108.23	0.1250	90.05	0.3091	121.48	0.1250	106.38
0.0909	110.47	0.2083	95.17	0.1887	108.39	0.2083	90.39	0.3273	121.76	0.2083	112.82
0.1636	110.47	0.2917	95.13	0.2642	108.39	0.2917	90.95	0.4384	121.76	0.2917	114.22
0.2364	111.40	0.3750	95.11	0.3019	110.01	0.3750	91.88	0.4384	122.10	0.3750	115.26
0.3091	111.40	0.4583	95.10	0.3208	110.01	0.4583	93.67	0.4809	122.10	0.4583	116.11
0.3091	112.49	0.5417	95.11	0.3366	110.83	0.5417	97.73	0.4809	122.41	0.5417	116.88
0.3836	112.49	0.6250	95.15	0.3682	110.83	0.6250	104.15	0.5818	122.41	0.6250	117.80
0.4384	113.57	0.7083	95.25	0.3682	111.09	0.7083	108.13	0.6000	122.56	0.7083	118.30
0.4809	113.57	0.7917	95.47	0.4340	111.09	0.7917	110.87	0.6809	122.56	0.7917	118.97
0.4809	114.35	0.8750	95.07	0.4328	111.58	0.8750	113.00	0.6809	122.87	0.8750	119.82
0.5435	114.35	0.9583	97.80	0.4808	111.58	0.9583	114.78	0.7836	122.87	0.9583	120.24
0.5836	115.43	1.0417	107.19	0.5084	112.33	1.0417	118.25	0.7836	123.18	1.0417	120.83
0.6182	115.43	1.1250	112.85	0.5472	112.33	1.1250	117.56	0.8182	123.18	1.1250	121.40
0.6182	115.80	1.2083	118.32	0.5472	112.85	1.2083	118.73	0.8182	123.80	1.2083	121.85
0.6545	115.80	1.2917	118.21	0.5848	112.85	1.2917	119.77	0.8273	123.80	1.2917	122.47
0.6727	116.32	1.3750	121.27	0.6038	113.42	1.3750	120.71	0.8273	123.98	1.3750	122.98
0.7081	117.45	1.4583	122.91	0.6804	113.42	1.4583	121.57	1.0182	124.11	1.4583	123.43
0.7273	118.32	1.5417	124.22	0.6782	114.50	1.5417	122.34	1.0727	124.27	1.5417	123.88
0.7836	117.45	1.6250	125.28	0.7170	114.50	1.6250	123.05	1.1636	124.27	1.6250	124.30
0.7818	118.07	1.7083	128.15	0.7170	115.43	1.7083	123.70	1.1818	124.73	1.7083	124.71
0.8384	118.07	1.7917	128.86	0.7738	115.43	1.7917	124.29	1.2182	124.73	1.7917	125.08
0.8545	118.00	1.8750	127.45	0.7738	115.80	1.8750	124.84	1.2884	124.89	1.8750	125.44
0.8809	118.00	1.9583	127.93	0.7825	116.21	1.9583	125.33	1.2809	124.89	1.9583	125.78
0.8809	118.82	2.0417	128.33	0.8113	115.80	2.0417	125.78	1.3081	125.35	2.0417	126.10
0.9435	118.82	2.1250	128.85	0.8491	116.21	2.1250	126.19	1.3818	125.35	2.1250	126.40
0.9435	120.39	2.2083	128.82	0.8491	116.87	2.2083	126.57	1.4000	126.88	2.2083	126.88
0.9818	120.39	2.2917	129.14	0.8878	116.87	2.2917	126.81	1.4545	126.88	2.2917	126.94
1.0182	120.88	2.3750	129.31	0.8807	117.78	2.3750	127.23	1.4727	126.87	2.3750	127.19
1.0584	121.83	2.4583	129.46	0.8245	117.29	2.4583	127.51	1.4809	126.87	2.4583	127.42
1.0545	120.88	2.5417	129.57	0.8434	117.78	2.5417	127.77	1.4809	126.28	2.5417	127.83
1.1081	121.83	2.6250	129.86	0.8825	118.22	2.6250	128.00	1.6182	126.28	2.6250	127.83
1.1273	122.10	2.7083	129.74	1.0000	118.22	2.7083	128.22	1.6182	126.59	2.7083	128.02
1.1636	122.10	2.7917	129.80	1.0000	118.84	2.7917	128.41	1.6384	126.59	2.7917	128.19
1.1836	122.58	2.8750	129.84	1.0189	118.84	2.8750	128.58	1.6727	126.75	2.8750	128.35
1.2000	122.58	2.9583	129.88	1.0377	119.48	2.9583	128.74	1.7081	126.75	2.9583	128.50
1.2000	123.34	3.0417	129.91	1.0755	119.48	3.0417	128.88	1.7273	126.90	3.0417	128.84
1.2182	123.80	3.1250	129.83	1.0755	120.24	3.1250	129.01	1.7818	126.90	3.1250	128.78
1.2545	123.34	3.2083	129.95	1.1321	120.24	3.2083	129.12	1.8000	127.08	3.2083	128.88
1.2545	123.80	3.2917	129.88	1.1508	120.35	3.2917	129.22	1.8545	127.08	3.2917	128.98
1.2727	124.27	3.3750	129.07	1.1887	120.35	3.3750	129.32	1.8809	127.37	3.3750	129.08
1.3273	124.27	3.4583	129.98	1.1887	120.86	3.4583	129.40	1.8081	127.37	3.4583	129.17
1.3435	124.89	3.5417	129.88	1.2075	121.32	3.5417	129.47	1.8836	127.32	3.5417	129.25
1.3818	124.89	3.6250	129.99	1.2453	120.86	3.6250	129.33	2.0000	127.32	3.6250	129.33
1.3818	125.35	3.7083	129.99	1.2830	121.32	3.7083	129.59	2.0727	127.99	3.7083	129.40
1.4727	125.82	3.7917	129.99	1.2830	121.84	3.7917	129.84	2.1435	127.99	3.7917	129.46
1.5081	125.35	3.8750	130.00	1.3019	122.25	3.8750	129.89	2.1836	128.30	3.8750	129.52
1.5273	125.82	3.9583	130.00	1.3019	122.87	3.9583	129.73	2.2545	128.30	3.9583	129.57
1.5273	126.59	4.0417	130.00	1.3208	121.84	4.0417	129.78	2.2809	128.45	4.0417	129.84
1.5818	126.59	4.1250	130.00	1.3388	122.25	4.1250	129.83	2.3081	128.45	4.1250	129.84
1.6182	126.75	4.2083	130.00	1.3585	122.87	4.2083	129.88	2.3273	128.81	4.2083	129.77
1.6727	127.08	4.2917	130.00	1.3882	123.49	4.2917	129.81	2.3818	128.81	4.2917	129.82
1.6809	128.75	4.3750	130.00	1.4717	123.49	4.3750	129.83	2.4000	128.78	4.3750	129.86
1.6809	127.21	4.4583	130.00	1.4717	124.11	4.4583	129.85	2.5273	128.78	4.4583	129.89
1.7273	127.08	4.5417	130.00	1.4908	124.42	4.5417	129.86	2.6384	129.07	4.5417	129.92
1.7836	127.21	4.6250	130.00	1.5283	124.11	4.6250	129.87	2.7081	129.07	4.6250	129.94
1.7818	127.83	4.7083	130.00	1.5472	124.42	4.7083	129.88	2.7435	129.38	4.7083	129.95
1.8545	127.83	4.7917	130.00	1.5472	124.58	4.7917	129.89	2.8000	129.38	4.7917	129.96
1.8545	127.99	4.8750	130.00	1.5880	125.20	4.8750	129.89	2.8545	129.89	4.8750	129.97
1.8809	128.30	4.9583	130.00	1.5848	124.58	4.9583	129.89	3.1435	129.89	4.9583	129.97
1.9273	127.99	5.0417	130.00	1.6038	125.20	5.0417	130.00	3.1636	129.85	5.0417	129.99
2.0000	128.30	5.1250	130.00	1.6415	125.88	5.1250	130.00	3.5081	130.00	5.1250	129.99
2.1091	128.81	5.2083	130.00	1.6804	125.88	5.2083	130.00	3.5273	130.16	5.2083	129.99
2.1836	128.81	5.2917	130.00	1.6881	125.82	5.2917	130.00	4.2000	130.16	5.2917	129.99
2.1836	128.92	5.3750	130.00	1.7547	125.82	5.3750	130.00				
2.2545	128.92	5.4583	130.00	1.7738	128.13	5.4583	130.00				
2.3435	129.23	5.5417	130.00	1.7825	128.28	5.5417	130.00				
2.6182	129.23	5.6250	130.00	1.8113	128.13	5.6250	130.00				
2.6545	129.89	5.7083	130.00	1.8113	128.39	5.7083	130.00				
2.8182	129.89	5.7917	130.00	1.8491	128.28	5.7917	130.00				
2.8384	129.34	5.8750	130.00	1.8491	128.90	5.8750	130.00				
3.0000	129.34	5.9583	130.00	1.8879	128.30	5.9583	130.00				
3.2809	128.85	6.0417	130.00	1.8434	128.90	6.0417	130.00				
3.8727	128.85	6.1250	130.00	1.8853	127.37	6.1250	130.00				
3.8909	130.00	6.2083	130.00	2.0377	127.37	6.2083	130.00				
4.0384	130.00	10.5000	130.00	2.0377	127.88	10.5000	130.00				
		11.5000	130.00	2.1132	127.88	11.5000	130.00				
		12.5000	130.00	2.1132	127.99	12.5000	130.00				
				2.3435	128.14						
				2.3019	128.30						
				2.4151	128.81						
				2.4340	128.78						
				2.4808	128.78						
				2.5084	128.82						
				2.5880	129.07						
				2.6228	128.92						
				2.6804	129.07						
				2.7738	129.38						
				3.0377	129.38						
				3.0755	129.34						
				3.2830	129.85						
				3.3618	129.34						
				3.7170	129.85						
				3.7388	130.16						
				4.1887	130.16						

Table 2 - Raw Temperature Data for Figure 12

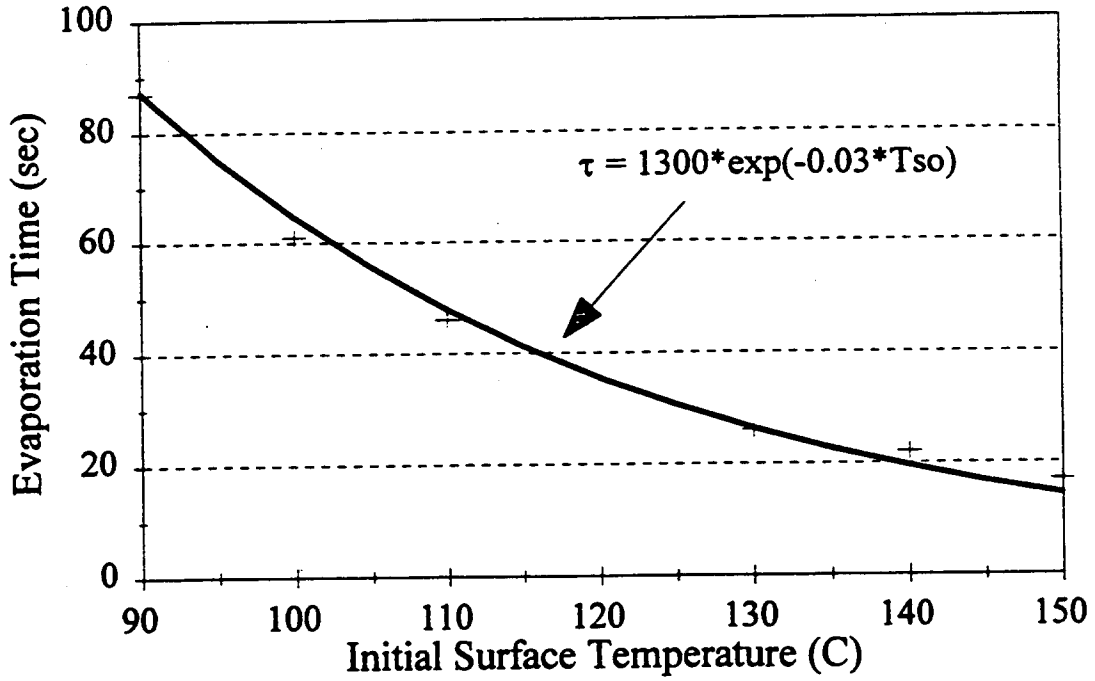


Figure 13 - Evaporation Time v. Initial Surface Temperature

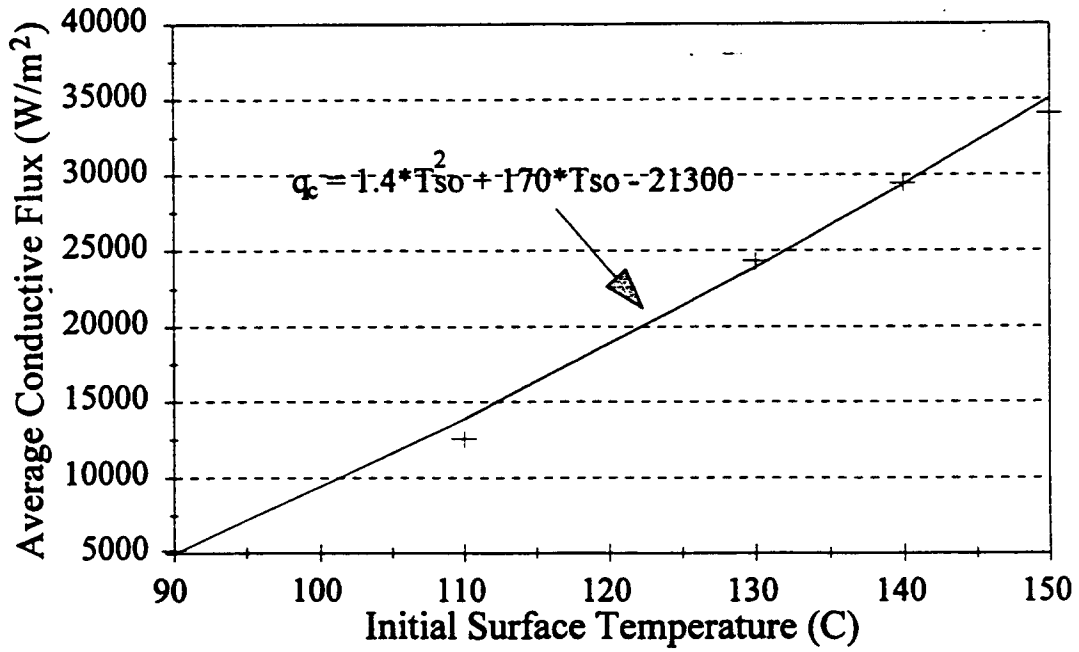


Figure 14 - Average Conductive Flux v. Initial Surface Temperature

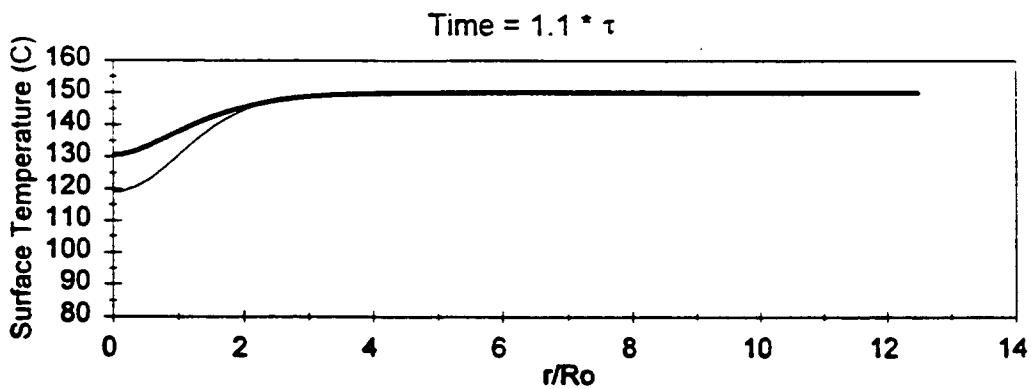
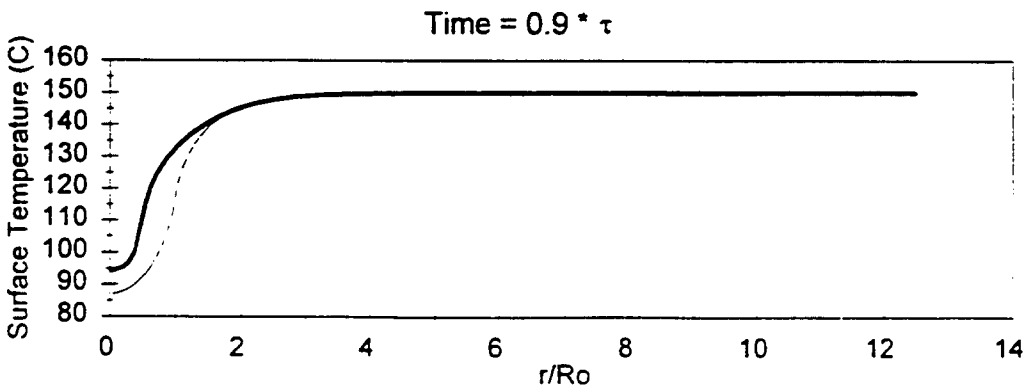
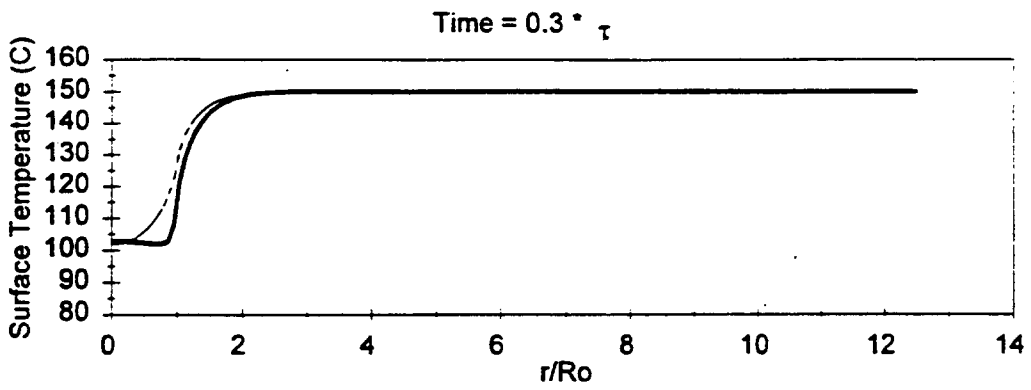


Figure 15 - Surface Temperature Distributions;
 $T_{so} = 150 \text{ } ^\circ\text{C}$

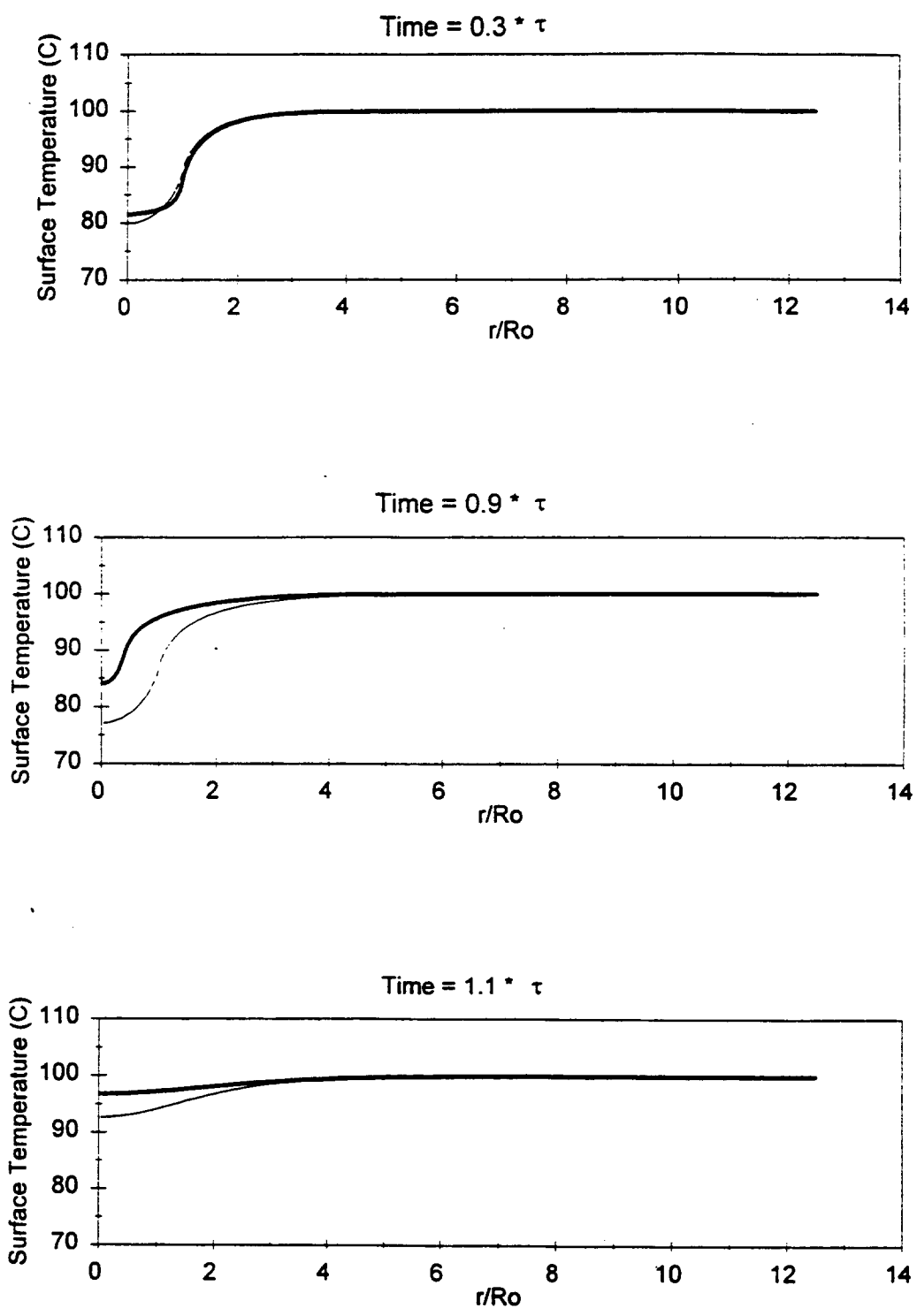


Figure 16 - Surface Temperature Distributions;
 $T_{so} = 100 \text{ }^\circ\text{C}$

r/Ro	Time = 0.3 * tau		Time = 0.9 * tau		Time = 1 * tau	
	Single Droplet Code	Closed-Form Solution	Single Droplet Code	Closed-Form Solution	Single Droplet Code	Closed-Form Solution
0.0417	102.66	101.89	94.29	87.04	130.58	118.98
0.1250	102.87	102.12	94.82	87.34	130.73	119.17
0.2083	102.85	102.52	95.50	87.89	131.02	119.56
0.2917	102.76	103.15	96.80	88.74	131.46	120.14
0.3750	102.63	104.00	99.73	89.87	132.01	120.89
0.4583	102.47	105.16	106.75	91.38	132.66	121.81
0.5417	102.29	106.61	114.85	93.23	133.38	122.87
0.6250	102.12	108.44	120.25	95.51	134.16	124.07
0.7083	102.00	110.72	124.00	98.29	134.97	125.37
0.7917	102.08	113.58	126.91	101.69	135.80	126.76
0.8750	103.00	117.31	129.32	105.99	136.63	128.22
0.9583	108.10	122.61	131.41	111.88	137.45	129.71
1.0417	120.84	131.40	133.25	121.28	138.26	131.21
1.1250	128.61	136.38	134.90	126.88	139.05	132.71
1.2083	133.70	139.63	136.39	130.77	139.81	134.18
1.2917	137.40	141.98	137.74	133.74	140.55	135.59
1.3750	140.20	143.79	138.98	136.17	141.25	136.85
1.4583	142.37	145.17	140.10	138.14	141.92	138.23
1.5417	144.07	146.25	141.12	139.60	142.56	139.43
1.6250	145.40	147.08	142.06	141.19	143.16	140.54
1.7083	146.45	147.72	142.90	142.37	143.73	141.56
1.7917	147.28	148.28	143.68	143.44	144.27	142.49
1.8750	147.92	148.64	144.38	144.28	144.77	143.33
1.9583	148.43	148.98	145.01	145.06	145.23	144.09
2.0417	148.82	149.22	145.59	145.71	145.67	144.78
2.1250	149.12	149.42	146.10	146.30	146.08	145.39
2.2083	149.35	149.57	146.57	146.80	146.45	145.93
2.2917	149.52	149.68	146.98	147.23	146.80	146.41
2.3750	149.65	149.75	147.36	147.59	147.12	146.84
2.4583	149.75	149.78	147.69	147.88	147.41	147.22
2.5417	149.82	149.84	147.98	148.18	147.68	147.56
2.6250	149.87	149.91	148.25	148.47	147.93	147.86
2.7083	149.91	149.93	148.48	148.67	148.15	148.12
2.7917	149.94	149.96	148.68	148.87	148.35	148.36
2.8750	149.96	149.96	148.86	149.01	148.54	148.56
2.9583	149.97	149.97	149.02	149.16	148.70	148.74
3.0417	149.98	150.00	149.16	149.30	148.85	148.90
3.1250	149.99	149.97	149.28	149.37	148.99	149.04
3.2083	149.99	150.00	149.39	149.48	149.11	149.17
3.2917	150.00	149.98	149.48	149.54	149.22	149.28
3.3750	150.00	150.00	149.55	149.62	149.32	149.37
3.4583	150.00	150.00	149.62	149.69	149.40	149.46
3.5417	150.00	150.04	149.68	149.77	149.48	149.53
3.6250	150.00	150.01	149.73	149.78	149.55	149.59
3.7083	150.00	150.00	149.77	149.81	149.61	149.65
3.7917	150.00	150.06	149.81	149.90	149.66	149.70
3.8750	150.00	150.00	149.84	149.86	149.71	149.74
3.9583	150.00	150.00	149.87	149.89	149.75	149.78
4.0833	150.00	150.00	149.90	149.91	149.80	149.82
4.2500	150.00	150.00	149.93	149.94	149.85	149.87
4.4167	150.00	150.01	149.95	149.97	149.89	149.91
4.5833	150.00	150.01	149.97	149.98	149.92	149.93
4.7500	150.00	150.01	149.98	149.99	149.95	149.95
4.9167	150.00	149.94	149.99	149.93	149.96	149.97
5.0833	150.00	150.02	149.99	150.01	149.97	149.98
5.2500	150.00	150.01	149.99	150.01	149.98	149.98
5.4167	150.00	150.02	150.00	150.01	149.99	149.99
5.5833	150.00	149.96	150.00	149.96	149.99	149.99
5.7500	150.00	150.00	150.00	150.00	149.99	150.00
5.9167	150.00	150.02	150.00	150.01	150.00	149.99
6.0833	150.00	149.97	150.00	149.97	150.00	149.99
6.2500	150.00	149.96	150.00	149.96	150.00	150.00
6.4167	150.00	150.00	150.00	150.00	150.00	150.00
6.5833	150.00	150.00	150.00	150.00	150.00	150.01
6.7500	150.00	149.99	150.00	149.99	150.00	150.01
6.9167	150.00	149.92	150.00	149.92	150.00	150.01
7.1667	150.00	149.92	150.00	149.92	150.00	149.99
7.5000	150.00	149.99	150.00	149.99	150.00	149.99
7.8333	150.00	149.99	150.00	149.99	150.00	150.01
8.1667	150.00	150.02	150.00	150.02	150.00	150.00
8.5000	150.00	150.02	150.00	150.02	150.00	150.00
8.8333	150.00	150.00	150.00	150.00	150.00	149.99
9.1667	150.00	149.98	150.00	149.98	150.00	150.00
9.5000	150.00	150.00	150.00	150.00	150.00	150.01
9.8333	150.00	149.98	150.00	149.98	150.00	150.00
10.5000	150.00	150.00	150.00	150.00	150.00	149.99
11.5000	150.00	149.99	150.00	149.99	150.00	150.00
12.5000	150.00	150.00	150.00	150.00	150.00	150.01

Table 3 - Raw Temperature Data for Figure 15

r/R0	Time = 0.3 * Lau		Time = 0.9 * Lau		Time = 1.1 * Lau	
	Single Droplet Code	Closed-Form Solution	Single Droplet Code	Closed-Form Solution	Single Droplet Code	Closed-Form Solution
0.0417	81.48	79.90	84.02	77.11	96.78	92.65
0.1250	81.59	80.00	84.40	77.21	96.79	92.67
0.2083	81.66	80.17	85.00	77.40	96.80	92.72
0.2917	81.76	80.44	85.14	77.68	96.82	92.79
0.3750	81.88	80.80	86.38	78.06	96.85	92.88
0.4583	82.05	81.28	90.88	78.56	96.88	92.99
0.5417	82.27	81.86	92.37	79.17	96.92	93.12
0.6250	82.55	82.58	93.36	79.93	96.97	93.27
0.7083	82.94	83.46	94.11	80.84	97.02	93.44
0.7917	83.48	84.54	94.71	81.95	97.07	93.62
0.8750	84.31	85.89	95.21	83.35	97.13	93.82
0.9583	85.85	87.75	95.64	85.25	97.20	94.02
1.0417	89.19	90.70	96.01	88.26	97.26	94.24
1.1250	91.30	92.47	96.34	90.08	97.33	94.46
1.2083	92.75	93.69	96.64	91.36	97.41	94.68
1.2917	93.85	94.64	96.91	92.36	97.48	94.91
1.3750	94.73	95.41	97.15	93.20	97.56	95.14
1.4583	95.46	96.04	97.37	93.89	97.63	95.37
1.5417	96.06	96.57	97.58	94.49	97.71	95.60
1.6250	96.57	97.02	97.77	95.00	97.79	95.83
1.7083	97.01	97.40	97.94	95.45	97.87	96.05
1.7917	97.39	97.75	98.10	95.86	97.95	96.27
1.8750	97.71	98.02	98.25	96.20	98.02	96.48
1.9583	98.00	98.28	98.38	96.52	98.10	96.68
2.0417	98.25	98.49	98.51	96.81	98.18	96.88
2.1250	98.47	98.69	98.63	97.07	98.25	97.06
2.2083	98.66	98.85	98.74	97.31	98.33	97.24
2.2917	98.83	99.00	98.84	97.52	98.40	97.41
2.3750	98.97	99.12	98.93	97.71	98.47	97.58
2.4583	99.10	99.22	99.02	97.87	98.54	97.73
2.5417	99.22	99.33	99.10	98.04	98.60	97.88
2.6250	99.32	99.42	99.18	98.20	98.67	98.01
2.7083	99.41	99.50	99.25	98.33	98.73	98.14
2.7917	99.48	99.57	99.31	98.46	98.79	98.26
2.8750	99.55	99.62	99.37	98.57	98.85	98.38
2.9583	99.61	99.67	99.43	98.68	98.91	98.49
3.0417	99.66	99.72	99.48	98.79	98.96	98.59
3.1250	99.71	99.75	99.52	98.87	99.02	98.68
3.2083	99.75	99.79	99.57	98.96	99.07	98.77
3.2917	99.78	99.81	99.61	99.03	99.12	98.85
3.3750	99.81	99.84	99.64	99.11	99.16	98.93
3.4583	99.84	99.87	99.68	99.18	99.21	99.00
3.5417	99.86	99.90	99.71	99.25	99.25	99.07
3.6250	99.88	99.91	99.74	99.30	99.29	99.13
3.7083	99.90	99.92	99.76	99.35	99.33	99.19
3.7917	99.92	99.95	99.78	99.42	99.37	99.25
3.8750	99.93	99.94	99.81	99.44	99.41	99.30
3.9583	99.94	99.95	99.83	99.48	99.44	99.34
4.0833	99.95	99.96	99.85	99.54	99.49	99.41
4.2500	99.97	99.97	99.88	99.61	99.55	99.49
4.4167	99.98	99.98	99.91	99.67	99.60	99.56
4.5833	99.98	99.99	99.93	99.72	99.65	99.62
4.7500	99.99	99.99	99.94	99.76	99.69	99.67
4.9167	99.99	99.99	99.95	99.78	99.73	99.71
5.0833	99.99	100.00	99.96	99.84	99.77	99.75
5.2500	100.00	100.00	99.97	99.86	99.80	99.79
5.4167	100.00	100.00	99.98	99.88	99.82	99.82
5.5833	100.00	99.99	99.98	99.89	99.85	99.84
5.7500	100.00	100.00	99.99	99.92	99.87	99.87
5.9167	100.00	100.00	99.99	99.93	99.89	99.89
6.0833	100.00	99.99	99.99	99.93	99.90	99.90
6.2500	100.00	99.99	100.00	99.94	99.92	99.92
6.4167	100.00	100.00	100.00	99.96	99.93	99.93
6.5833	100.00	100.00	100.00	99.97	99.94	99.94
6.7500	100.00	100.00	100.00	99.97	99.95	99.95
6.9167	100.00	99.98	100.00	99.95	99.96	99.96
7.1667	100.00	99.97	100.00	99.96	99.97	99.97
7.5000	100.00	100.00	100.00	99.99	99.98	99.98
7.8333	100.00	100.00	100.00	99.99	99.98	99.98
8.1667	100.00	100.00	100.00	100.00	99.99	99.99
8.5000	100.00	100.01	100.00	100.00	99.99	99.99
8.8333	100.00	100.00	100.00	100.00	99.99	99.99
9.1667	100.00	99.99	100.00	99.99	100.00	100.00
9.5000	100.00	100.00	100.00	100.00	100.00	100.00
9.8333	100.00	99.99	100.00	99.99	100.00	100.00
10.5000	100.00	100.00	100.00	100.00	100.00	100.00
11.5000	100.00	100.00	100.00	100.00	100.00	100.00
12.5000	100.00	100.00	100.00	100.00	100.00	100.00

Table 4 - Raw Temperature Data for Figure 16

5. EFFECTS OF DISSOLVED GASES ON THE SPARSE SPRAY COOLING OF SURFACES

An experimental study performed previously examined the evaporative cooling of a radiantly heated, low thermal conductivity material subjected to a sparse spray of deionized and degassed water [9]. The transient behavior of the surface with respect to the average temperature and the spatial surface temperature distribution was quantified and is used in Chapter 6 to validate the sparse spray model results. The experimental work is extended here to include the effects of dissolved gases in the water on the transient thermal behavior of the surface.

5.1 Description of the Experiment

The experimental setup and procedures basically follow those described in more detail by Dawson and diMarzo [9]. A brief description of the experimental setup and procedures is provided here.

5.1.1 Experimental Setup

The schematic of the experimental setup is shown in Figure 9 of Chapter 4. The setup consists of a ceramic macor tile that is heated by three conical radiant panels from above and maintained at a constant temperature below by means of a chill plate. Two of the radiant panels are the same size and mounted above the macor surface at angles of 30° from the vertical on either side. The third panel is larger in diameter and shallower in depth and surrounds the perimeter of the tile. The temperature of the panels are controlled by an Omega CN-7100 digital process

controller and can achieve a maximum temperature of 800 °C.

A droplet dispenser, shown in detail in Figure 17, hangs above the surface and, together with a set of solenoidal-controlled bumpers, provides a random spray of water to the surface. The dispenser was designed and tested previously [15]. The dispenser consists of a tapered, conical, aluminum body with a bored out center. The cavity exits through a hole at the bottom of the main body. This cavity is filled with water and sealed at the top with a plastic diaphragm and o-ring. A size 20 IV needle screws into the hole at the bottom of the cavity. A steel piston rests on top of the diaphragm while a solenoid-spacer mechanism is fitted to the top of the piston. The spacer provides a gap, which can be adjusted by a small screw, between the solenoid core and solenoid body. When the solenoid is energized, it pushes down on the spacer, closing the gap and causing the piston to deflect the diaphragm and thus produce a droplet from the needle. The size of the droplet is controlled by adjustment of the gap and the frequency of droplet deposition is controlled by the solenoid.

The cavity in the dispenser is kept filled by a feedwater line which, at one end, fits into a small inlet located just below the diaphragm. The other end connects to a reservoir of water that produces a static head of almost zero. The height of this reservoir is adjusted throughout the experiment to maintain the near zero static head.

An infrared camera looks through a chill pipe that ends just above the macor tile. The chill pipe is painted black on the inside and serves as a means of absorbing

any stray reflections from surrounding objects. The infrared camera can then focus on the surface of interest and record its thermal variations.

5.1.2 Experimental Procedure

A series of experiments were run for various initial surface temperatures ranging from approximately 110 °C to 180 °C. At each initial surface temperature in an experimental session, three mass fluxes of the gassed water impinging on the surface were tested. The initial surface temperature and mass fluxes were selected to closely match those from Dawson's experiments with degassed water. The procedure that was followed for each experimental session is outlined below.

- (1) The macor surface is cleaned with ethyl alcohol and a soft cloth, lightly rinsed with distilled water, and allowed to dry.
- (2) The radiant heaters are turned on and allowed to heat up for approximately two hours.
- (3) The infrared camera is turned on, also two hours prior to experimentation.
- (4) The reservoir is filled with distilled water and adjusted to create a zero static head so that no water flows from the IV needle.
- (5) The droplet generator is turned on and allowed 10 - 15 minutes to stabilize. Once stabilized, 50 droplets are collected in a beaker which is quickly capped to avoid evaporation. The beaker and drops are weighed and the volume of a single droplet is determined.
- (6) Once the droplet size is adjusted and determined, the frequency of the solenoid motion is set to the desired mass flux. The mass flux is given by

$$G = \frac{\rho V f}{A_w} \quad (13)$$

where ρ is the density of water, V is the droplet volume, f is the frequency of droplet impingement, and A_w is the droplet impingement area determined by Dawson to be 0.0033 m^2 .

- (7) Once the surface temperature has reached the desired, steady value (as indicated by an Omega thermocouple probe), the droplet dispenser is set in motion with the solenoidal bumpers and allowed to stabilize.
- (8) After the above procedures are completed, experiments begin. Droplets are allowed to fall for about twenty-five minutes. Each run is recorded by the infrared camera onto 8 mm videotapes from which the data is later processed.

5.1.3 Data Acquisition and Reduction

The transient thermal behavior of the surface is captured using infrared thermographic techniques that were developed and implemented previously by Klassen [6]. An Inframetrics Model 525 infrared camera detects radiation wavelengths from 8 microns to 12 microns and translates thermal variations of an object into a real time gray image. These images are made up of dark shades that represent cool regions and light shades that represent hot regions. The camera records the thermal image of the surface onto 8 mm videotape for future processing and convenient storage.

The means of reducing the stored data was developed and used by Dawson [9] for his multi-droplet evaporative cooling experiments. A Matrox MVP-AT frame grabber board is installed in an IBM PC-AT and used to digitize single frames of the filmed images. Once digitized, each frame can be analyzed pixel by pixel using Imager-AT software. Each frame is calibrated using a temperature versus intensity relationship so that shades of gray may be translated into corresponding temperatures.

For the purposes of the multi-droplet evaporative cooling experiments, the infrared camera records a region of the macor surface of approximately 0.075 m x 0.055 m. The pixels contained in this viewing area are 512 by 480 in the horizontal and vertical direction, respectively. Thus, the average spatial resolution is 0.00013 meters per pixel. There are 130 shades of gray to represent an average temperature range of 100 °C. The temperature resolution is, therefore, calculated as 0.77 °C / gray shade.

5.2 Results

The results of both the dissolved gases and degassed experiments are presented and compared in Figures 19 through 32 and in Tables 6 through 12. The transient thermal behavior of the surface is represented in the form of average surface temperature versus time plots and in the form of surface temperature contour plots.

5.2.1 Transient Average Surface Temperature

Figures 19 through 23 contain plots of transient average surface temperatures. These plots were made using the computer program, PIXAV [9]. PIXAV is used to average across 3717 pixel values contained in an area of 0.046 m x 0.034 m and provide the corresponding average temperature. The average surface temperature is obtained in this way at 30-second intervals throughout an experimental recording.

Seven experiments are compared. These experiments consist of initial surface temperatures of 111 °C , 131 °C, 151 °C, 162 °C, and 182 °C. The lowest three temperatures correspond to evaporative cooling, while the highest two temperatures

correspond to the onset of nucleate boiling and full nucleate boiling, respectively. At least one mass flux is compared at each initial surface temperature with an additional mass flux for initial temperatures of 151 °C and 162 °C.

Each plot contains both raw data points from the dissolved gases and degassed experiments and a best fit line corresponding to each set of raw data. The general trend apparent in each plot is the decay of the average surface temperature from its initial value to some steady state value. The deviation of the data points from a smooth decay occurs due to the nature of the data acquisition. Because only a portion of the sprayed area is viewed and averaged, at any instant the number of droplets that can be seen may be different than at other instants thus resulting in fluctuations of the average surface temperature.

The method used to determine the best fit curve to the data is the same method used by Dawson [9]. An equation of the following form is used as a curve fit to the temperature data

$$T = (T_0 - T_{ss}) e^{-\frac{t}{\tau}} + T_{ss} \quad (14)$$

This equation is basically a decaying exponential with T_0 = initial surface temperature, T_{ss} = steady state surface temperature, and τ = time constant. The steady state temperature and time constant are adjusted so that an equal number of data points fall above and below the curve.

Dawson suggests that the time constant is a function of the material as opposed to a function of mass flux [9]. Table 5 lists the time constants corresponding to the

various initial surface temperatures and mass fluxes for both sets of experiments. The time constants listed are fairly constant ranging from 126 to 270 seconds, where the average value is 186 seconds with a standard deviation of 11.5 seconds. The unchanging time constant supports Dawson's conclusion of the material dependence of this parameter.

Table 5 - Time Constants for Sparse Spray Cooling Experiments
 (* indicates dissolved gases experiments)

T_0 (°C)	G (g/m ² -s)	τ (min)
111	* 0.21 0.24	* 4.20 4.50
131	* 0.57 0.50	* 2.50 3.33
151	* 0.96 0.96	* 2.90 2.90
151	* 1.30 1.30	* 2.70 2.80
162	* 0.97 0.97	* 2.50 2.50
162	* 1.50 1.50	* 4.00 4.00
182	* 1.60 1.60	* 2.40 2.10

Using the limiting values found for the time constant, the penetration depth, l , of the solid can be found from

$$l = \sqrt{\alpha_s \tau} \quad (15)$$

where, α_s is the thermal diffusivity and has a value of $5.79 * 10^{-7} \text{ m}^2/\text{s}$ for macor. The penetration depth is then calculated to be between 0.85 and 1.25 cm. The radius of influence of the droplet on the solid surface is a circular region with a radius of 3.5 to 5 times the deposited droplet's radius [16]. For a 9 microliter droplet with a shape factor of 2.3, which are the conditions used for the single droplet validation, the radius of influence is approximately 1.05 cm to 1.5 cm. These values are of the same order of magnitude as the range above and, again, indicate that the time constant is a function of the solid material.

Overall, the plots indicate that dissolved gases in the water do not affect the cooling of the surface. This is indicated by the temperature correlations to the best fit curves. For comparable initial surface temperatures and mass fluxes, the best fit equations to the data are similar in all cases. In light of the relative independence of the time constant discussed previously, the steady state temperature becomes the parameter of interest for comparison purposes. The average difference in steady state temperatures for the cases presented is 3.4 °C. The largest difference is 8 °C and is found at initial surface temperatures of 111 °C and 131 °C. Part of this difference may be explained by the difference in mass flux used for the dissolved gases experiment, thereby altering the steady state temperature. Additionally, the droplet distribution may not be the same in both experiments and therefore calculating an average surface temperature over only a portion of the entire surface could bias the results.

5.2.2 Surface Temperature Contours

Spatial surface temperature results of the dissolved gases and degassed experiments can be found in Figures 24 through 32. These results are in the form of surface temperature contour plots.

Three of the cases that are contained in Figures 24 through 32 are shown in order to convey the overall qualitative behavior of the surface. The cases shown are for initial surface temperatures of 111 °C, 151 °C, and 162 °C with mass fluxes of approximately 0.2 g/m²s, 0.96 g/m²s, and 0.97 g/m²s, respectively.

Each figure contains two contour plots that correspond to the dissolved gases and degassed experiments. Three different times during an experimental run are selected. The times are chosen to show 1) a very early time in the transient when the surface temperature is close to its initial value, 2) a time fairly far into the transient, but before steady state has been reached, and 3) a time after steady state has been reached.

The contour plots for both the dissolved gases and degassed experimental results contain some features that are similar. Both sets of results show very distinct locations where droplets are evaporating on the surface, or have just evaporated from the surface. These places are marked by concentric contours that increase in temperature as the outer contour is approached. Places where droplets have recently evaporated will still have concentric contours but the inner contour will be associated with a temperature higher than that of evaporating droplets. At a given time, roughly the same number of droplet locations can be seen on each contour plot. There may be

slightly more or less drops shown due to the fact that some of the droplets fall outside of the area showed by the contour plots. Another similarity between the contour plots for experiments is the way in which the plots progress with time. At later times, the effects on the surface temperature due to individual droplets tend to merge. While at earlier times, temperature effects are contained within a local region around the droplet. Lower temperature contours are found near the perimeter of the plot at later times than those found at early times, indicating that the entire surface is cooling. By a time of 600 seconds, the average surface temperature, which is labelled at the top of each plot, has approached the steady state temperature.

Alternatively, there are features of the contour plots that distinguish the behavior of the water containing dissolved gases from the behavior of the degassed water. The most noticeable difference between the two sets of results is the size of the concentric contours surrounding a droplet. Experimental results using water with dissolved gases show contours that are larger in the region surrounding a droplet than those corresponding to degassed water experimental results. Furthermore, the temperature gradients surrounding the water droplets containing dissolved gases are also larger. Large temperature gradients are illustrated by the proximity of two concentric contours.

The explanation for these differences stems from the make up of the two types of water droplets. Figure 18 depicts a general concept of the two types of water droplets and the behavior of the conductive heat flux associated with them. Note that no study was performed on the actual make up and behavior of a single droplet,

rather Figure 18 represents what the author believes to be occurring. The larger contours associated with a droplet of water containing dissolved gases can be attributed to the spreading of the droplet on the surface due to the gases. For droplets of equivalent mass, a droplet containing dissolved gases requires more area on the surface due to the relatively larger volume taken up by the gas. Consequently, the dissolved gases push the liquid outward. Higher temperature gradients are also explained by the presence of the gases. In locations where gas bubbles exist, a degradation in heat flux through the droplet occurs. Significantly larger heat fluxes are therefore found at the droplet's edge. These large heat fluxes cause high temperature gradients at the edge of the droplet. In contrast, the heat flux through a degassed water droplet is fairly constant with a smaller increase at the edge. Most likely, overall surface temperatures do not differ significantly for the two experiments because the average heat fluxes associated with the droplets are similar.

5.4 Summary

Transient average surface temperatures and surface temperature contours were compared for water containing dissolved gases and degassed water. The results showed that there is no significant effect on the cooling of the surface when using water containing dissolved gases as opposed to degassed water. The characteristics of surface temperature contours differ for the two types of water. The spreading of the droplet on the surface and the high temperature gradients at the droplet's edge result from the dissolved gases in the water and are portrayed in the contour plots.

The work presented in this chapter does not represent an in depth study of the evaporative behavior of water containing dissolved gases, but rather represents a general comparison of the spray cooling of surfaces using water containing dissolved gases against degassed water. In the next chapter a model for sparse spray cooling is presented and is based on degassed water.

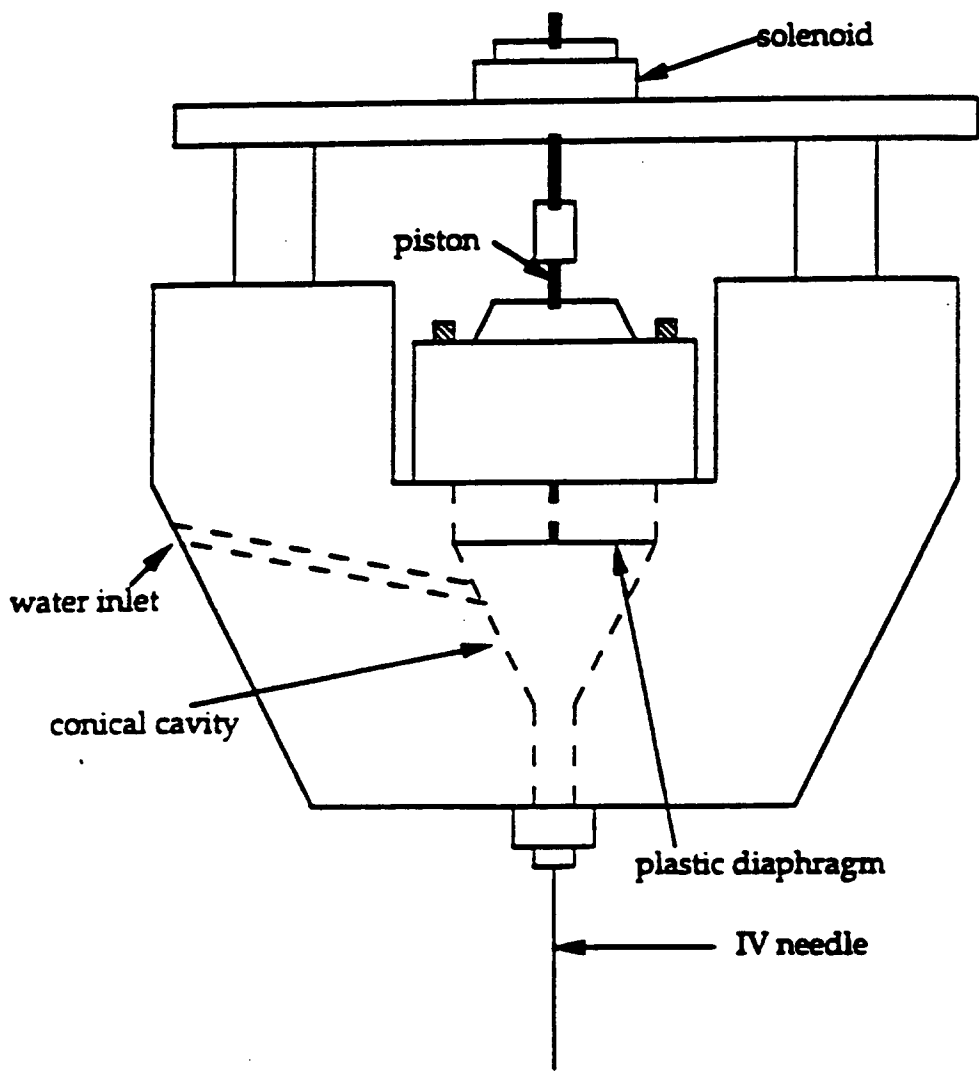


Figure 17 - Droplet Dispenser

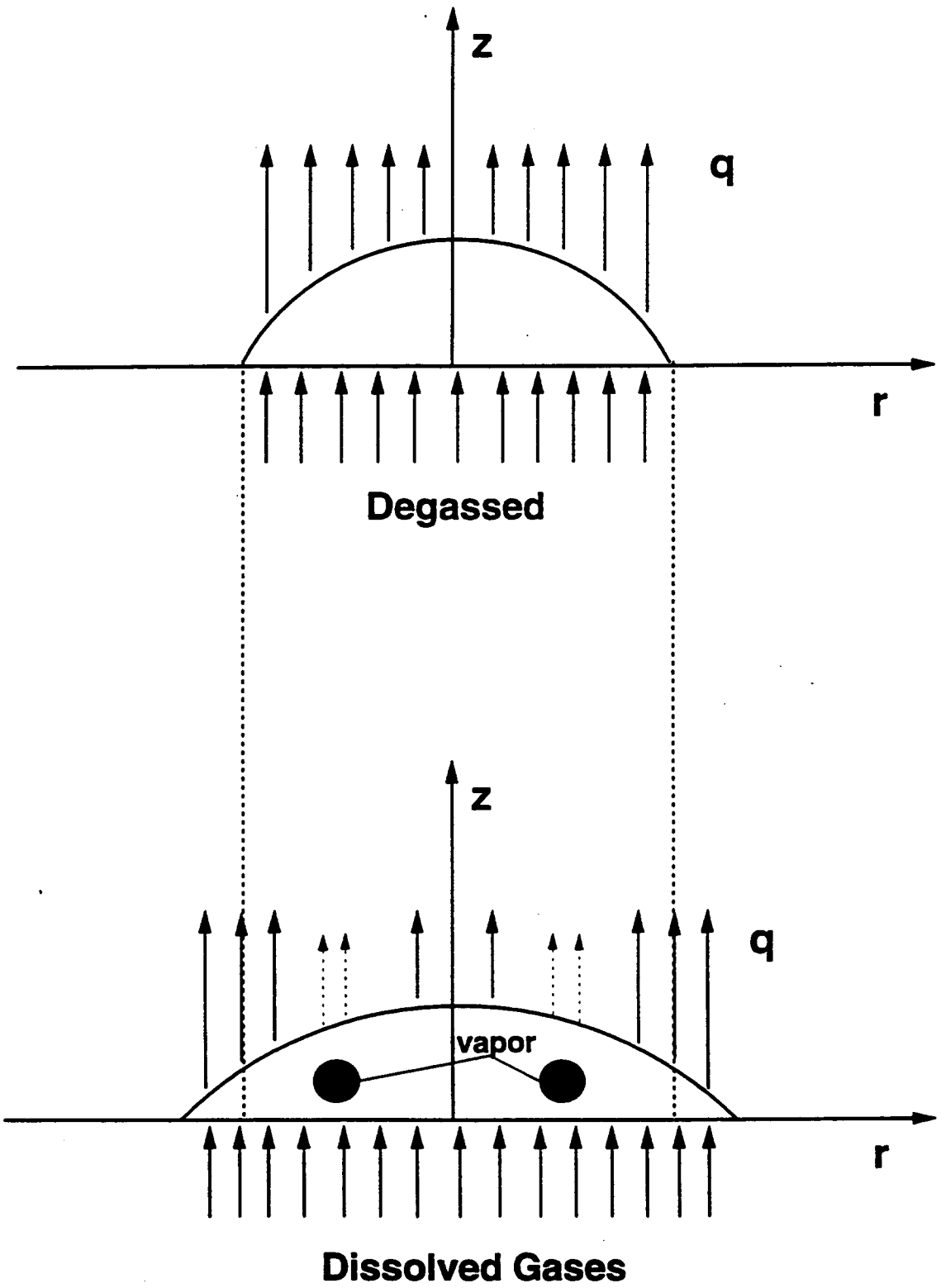


Figure 18 - Comparison of Water Droplets

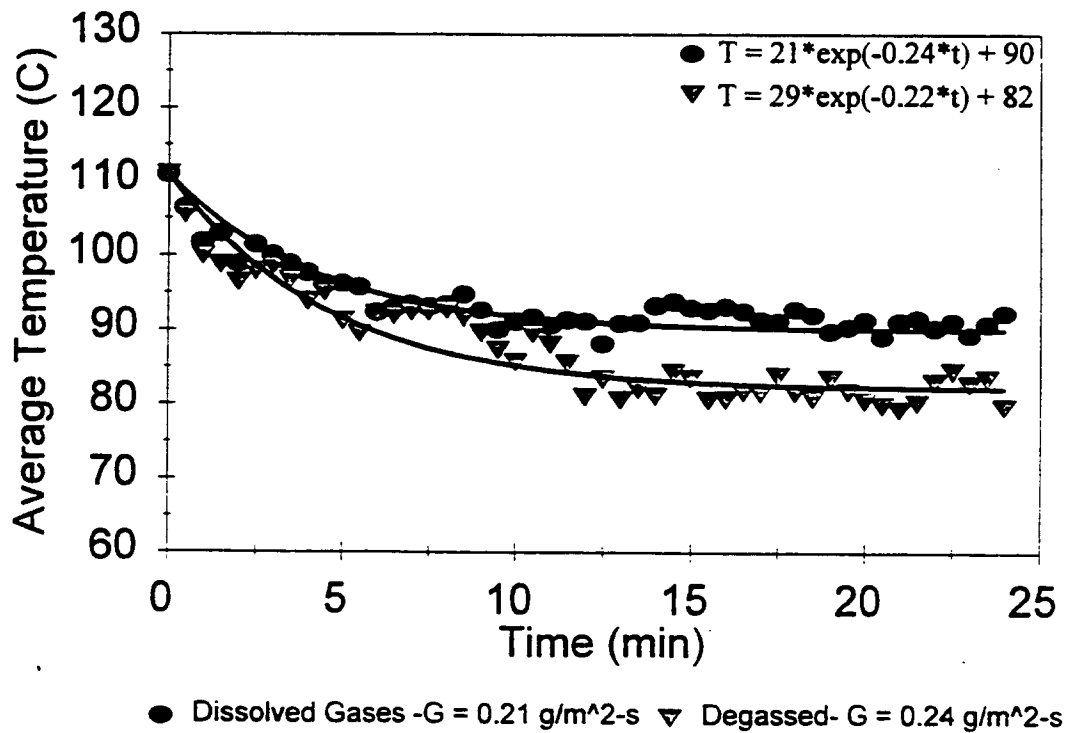


Figure 19 - Transient Temperature Plot: $T_{so} = 111 \text{ }^\circ\text{C}$

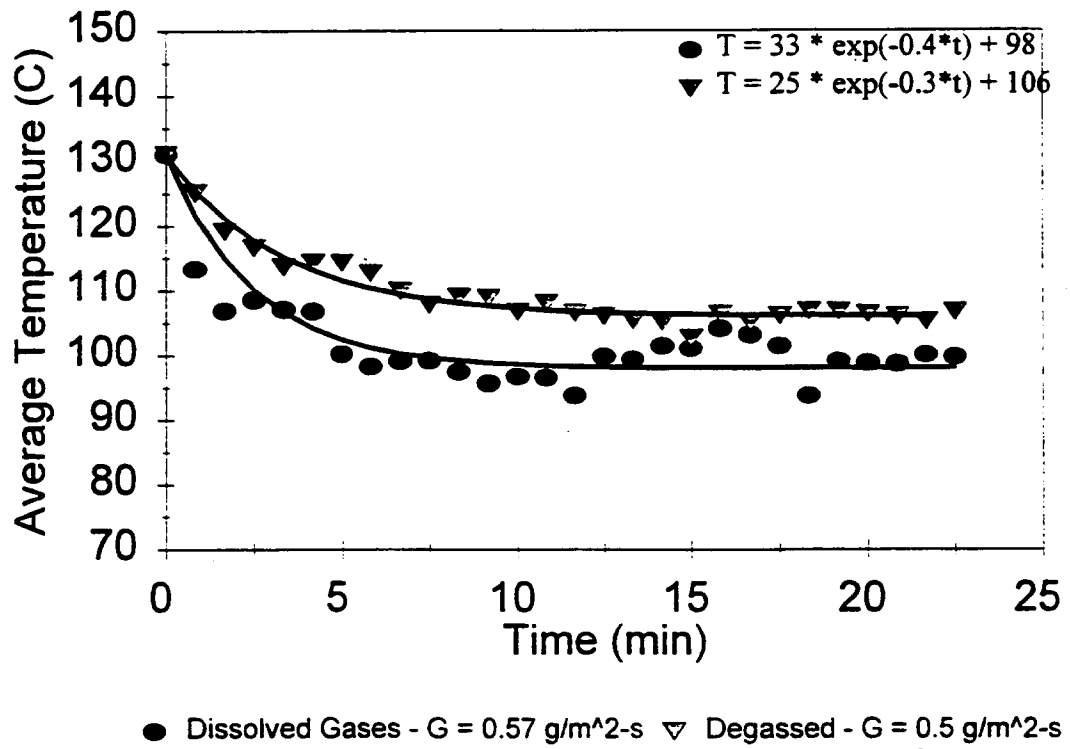


Figure 20 - Transient Temperature Plot: $T_{\infty} = 131 \text{ }^{\circ}\text{C}$

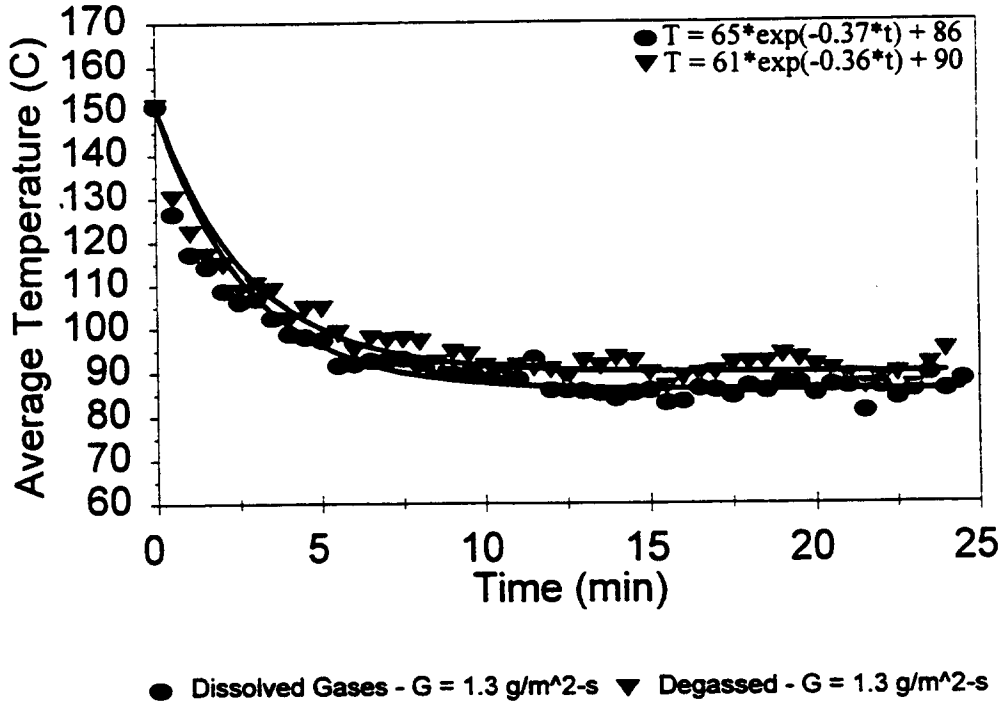
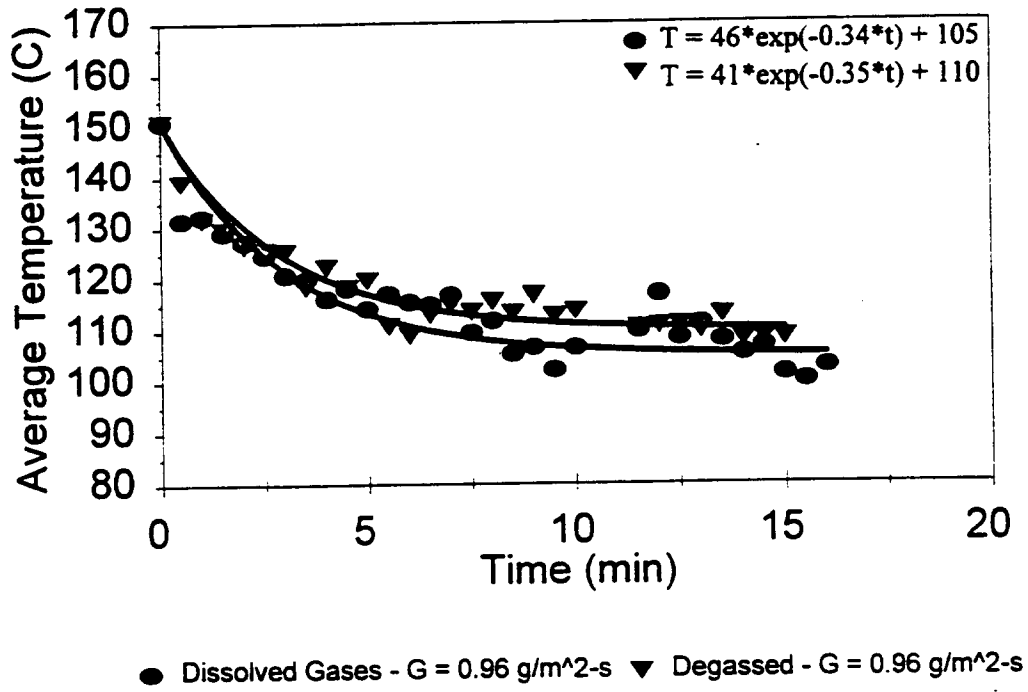


Figure 21 - Transient Temperature Plot: $T_{so} = 151 \text{ }^\circ\text{C}$

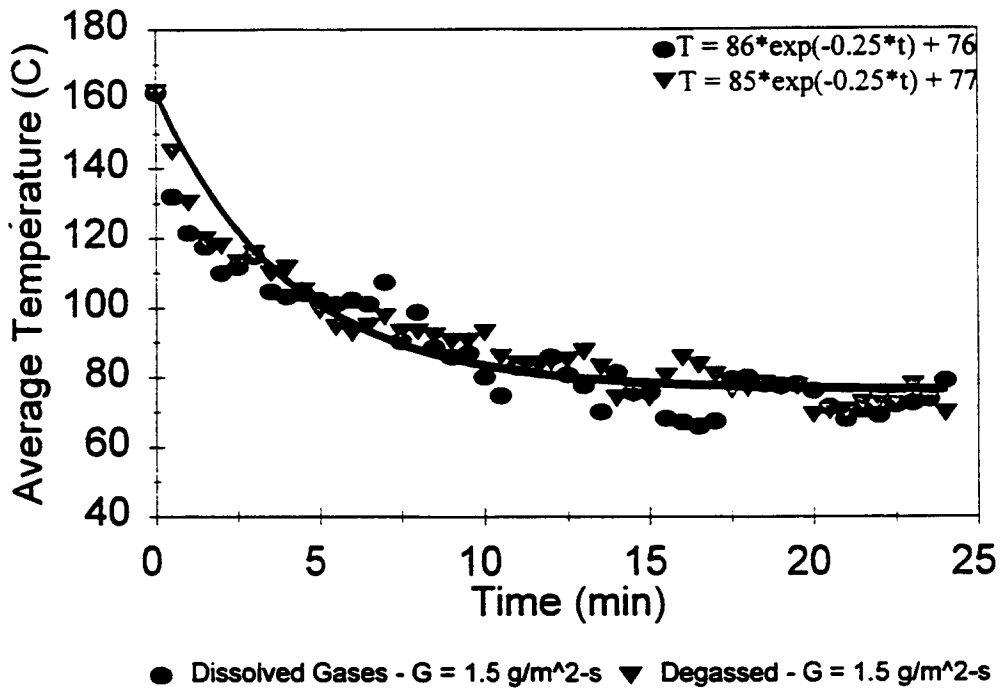
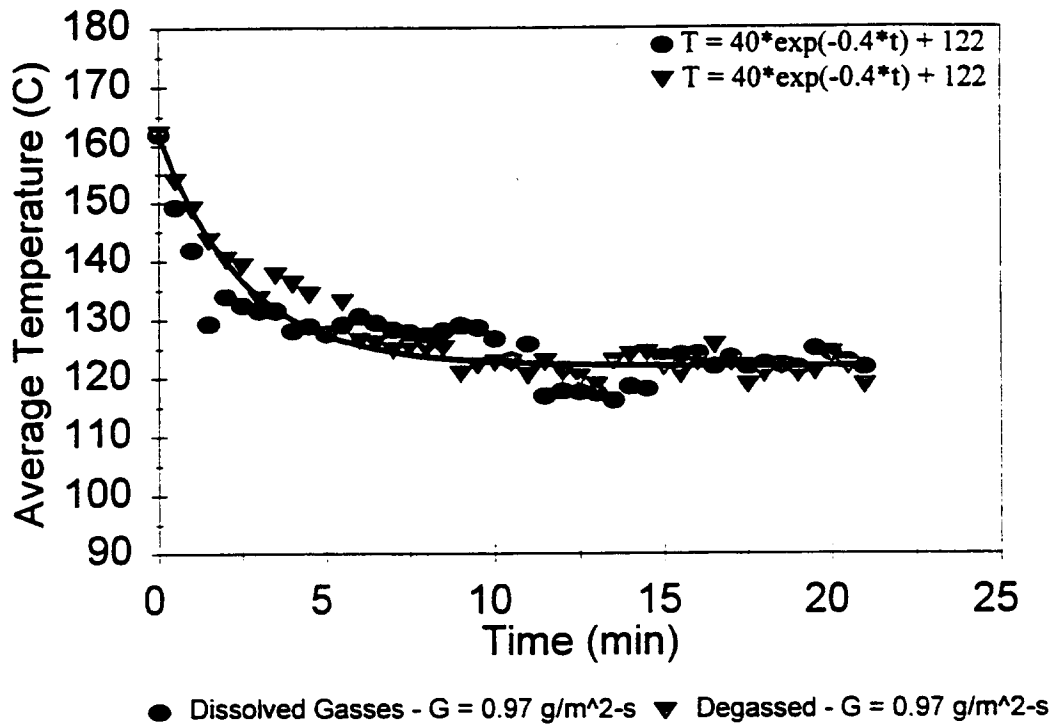


Figure 22 - Transient Temperature Plot: $T_{so} = 162 \text{ }^\circ\text{C}$

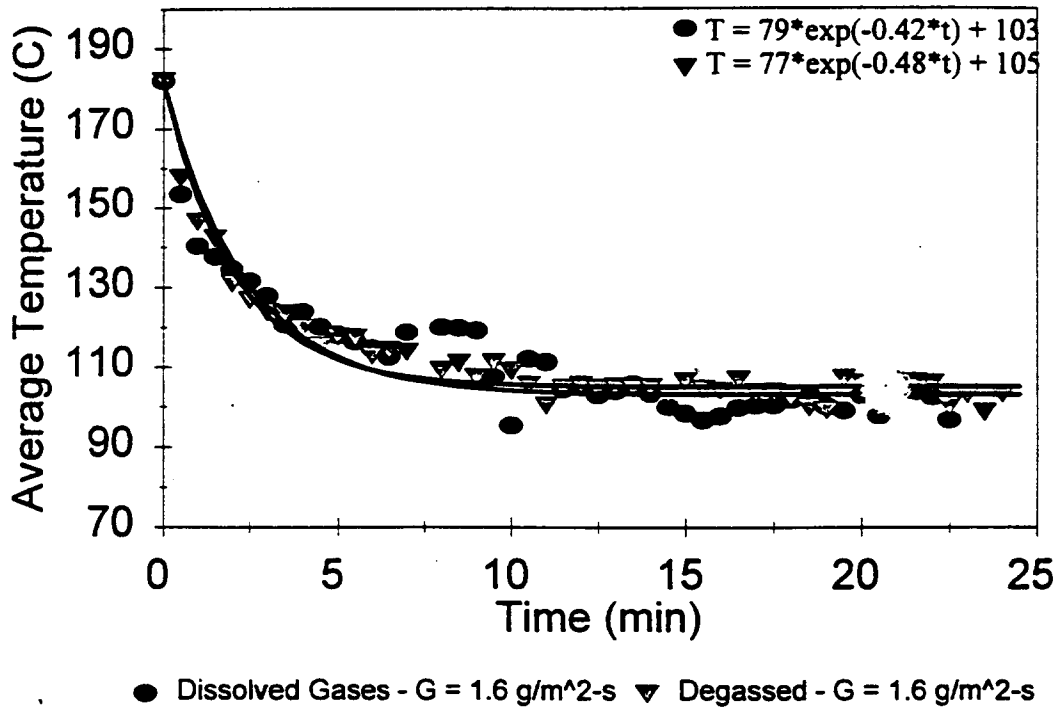


Figure 23 - Transient Temperature Plot: $T_{so} = 182 \text{ }^\circ\text{C}$

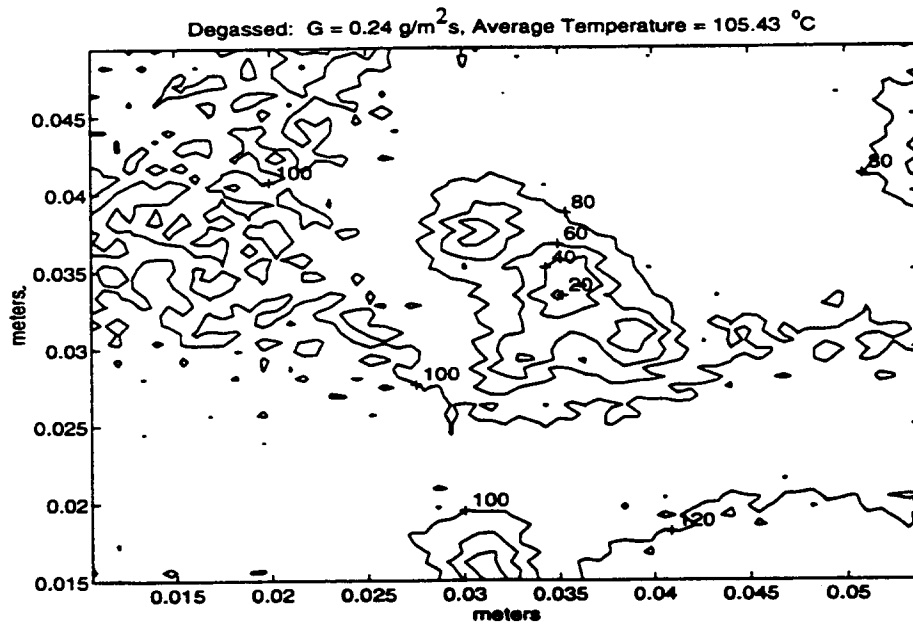
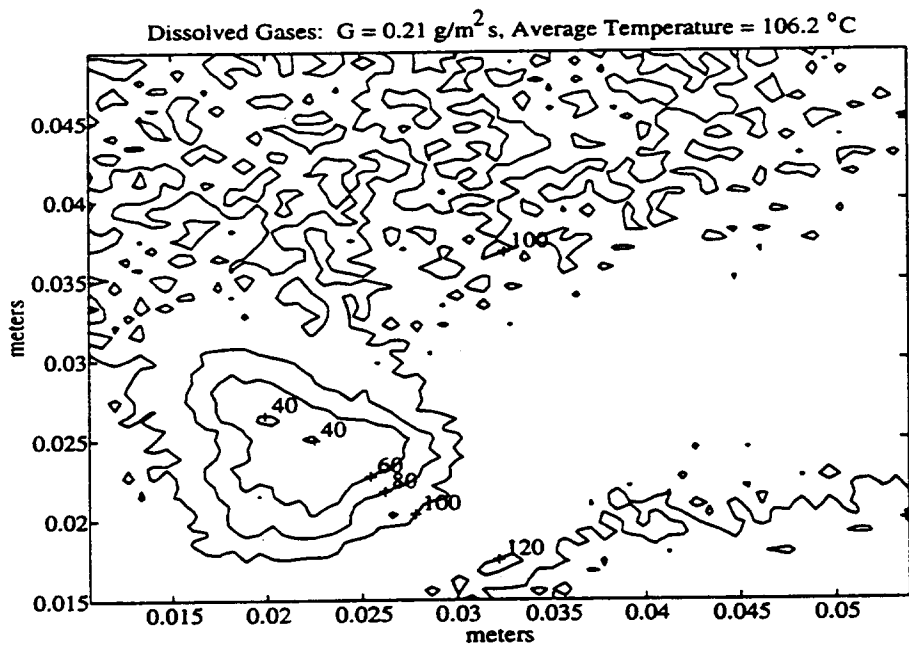


Figure 24 - Contour Plot: $T_{so} = 111 \text{ }^\circ\text{C}$, Time = 30 seconds

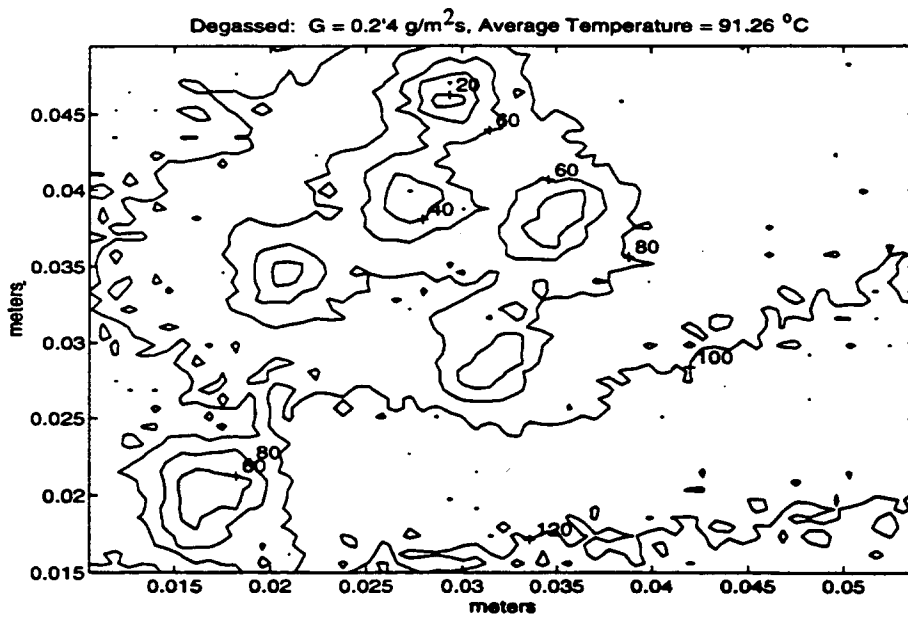
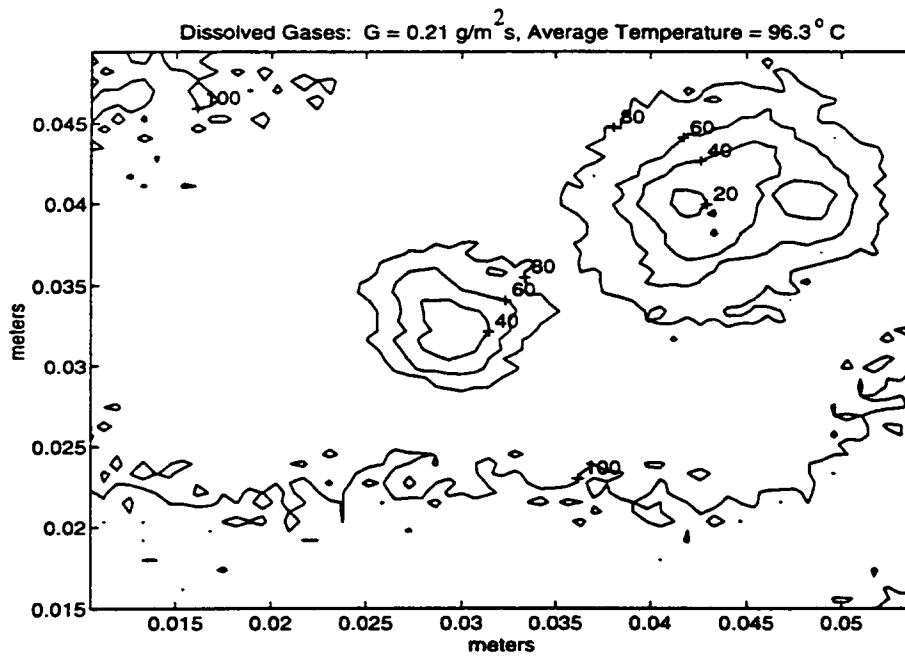


Figure 25 - Contour Plot: $T_{so} = 111^\circ \text{C}$, Time = 300 seconds

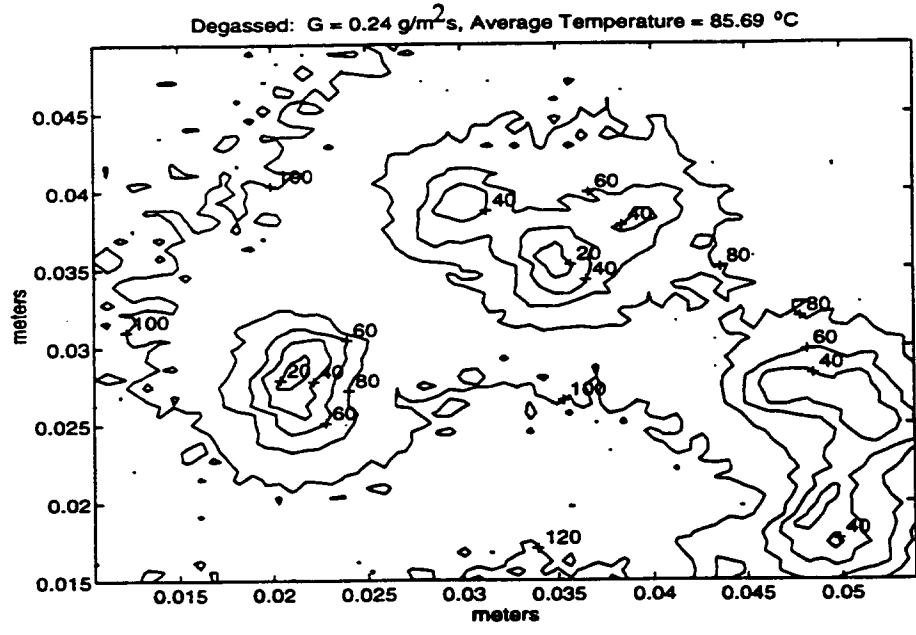
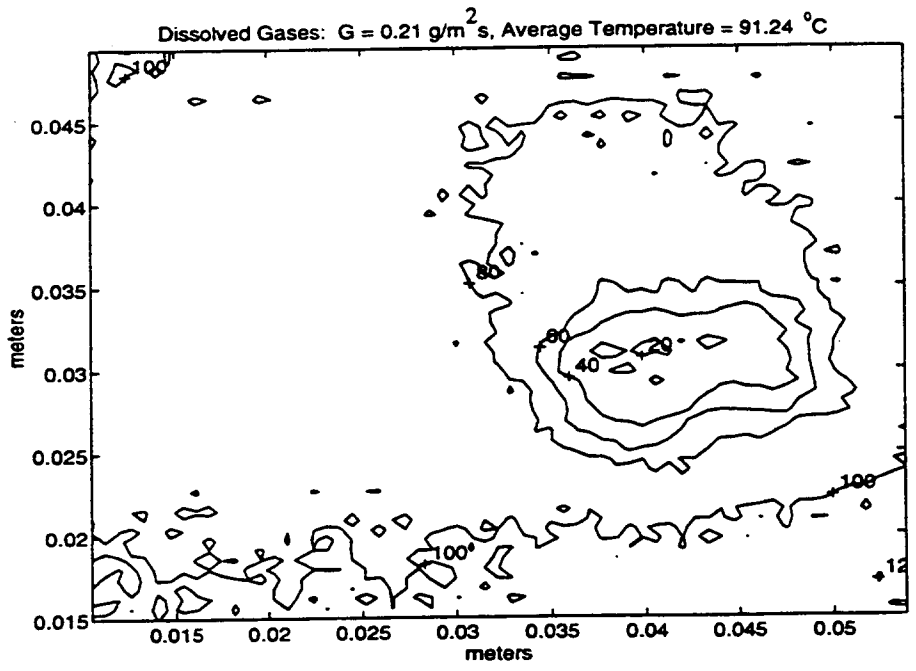


Figure 26 - Contour Plot: $T_{so} = 111 \text{ }^\circ\text{C}$, Time = 600 seconds

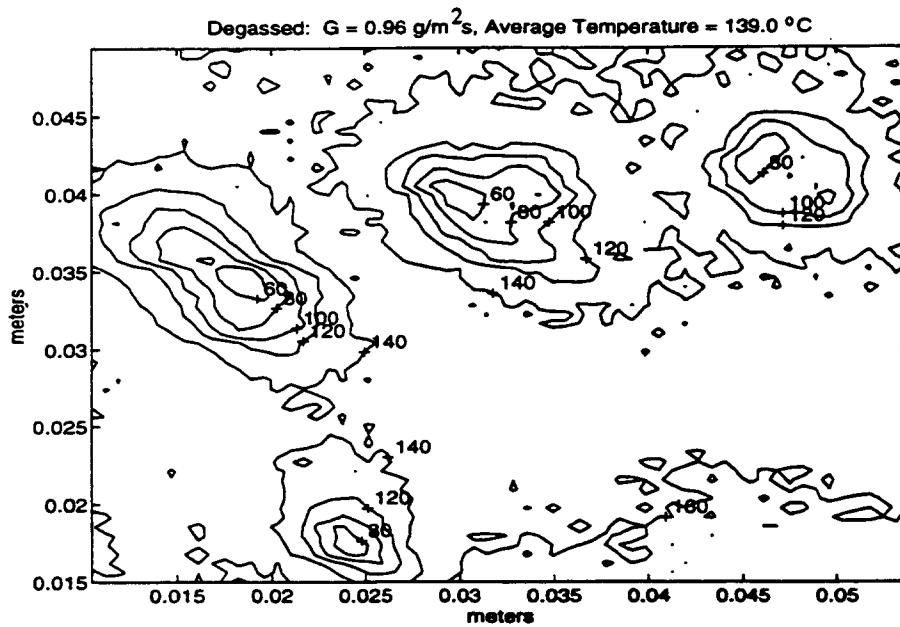
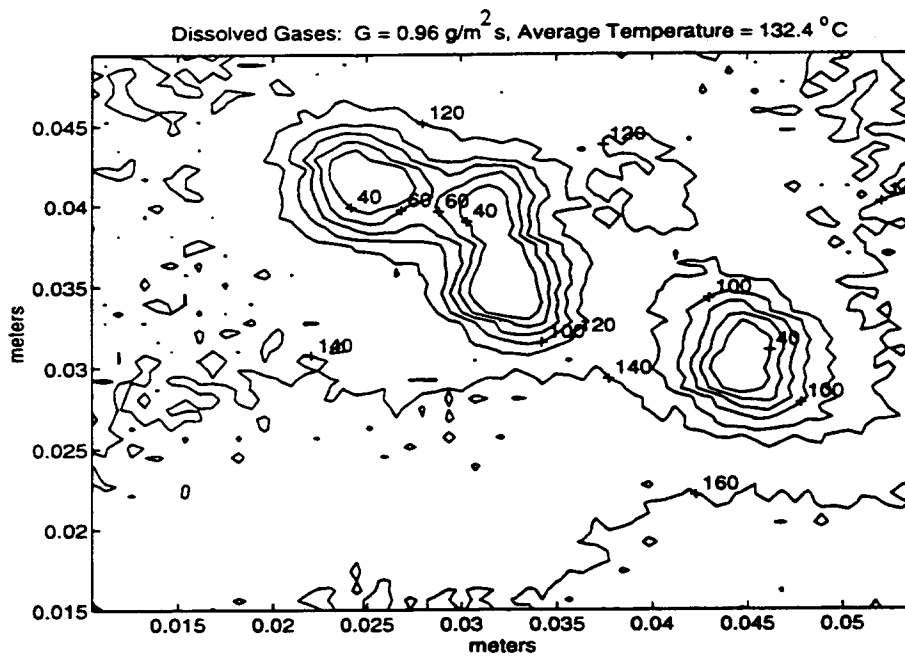


Figure 27 - Contour Plot: $T_{so} = 151 \text{ }^\circ\text{C}$, Time = 30 seconds

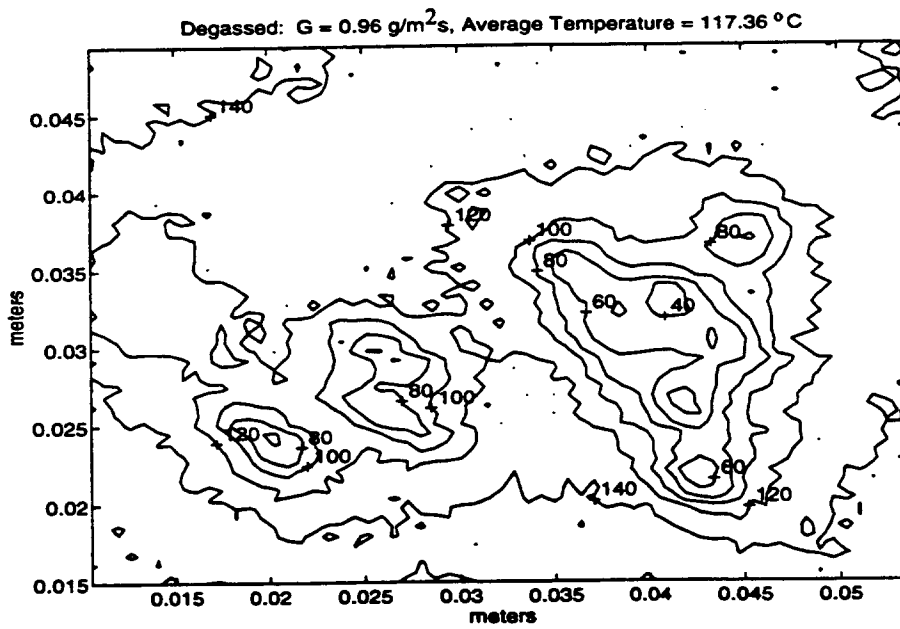
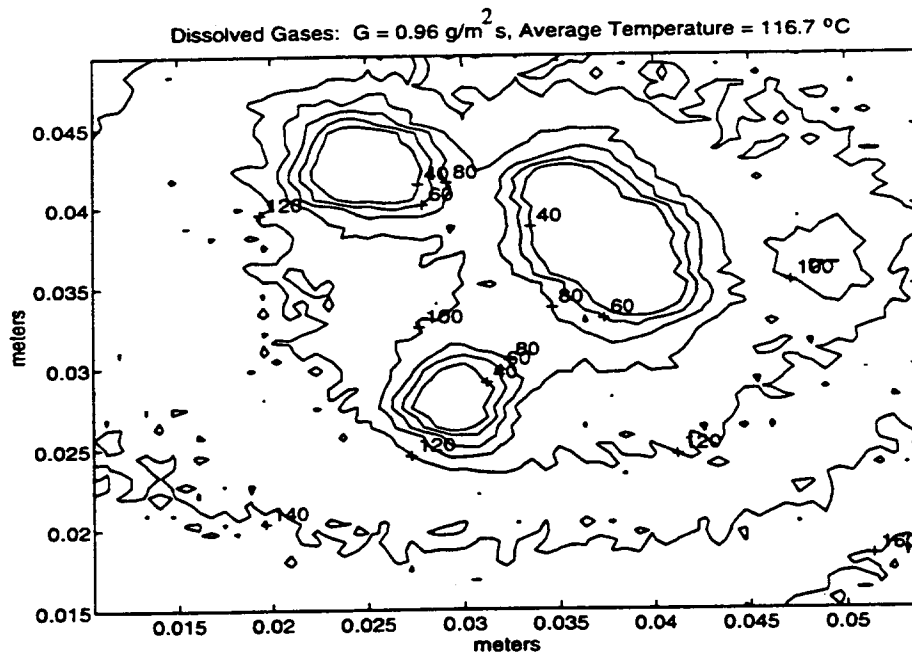


Figure 28 - Contour Plot: $T_{s0} = 151 \text{ }^\circ\text{C}$, Time = 300 seconds

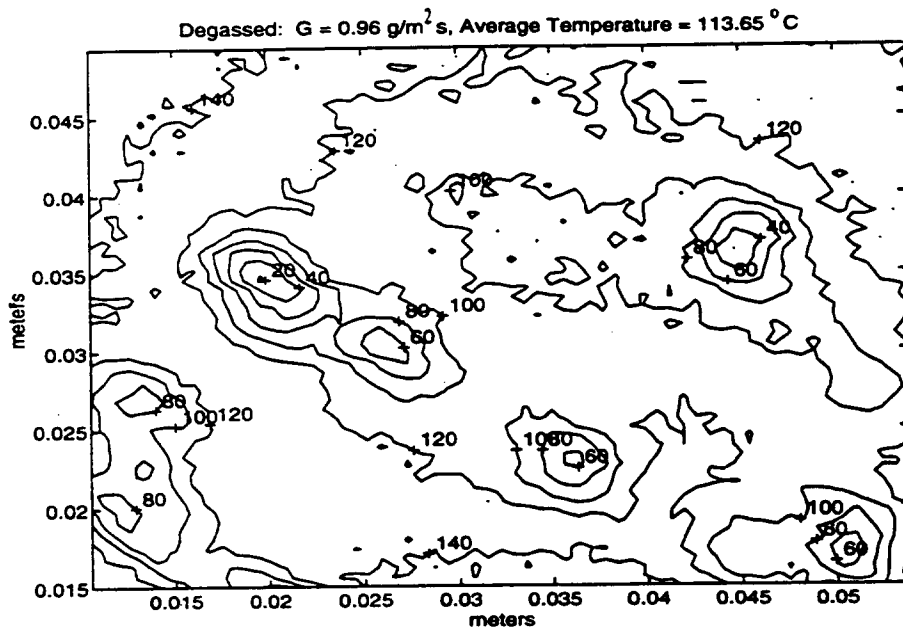
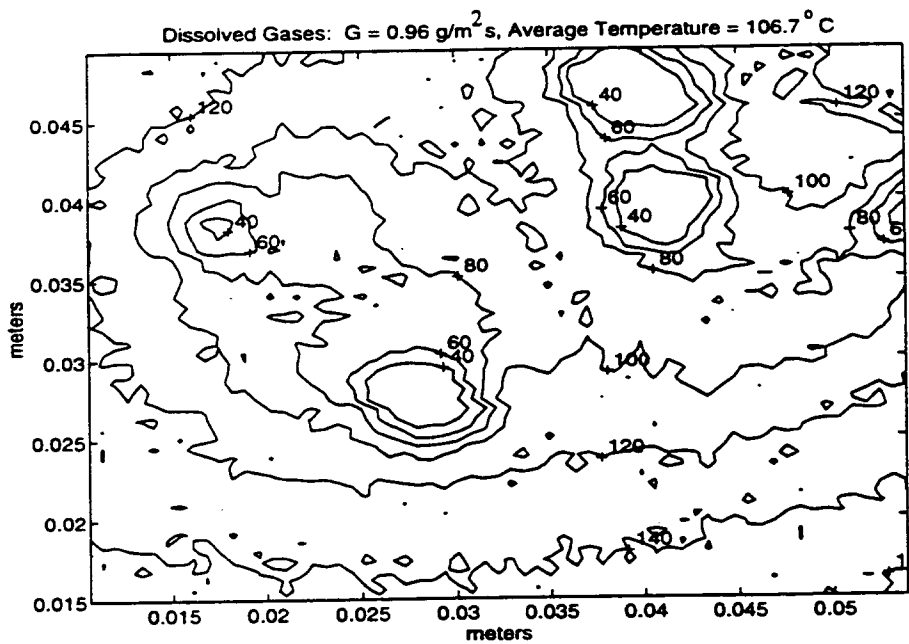


Figure 29 - Contour Plot: $T_{so} = 151^\circ \text{ C}$, Time = 600 seconds

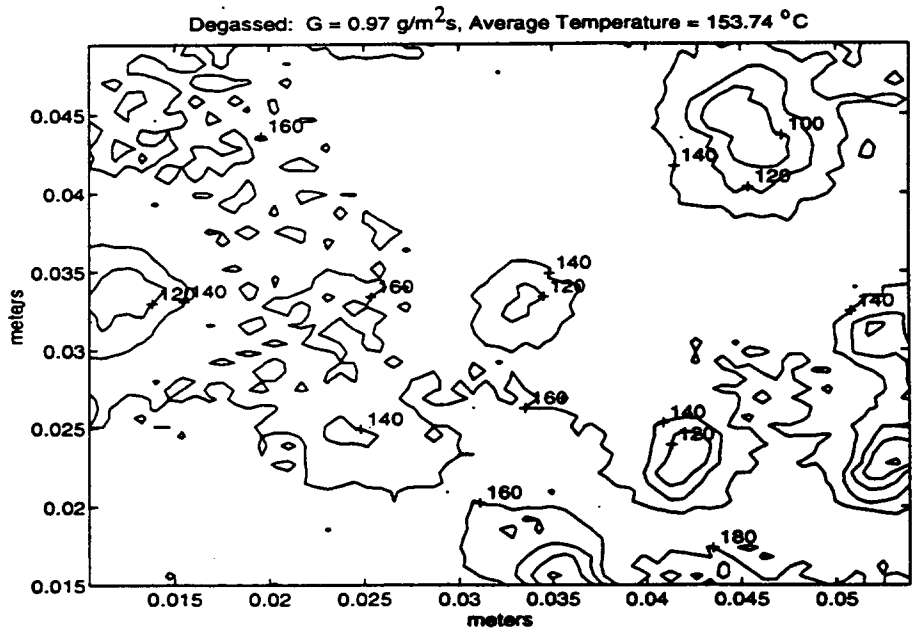
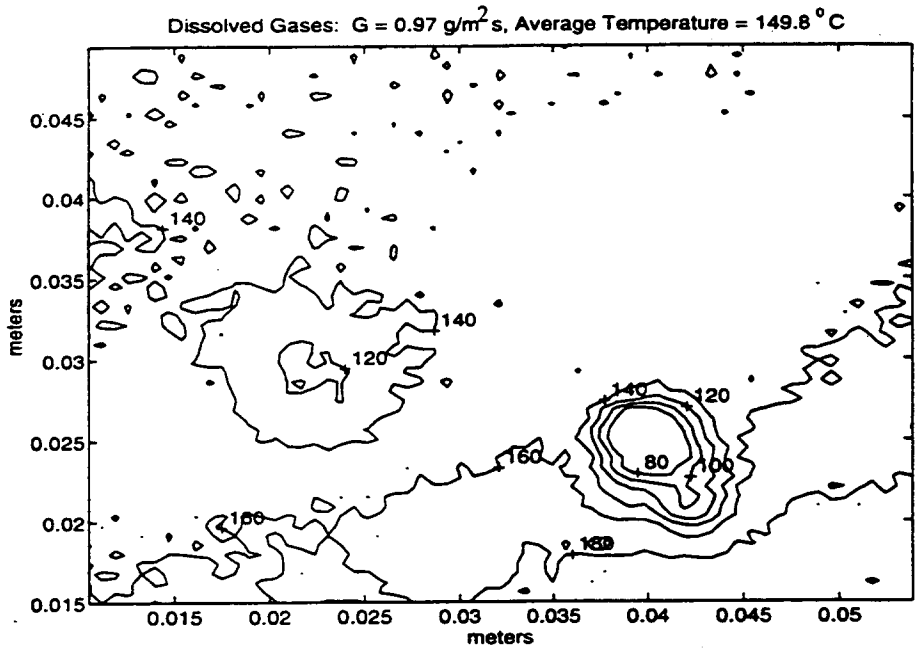


Figure 30 - Contour Plot: $T_{s0} = 162 \text{ }^\circ\text{C}$, Time = 30 seconds

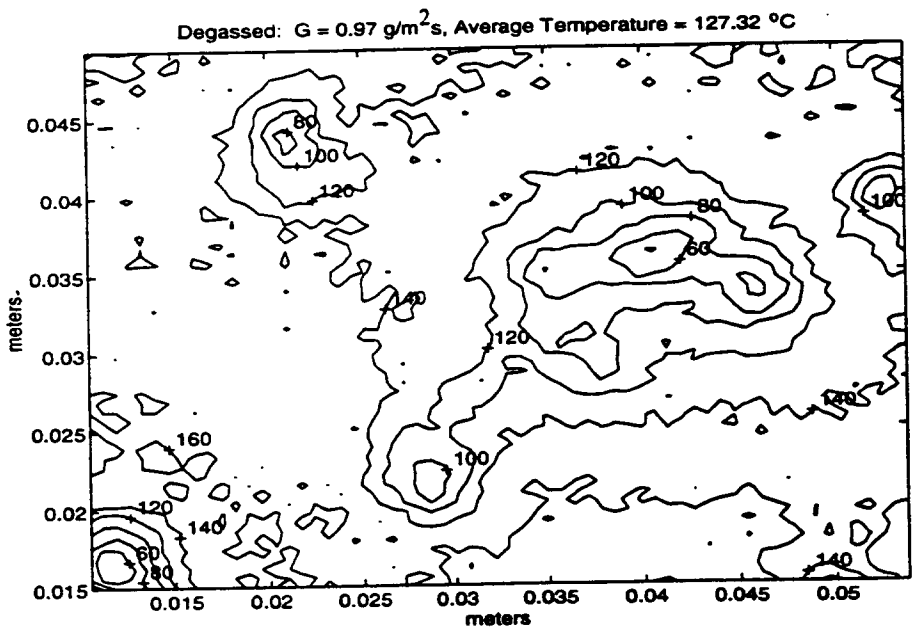
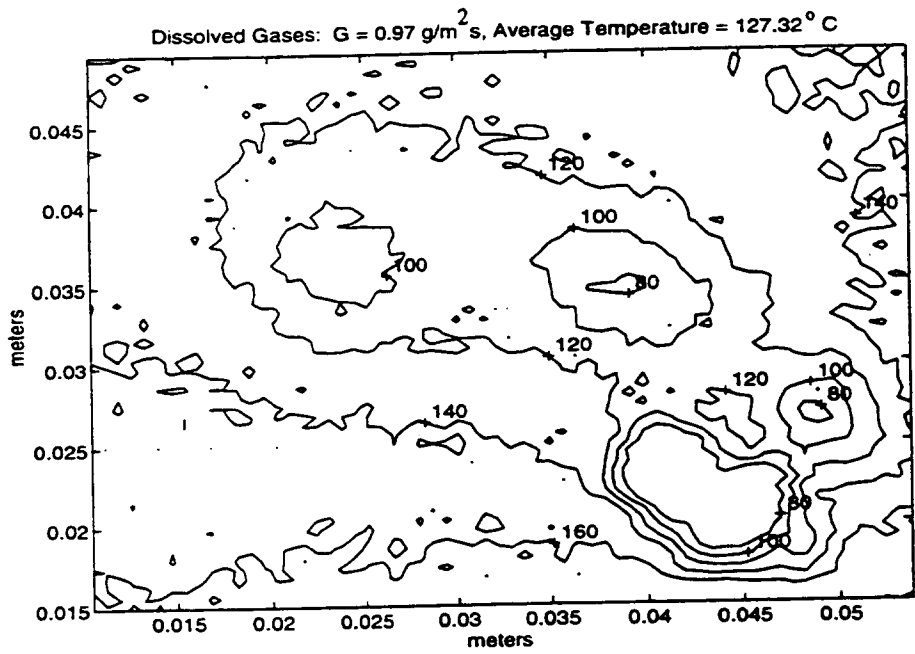


Figure 31 - Contour Plot: $T_{so} = 162^\circ \text{ C}$, Time = 300 seconds

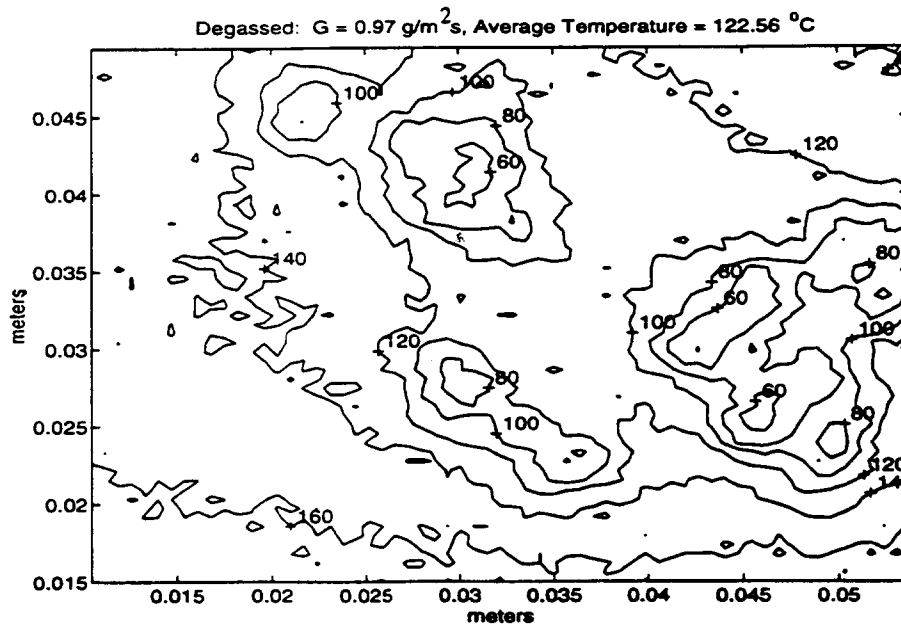
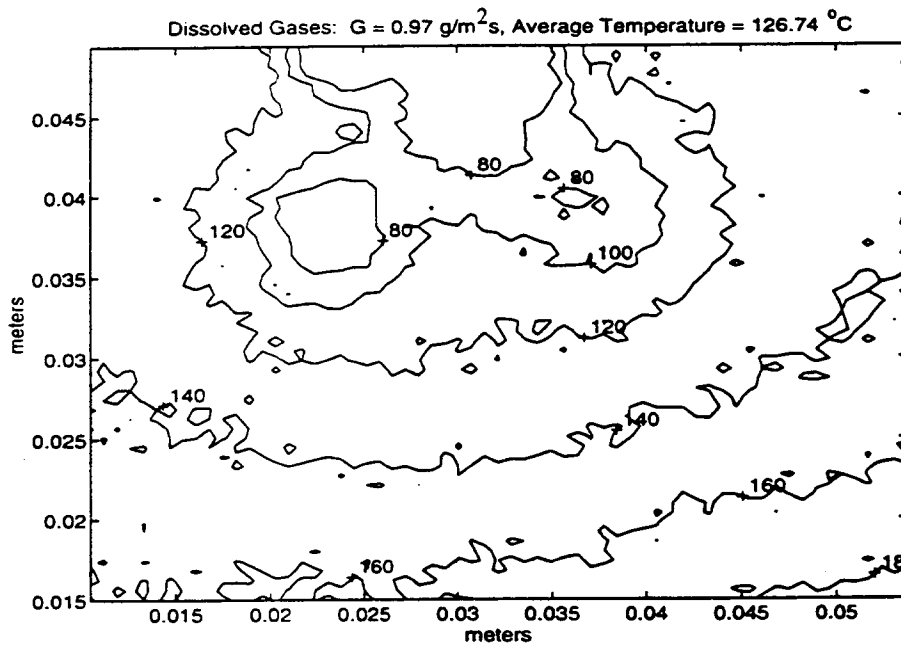


Figure 32 - Contour Plot: $T_{s0} = 162 \text{ }^\circ\text{C}$, Time = 600 seconds

Time (min)	Dissolved Gases (C)	Degassed (C)
0	111.00	111
0.5	106.49	105.43
1	101.86	100.02
1.5	103.04	98.77
2	98.92	96.43
2.5	101.50	97.9
3	100.18	98.56
3.5	98.94	96.68
4	97.75	93.87
4.5	96.29	95.01
5	96.29	91.26
5.5	95.79	89.56
6	92.44	92.22
6.5	93.03	91.97
7	93.50	92.51
7.5	93.16	92.46
8	93.48	92.77
8.5	94.80	91.74
9	92.74	89.63
9.5	90.08	87.36
10	91.24	85.69
10.5	91.84	89.57
11	90.63	88.08
11.5	91.43	85.6
12	91.26	81.1
12.5	88.28	83.43
13	90.98	80.68
13.5	91.08	82.1
14	93.36	81.22
14.5	93.94	84.37
15	93.15	83.6
15.5	92.72	80.65
16	93.22	80.69
16.5	92.67	81.71
17	91.50	81.57
17.5	91.25	83.94
18	92.91	81.64
18.5	92.13	80.86
19	89.90	83.54
19.5	90.46	81.79
20	91.38	80.53
20.5	89.18	79.9
21	91.19	79.27
21.5	91.69	80.24
22	90.35	83.06
22.5	91.27	84.5
23	89.42	82.68

Table 6 - Raw Temperature Data: $G = 0.21 \text{ g/m}^2\text{s}$

Time (min)	Dissolved Gases (C)	Degassed (C)
0.00	131.00	131.00
0.83	113.35	125.12
1.67	106.93	119.19
2.50	108.58	116.65
3.33	107.16	113.60
4.17	106.80	114.32
5.00	100.26	114.25
5.83	98.31	112.64
6.67	99.17	109.91
7.50	99.22	107.80
8.33	97.51	108.96
9.17	95.74	108.80
10.00	96.77	106.63
10.83	96.66	107.96
11.67	93.85	106.54
12.50	99.84	106.00
13.33	99.43	105.37
14.17	101.47	105.12
15.00	101.03	102.58
15.83	104.18	106.33
16.67	103.16	105.11
17.50	101.41	106.04
18.33	93.79	106.76
19.17	99.06	106.72
20.00	98.89	106.37
20.83	98.68	105.94
21.67	100.08	105.15
22.50	99.71	106.63

Table 7 - Raw Temperature Data: $G = 0.5 \text{ g/m}^2\text{s}$

Time (min)	Dissolved Gases (C)	Degassed (C)
0	151	151
0.5	131.55	139
1	132.31	131.62
1.5	129.12	129.64
2	127.31	126.57
2.5	124.64	125.62
3	120.9	125.41
3.5	120.01	118.6
4	116.3	122.42
4.5	118.27	118.45
5	114.35	119.79
5.5	117.16	110.91
6	115.55	109.05
6.5	114.98	113.08
7	116.9	115.05
7.5	109.65	113.57
8	111.89	115.52
8.5	105.475	113.24
9	106.73	116.71
9.5	102.35	112.66
10	106.68	113.65
11.5	109.98	110.45
12	116.96	110.71
12.5	108.5	110.97
13	111.23	109.86
13.5	108.03	112.78
14	105.47	108.06
14.5	106.86	108.34
15	101.57	108.3
15.5	100.17	
16	102.91	

Table 8 - Raw Temperature Data: $G = 0.96 \text{ g/m}^2\text{s}$

Time (min)	Dissolved Gases (C)	Degassed (C)
0	151	151
0.5	126.64	130.13
1	117.36	122.12
1.5	114.36	116.88
2	108.9	114.85
2.5	106.32	108.65
3	107.02	110.21
3.5	102.58	108.85
4	98.87	102.13
4.5	98.16	104.64
5	97.46	104.68
5.5	91.74	99.04
6	92.1	95.06
6.5	92.82	97.77
7	92.85	97.19
7.5	93.21	97.54
8	92.07	96.99
8.5	90.63	92.05
9	89.71	94.48
9.5	89.83	93.87
10	89.7	91.28
10.5	89.88	90.32
11	88.46	91.29
11.5	93.2	90.98
12	86.01	90.45
12.5	85.96	88.34
13	85.79	92.33
13.5	85.26	91.17
14	84.02	93.12
14.5	85.35	92.29
15	85.85	89.59
15.5	83.04	86.49
16	83.36	88.48
16.5	86.3	89.34
17	85.94	89.82
17.5	84.56	91.72
18	86.82	91.84
18.5	85.77	91.87
19	87.85	93.65
19.5	87.56	92.75
20	85.22	91.14
20.5	87.03	90.21
21	86.79	88.85
21.5	81.21	86.53
22	86.67	87.55
22.5	84.18	89.45
23	85.97	86.24

Table 9 - Raw Temperature Data: $G = 1.3 \text{ g/m}^2\text{s}$

Time (min)	Dissolved Gases (C)	Degassed (C)
0	162	162
0.5	149.27	153.74
1	141.89	148.92
1.5	129.32	143.44
2	133.98	140.18
2.5	132.47	139.07
3	131.59	133.52
3.5	131.55	137.56
4	128.08	136.15
4.5	128.98	134.22
5	127.64	127.32
5.5	129.2	132.99
6	130.55	126.38
6.5	129.42	125.85
7	128.28	124.64
7.5	127.85	125.19
8	127.26	124.86
8.5	128.06	125
9	129.04	120.65
9.5	128.61	122.04
10	126.74	122.56
10.5	123.03	122.57
11	125.83	120.33
11.5	116.97	122.63
12	117.78	120.84
12.5	117.56	120.01
13	117.37	118.6
13.5	116.2	122.72
14	118.58	123.84
14.5	118.13	124.19
15	123.58	121.72
15.5	124.04	120.36
16	124.15	122.58
16.5	121.93	125.46
17	123.4	122.43
17.5	121.88	118.63
18	122.43	120.55
18.5	122.19	121.83
19	121.75	120.44
19.5	125.05	120.83
20	124.19	124.01
20.5	122.68	121.76
21	121.78	118.57

Table 10 - Raw Temperature Data: $G = 0.97 \text{ g/m}^2\text{s}$

Time (min)	Dissolved Gases (C)	Degassed (C)
0	162	162
0.5	132.12	144.79
1	121.77	130.3
1.5	117.69	119.73
2	110.19	117.91
2.5	111.9	113.21
3	115.06	115.75
3.5	104.88	109.85
4	103.21	111.48
4.5	104.27	105.02
5	102.36	99.12
5.5	101.06	94.34
6	102.45	92.63
6.5	101.18	94.65
7	107.6	97.49
7.5	90.45	93.06
8	98.88	93.23
8.5	88.62	91.9
9	86.02	90.33
9.5	86.96	90.36
10	80.2	92.88
10.5	74.81	85.71
11	82.98	83.74
11.5	83.86	82.74
12	85.88	84.45
12.5	80.78	85
13	77.83	87.36
13.5	70.25	82.89
14	81.4	74.12
14.5	75.85	75.34
15	75.91	74.15
15.5	68.33	80.4
16	67.33	85.57
16.5	66	83.39
17	67.62	80.67
17.5	79.62	76.29
18	80.26	76.87
18.5	78.15	78.33
19	77.74	77.09
19.5	78.19	77.36
20	76.26	69.14
20.5	71.67	70.27
21	68.15	70.39
21.5	70.81	72.74
22	69.27	73.74
22.5	72.27	74.15
23	72.82	77.83

Table 11 - Raw Temperature Data: $G = 1.5 \text{ g/m}^2\text{s}$

Time (min)	Dissolved Gases (C)	Degassed (C)
0	182	182
0.5	153.63	157.69
1	140.44	146.49
1.5	137.74	142.32
2	134.64	131.1
2.5	131.67	126.87
3	127.93	123.98
3.5	120.89	123.47
4	123.88	119.93
4.5	120.13	115.41
5	118.21	117.76
5.5	116.47	117.49
6	114.73	112.98
6.5	112.73	114.34
7	118.82	113.9
8	120.15	109.33
8.5	119.96	111.07
9	119.29	107.48
9.5	107.6	111.25
10	95.47	109.08
10.5	112.23	105.61
11	111.32	100.46
11.5	104.49	104.77
12	105.03	105.69
12.5	103.02	104.78
13	104.07	105.24
13.5	105.84	104.78
14	103.35	105.06
14.5	100.08	103.52
15	98.43	106.48
15.5	96.79	104.56
16	97.88	104.06
16.5	99.9	106.93
17	100.36	103.79
17.5	100.44	103.89
18	101.95	102.36
18.5	103.31	99.84
19	100.24	98.99
19.5	99	107.14
20	102.86	106.06
20.5	97.87	101.05
21	107.01	104.16
21.5	103.77	106.28
22	102.55	105.94
22.5	96.76	100.29

Table 12 - Raw Temperature Data: $G = 1.6 \text{ g/m}^2\text{s}$

6. SPARSE SPRAY COOLING MODEL

The spray cooling of a hot surface is used in many engineering applications. Spray cooling involves the evaporation of water droplets and, due to the high latent heat, represents a way to remove large amounts of heat from a surface.

In the field of fire suppression, spray cooling from sprinklers is often used for extinguishment purposes as well as for the protection of surfaces. A model for the sparse spray cooling of a radiantly heated, semi-infinite, low thermal-conductivity solid surface is now presented. This model provides a relatively simple means of determining the transient thermal behavior of a surface that is being cooled by a sparse spray of water. Specifically, the code calculates transient average surface temperatures and spatial surface temperature distributions. The surfaces under consideration here are below the Leidenfrost temperature.

6.1 Development of the Computer Model

A previous computer model for the sparse spray cooling of a surface was developed by Liao [7]. This computer model predicted transient average surface temperatures and spatial temperature distributions for surfaces that are heated by conduction from below. Both a high thermal-conductivity surface (aluminum) and a low thermal-conductivity surface (macor) were modelled.

The computer model presented here differs from the previous one in several ways. The main features that distinguish the current code from the previous code are listed below.

- (1) model is for the evaporative cooling of a surface that is radiantly heated from above
- (2) includes accurate description of droplet distribution on the surface
- (3) closed-form solution replaces database to provide temperature drops for locations within 5 droplet radii from a droplet
- (4) validation of the model performed for the specific experimental setup of Dawson [9]

A listing of the computer code, entitled PROGRAM MDEC, can be found in the appendix .

6.1.1 Assumptions and Governing Equations

This section contains the overall equations that govern the cooling of the surface and describe the physical problem. Several assumptions are made that lead to the final form of these equations. The governing equation and boundary and initial conditions for the semi-infinite solid are

$$\frac{\partial T}{\partial t} = \alpha_s \nabla^2 T \quad (16)$$

$$T = T_{so} - \frac{q_o z}{k_s} \quad t=0 \quad (17)$$

$$-k_s \frac{\partial T}{\partial z} = q_c \quad z=0, 0 \leq r \leq R \quad (18)$$

$$-k_s \frac{\partial T}{\partial z} = h(T - T_\infty) - F_s \quad r > R, z=0 \quad (19)$$

$$-k_s \frac{\partial T}{\partial z} = q_o \quad z \rightarrow -\infty \quad (20)$$

$$\frac{\partial T}{\partial r} = 0 \quad r \rightarrow \infty, z \leq 0 \quad (21)$$

The initial condition of each droplet is the surface temperature corresponding to the location and time at which a droplet lands. This condition can be written as

$$T = T_{jso} \quad (22)$$

@ location j , $t = t_j$ $j = 1, ND$

With T_{jso} known, the temperature distribution associated with droplet j can be determined throughout its evaporation as was shown in Chapter 4. Therefore, for each droplet that impinges the surface the corresponding surface temperature prior to impingement must be calculated. The assumption required by this condition is that the temperature is uniform in a small region where the droplet is deposited. For a small droplet size and small temperature gradients, the assumption is valid. However, near the edge of a droplet the temperature profiles shown in Chapter 4 depict large temperature gradients. For droplets landing near other droplets, the overestimation and underestimation of the droplet's initial surface temperature is expected to average out and cause no significant errors in predicting the overall surface cooling behavior.

In the computer model, the quantity of interest is a temperature difference on the solid surface. In general, equations (16) through (21) are written in terms of the following quantity

$$U(r, z, t) = T(r, z, t) - T_{so} + \frac{q_o z}{k_s} \quad (23)$$

where on the surface ($z = 0$), U is simply the difference between the temperature at a location and time and the initial surface temperature.

Equations (16) through (21) take the following form when written in terms of U .

$$\frac{\partial U}{\partial t} = \alpha_s \nabla^2 U \quad (24)$$

$$U = 0 \quad t = 0 \quad (25)$$

$$-k_s \frac{\partial U}{\partial z} = q_c - q_o \quad 0 \leq r \leq R, z = 0 \quad (26)$$

$$-k_s \frac{\partial U}{\partial z} = h(T - T_\infty) - F_s - q_o \quad r > R, z = 0 \quad (27)$$

$$-k_s \frac{\partial U}{\partial z} = 0 \quad z \rightarrow -\infty \quad (28)$$

$$\frac{\partial U}{\partial r} = 0 \quad r \rightarrow \infty, z \leq 0 \quad (29)$$

6.1.2 Superposition

The governing equations and boundary and initial conditions developed in the previous section describe the evaporation of a single droplet on a surface. In the

sparse spray cooling of a surface, several droplets will be evaporating, and thus removing heat, on the surface. To determine the temperature drop at a location on the surface, the effects of all the droplets on the surface must be superimposed. The governing equations and boundary conditions can be written in terms of the effects of each droplet. First, the temperature difference, U_j , is defined as

$$U_j = T_j - T_{jso} + \frac{q_o z}{k_s} \quad (30)$$

where T_{jso} is the initial, uniform surface temperature at the deposition location of droplet j and T_j is the surface temperature at a given location due to the effect of droplet j . The governing equation for the solid and the initial and boundary conditions given in Equations (24) through (29) can then be written in terms of U_j .

Superposition is used to obtain the total temperature difference, U , due to the contributions from all evaporating drops. In this way,

$$U = \sum_{j=1}^{ND} U_j \quad (31)$$

Substituting equation (31) into equations (24) through (39), the surface temperature at any point on the surface and at any time will have the following form

$$T(r, t) = T_{so} + \sum_{j=1}^{ND} (U_j) = T_{so} + U \quad (32)$$

Two core assumptions are made when employing superposition. The first, which has already been stated, is the assumption of a uniform temperature underneath the droplet. The second assumption is that the evaporation of a droplet depends only

on the initial temperature which is associated with the droplet. That is, droplets landing on the surface after a droplet, j , has landed have no effect on droplet j , while droplets landing before only affect the initial surface temperature, T_{jso} , which governs the droplet's evaporation.

6.1.3 Calculation Procedure

A simplified flow chart of the computer code is displayed in Figure 33. The code calculates the temperature distribution and the average temperature for a portion of the entire region on which droplets are impinging. The calculation domain is divided into a grid and a temperature is determined at each grid point. This temperature represents the effects due to all droplets which have landed on the surface up until a particular time. It is important to realize that the effects of droplets that have fallen outside of the calculation domain are also accounted for in the temperature calculation. The dimensions of the grid are such that the spatial resolution matches that used to obtain the experimental data, that is 0.00013 meters/pixel.

At any time during the cooling of the surface, the temperature distributions and average temperature can be determined. At a grid point, the distance to each droplet that has impinged on the surface is calculated. Droplets within a distance of 5 droplet radii from the grid point are considered to be in the near-field. The temperature drops corresponding to droplets in the near-field are calculated using the closed-form solution presented in Chapter 4. Thus, the temperature drop has the form

$$U = -0.9 * \frac{(q_c - q_o) R}{k_s} \int_0^\infty J_0\left(\frac{\lambda r}{R}\right) J_1(\lambda) \left[\operatorname{erf}\left(\frac{\lambda \sqrt{\alpha_s t}}{R}\right) - \operatorname{erf}\left(\frac{\lambda \sqrt{\alpha_s (t - \tau)}}{R}\right) \right] \frac{d\lambda}{\lambda} \quad (33)$$

with the term $(t - \tau)$ is set equal to 0 for t less than or equal to τ .

Droplets farther than a distance of 5 radii from the grid point are considered to be in the far field. The temperature drop associated with droplets in the far field is obtained using an instantaneous point sink solution developed by Carslaw and Jaeger [14]. The solution has the following form

$$U = \frac{Q^*}{8 (\pi \alpha_s t)^{3/2}} e^{-\frac{r^2}{4 \alpha_s t}} \quad (34)$$

The term Q^* is the strength of the instantaneous point sink. For the case of a radiantly heated surface, the strength is given as

$$Q^* = -\frac{2Q_c}{\rho_s c_s} \quad (35)$$

The factor of 2 in Equation (35) accounts for the fact that the droplet acts in a semi-infinite space rather than an infinite space. Q_c is the total conductive heat that leaves the surface and acts to vaporize the droplet.

The solution given by (34) assumes an instantaneous point sink, the effects of which are generated at a time, t . However, an evaporating droplet removes heat over its entire evaporation time. For this reason, the time, t , is modified by determining when the average heat removal occurs during the droplet's evaporation. Figure 34 shows for various initial surface temperatures, the average conductive heat removal as

a function of normalized time. The curves were obtained using PROGRAM EVAP [10]. Referring to Figure 34, the average conductive heat removal over the evaporation time occurs at a time equal to 60% of the total evaporation time. Therefore, a delay in the deposition time of 0.6τ occurs for the instantaneous point sink. Equation (34) is rewritten as

$$U = \frac{Q^*}{8 (\pi \alpha_s (t - 0.6\tau))^{3/2}} e^{-\frac{r^2}{4\alpha_s(t-0.6\tau)}} \quad (36)$$

When using the far-field solution, any droplet that has not been on the surface for longer than 60% of its evaporation time has a zero temperature drop associated with it.

The choice to use the far-field solution at distances greater than 5 radii is made based on two factors. At approximately 5 droplet radii, the near-field solution exhibits some computational oscillations for times prior to the droplet's evaporation. The oscillations result from the oscillatory nature of the integrand and the numerical solution to the integral. Though the resulting oscillations are found to be less than 0.15°C , they are nonetheless undesirable. Additionally, a radius of influence of approximately 3 to 4 droplet radii has been determined from previous studies [16] and was discussed in Chapter 5. This suggests that at a distance of 5 radii from a droplet, the cooling effects are felt only in a remote sense and the far-field solution provides this type of result. Figure 35 shows the difference between the results obtained using the far-field solution and the near-field solution at a distance of 5 radii for various initial surface temperatures. The figure shows that the difference is always contained

in a narrow band of 0.15 °C.

6.1.4 Droplet Distribution

Prior to calculating the temperature at the grid points, information on the droplets that have impinged the surface over a specified time period is obtained using a droplet distribution subroutine (SUB DDIST). This subroutine provides the location of the droplet on the surface, the deposition time, the temperature at the point where the droplet landed, and the evaporation time of the droplet. Of these pieces of information, the positions of the droplet on the surface needed clarification with respect to the initially proposed random distribution.

In the sparse spray cooling experiments [9], attempts were made to distribute the droplets in a random fashion over a circular area of the solid surface. Such a random distribution was thought to simulate a spray cooling process more accurately. To this end, a positioning mechanism that consists of three solenoid-controlled bumpers was built to collide with and impart motion to the vertically-suspended droplet generator. The droplet generator, which hung from wires, would swing in a predetermined area as it impacted with the various bumpers. To keep the motion from decaying or falling into a particular pattern, a motorized cam was used to periodically pluck one of the suspension wires.

In the previous sparse spray cooling model, Liao [7] attempted to simulate the droplet distribution by assuming a constant velocity distributor moving within a circular area. Upon hitting the perimeter, the distributor bounces back on a new

trajectory according to a perfectly elastic collision.

Keeping in mind the ideal random droplet distribution, initial versions of the current model used a random number generator to assign the droplet positions. Positions were assigned in polar coordinates with a random angular and radial position. To ensure an evenly-distributed droplet density over the entire circular area, the square root of the random number was taken and assigned as the radial location.

After preliminary testing of the model, an attempt was made to more accurately describe the droplet distribution that occurred in the laboratory. Figure 36 shows the droplet distribution recorded during a typical experiment. The distribution corresponds to the area that is viewed by the infrared camera, with the outside radius equal to 3 cm. The total area that droplets impinge upon is approximately 3.25 cm in radius. Considering a circular area with a radius of 2 cm within the distribution shown in Figure 36, the ratio of the number of droplets that fall within this area to the total number of droplets shown is 74 to 1. Thus, the assumption of a uniform droplet density over the wetted area is incorrect. Clearly, the density is higher for the inner circular area, which represents about half of the total area.

In order to determine the experimental distribution, the first step was to characterize the motion of the droplet generator. As mentioned previously, the generator swings back and forth in a region that is confined by a set of bumpers. The bumpers move in and out in the horizontal plane in a synchronous fashion. During their motion, the bumpers have an outermost position that corresponds to a radius of 3.25 cm and an innermost position that corresponds to a radius of roughly 1.8 cm.

These positions suggest that the droplet generator can move freely only in a 1.8 cm radius. The generator is not expected to have a radial position of the maximum 3.25 cm because the bumpers will impede the generator as they move back toward the center after reaching this radius. Studying the distribution shown in Figure 36 confirms the generator motion expected from the experimental setup.

To model the droplet distribution, a relationship between the random number produced by the random number generator and the radial location needs to be determined. In this way, the randomness of the droplet position is maintained while distribution characteristics are accounted for. diMarzo [17] realized that the integral of the function describing the droplet distribution constituted the aforementioned relationship. The function describing the droplet distribution has the following boundary conditions based on a normalized radius.

- $d = 0$ @ $r = 0$: ensures the correct random distribution for the free area of motion
- $d' = 2$ @ $r = 0$:
- $d' = 0$ @ $r = \xi$: where ξ is the radius of free motion, requires a continuous function with a maximum at this radius
- $d = 0$ @ $r = 1$: requires generator to never reach outermost position
- $\int_0^1 d \, dr = 1$: requires all droplets to fall in the given area (normalized function)

The form of the function d , then, is

$$d = ar^4 + br^3 + cr^2 + dr + e \quad (37)$$

With $\xi = 0.56$ ($\sim 1.8/3.25$), the coefficients in (37) can be solved for to obtain Integrating (38) yields the desired relationship between the random number, D , and the

$$d = 9.15r^4 - 22.64r^3 + 11.49r^2 + 2r \quad (38)$$

radial position, r , of a droplet. Therefore,

$$D = 1.83r^5 - 5.66r^4 + 3.83r^3 + r^2 \quad (39)$$

Note that $D(0.707) = 0.76$. This quantity represents the ratio of the number of droplets falling in an area equal to half that of the entire impingement area to the total number of drops. The ratio obtained using Figure 36 is 0.74, indicating that the function d given by (38) provides a reasonable representation of the experimental droplet distribution. To further check the validity of the function given in Equation (39), the percentage of droplets falling in any particular radius in Figure 36 can be calculated. By dividing the area of droplet impingement into evenly-spaced concentric circles, a range of percentages corresponding to each radial location can be calculated. The ranges are determined based on two positions of the outermost concentric ring with respect to the outermost droplet. These two positions are determined such that the outermost droplet lies along either the inner radius or the outer radius of the last concentric ring. Figure 37 shows the relationship between the random number, D , and the normalized radial position for the distributions given a linear relationship, a spatial relationship, and the relationship given in (39). The droplet percentage range at incremental radial locations is also plotted. The fact that the function given in Equation (39) falls within these ranges further supports that the droplet distribution has been characterized correctly. A typical droplet distribution computed by the subroutine SUB DDIST is shown in Figure 38. The distribution is for a mass flux of

0.5 g/m²s.

6.2 Results and Analysis

The results of the sparse spray cooling model and sparse spray cooling experiments [9] are found in Figures 39 through 55 , with raw data contained in Tables 13 through 16. Dawson's experimental data includes initial surface temperatures ranging from 110 °C to 182 °C and water mass fluxes ranging from 0.2 g/m²s to 1.7 g/m²s. Calculated results are compared against four data sets corresponding to the degassed water experiments. The cases selected for comparison represent a relatively wide span of both initial surface temperature and mass flux that are found in evaporative cooling. Large experimental mass fluxes that produced steady state temperatures below 100 °C were not used for comparison because these temperatures are not relevant to evaporative cooling applications. Additionally, experiments with initial surface temperatures of 182 °C could not be used because nucleate boiling occurs at this temperature. The four experiments selected allow for a comparison of both mass flux and initial surface temperature effects. Thus, the results are for initial surface temperatures of 131 °C and 162 °C, each having a mass flux of 0.5 g/m²s, and for initial surface temperatures of 151 °C and 162 °C, having mass fluxes of 0.96 g/m²s and 0.97 g/m²s, respectively.

Although only four data sets are selected to validate the code, it is important to realize how a data point is obtained. Each infrared snapshot of the surface represents a grid of approximately 354 pixels x 262 pixels. A data point is calculated by

averaging every fifth pixel intensity values, or approximately 3710 pixel values. Transient average surface temperatures are comprised of data points at every 50 seconds for 24 minutes. Therefore, each data set contains averages of approximately 107,000 pixel values.

6.2.1 Transient Average Surface Temperature

In Figure 39 through Figure 42 the average surface temperature is plotted versus time for the four cases listed in Section 6.2. Experimental data is plotted using open symbols while the calculated results are plotted using closed symbols. With the exception of the results corresponding to an initial surface temperature of 162 °C and a mass flux of 0.5 g/m²s, the calculated and experimental results agree well. The code is able to predict steady state temperatures that agree with those found in the experiment. Additionally, the code is able to capture the transient behavior of the surface.

Experimental data for an initial surface temperature of 151 °C and a mass flux of 0.96 g/m²s does not exist past a time of approximately 15 minutes. The code was run for a longer time, however, in order to observe the predicted steady state behavior. The initial portion of the calculated results agrees with the experimental data and it appears that if experimental data existed for longer times it would follow the trend observed in the calculated results. The largest disagreement between the calculated results and the experimental data is found for the case having an initial surface temperature of 162 °C and a mass flux of 0.5 g/m²s. In the first five minutes of

cooling, the experimental temperatures are lower than the predicted temperatures. At a time of five minutes, the experimental data exhibits a discontinuity where the surface appears to have overcooled, recovered slightly, and cooled again. At ten minutes into the cooling, the surface appears to begin to approach the steady state temperature predicted by the code. A simple linear extrapolation of the experimental data points indicates that the surface would reach its steady state temperature at a time of approximately 58 minutes. The most likely reason for the deviant behavior of this data set is that an initial surface temperature of 162 °C is near the range of nucleate boiling. The data suggests that nucleate boiling may have occurred during the initial cooling period causing the surface to cool to lower temperatures than expected. After the initial sharp cooling of the surface, it appears that the continual impingement of water on the surface causes a suppression of the nucleate boiling. The suppression allows for a slight recovery of the surface and for the remaining of the surface cooling to be governed by evaporation. The deviant behavior is not seen in the data corresponding to an initial surface temperature of 162 °C and mass flux of 0.97 g/m²s because the relatively high mass flux is able to suppress the nucleate boiling.

From the experimental results shown in Chapter 5 and contained in reference [9], two important parameters that govern the cooling of the surface are evident. These parameters are the steady state surface temperature and the behavior of the surface as it cools to the steady state temperature. The latter parameter is described by a time constant. Various quantities, such as the mass flux, the initial surface temperature, or the solid material properties, may affect these two parameters. It is

important to determine any relationships between these parameters and the quantities that may affect them.

A maximum temperature difference is defined in the following way

$$\Delta T_m = T_{SO} - T_{SS} \quad (40)$$

Dawson [9] found a relationship between the surface temperature and time of the following form

$$T = \Delta T_m e^{-\frac{t}{\tau}} + T_{SS} \quad (41)$$

A normalized temperature can now be defined as

$$\Theta = \frac{T - T_{SS}}{\Delta T_m} \quad (42)$$

In terms of Θ , equation (41) becomes

$$\Theta = e^{-t/\tau} \quad (43)$$

In this equation, τ , is the time constant mentioned previously.

The experimental and calculated data are plotted in the form of Θ versus t in Figure 43. The steady state temperature used to plot the data is obtained using the calculated results. With the exception of the experiment consisting of an initial surface temperature of 162 °C and mass flux of 0.5 g/m²s, the experimental and calculated data collapses. The transient results plotted in this form indicate that the transient thermal behavior of the surface is independent of mass flux and initial surface temperature. The calculated results corresponding to an initial surface

temperature of 162 °C and mass flux of 0.5 g/m²s are consistent with the other sets of data, indicating that the experimental data for that case represents an anomaly and that the experimental conditions may not have been conducive to evaporative cooling. Figure 43 gives both theoretical and experimental support to the conclusion that the time constant, τ , is independent of mass flux and initial surface temperature.

To determine the time constant, a curve is fit to the calculated results in the form of $e^{-t/\tau}$. To do this, $\ln\Theta$ is plotted against t and a linear regression is performed. A regression is performed only for the initial transient ($t < 3.5$ min) because this is the region where calculated results have the least scatter. A value of τ equal to 230 seconds was calculated in this way.

Since τ was found to be independent of the mass flux and initial surface temperature, one might expect that it instead depends on the properties of the solid. At steady state, cooling effects are expected to be felt within a certain depth of the solid. This depth is called the penetration depth, l , and is given as

$$l = \sqrt{\alpha_s \tau} \quad (44)$$

Using $\alpha_s = 5.79 \cdot 10^{-7}$ m²/s for macor and $\tau = 230$ seconds as calculated, l is found to be 1.15 cm. A radius of influence was discussed in Section 5.2.1 and determined to be between 1.05 cm and 1.5 cm for the experimental conditions under consideration. Therefore, the model supports the experimental data in suggesting that the time constant is a function of the solid properties, and that the penetration depth defined by (44) is of the same order of magnitude as radius of influence of a single droplet on the surface.

6.2.2 Surface Temperature Contours

A more qualitative validation of the sparse spray cooling code is found in the temperature contour plots contained in Figures 44 through 55. The contour plots are simply snapshots of the surface taken at three different times during each experimental run. The times are chosen to represent the early portion of the surface cooling ($t = 50$ seconds), an intermediate portion of the surface cooling ($t = 300$ seconds), and a steady state portion of the surface cooling ($t = 600$ seconds). Again, the cases used for the qualitative validation are those described in the previous section. Two contour plots, corresponding to experimental results and calculated results, respectively, are shown in each figure.

Several features are similar in both the experimental and calculated contour plots. The first feature is that both plots contain local concentric rings of contour lines indicating locations of evaporating droplets. At a given time, the number of droplets indicated by the contours are approximately the same for both experimental and calculated results. There may be slight differences in the number of droplets due to the fact that the snapshot represents only a portion of the surface and droplets may fall outside of the displayed region. Another observable trend seen in both sets of results is that the number of droplets increases with time. This is expected because the evaporation times are longer as the surface cools.

The temperatures indicated on the contours also agree between the experiments and the code. The innermost contours have the lowest temperatures while the outermost have the highest. The innermost contour temperatures for the experiments

are generally lower than those for the code. However, these contours represent regions underneath the droplets where the infrared camera yields erroneous data. The more important temperatures are those associated with the contours that run through the main portion of the plots. These contours indicate how the surface behaves as a whole, not just in the local region where droplets exist. These temperatures are consistent between the experimental and calculated results. A decrease in these temperatures occurs as time increases and the surface cools.

The main difference between the experimental and calculated contour plots is that the calculated contours appear smoother than the experimental contours. The jagged contour lines in the experimental results occur because of the fluctuation in the intensities at the various surface points.

6.3 Summary

A model for the prediction of the transient thermal behavior of a low thermal conductivity, semi-infinite solid subjected to a random array of water droplets has been presented and tested against experiments. The model uses superposition and closed-form solutions to calculate surface temperature drops caused by all droplets that have impinged the surface. A detailed description of the droplet distribution that occurred during experiments is incorporated in the model.

Validation of the model against experimental data shows that the model is able to predict the transient thermal behavior of the solid both quantitatively and qualitatively. The code is able to calculate the steady state temperature of the surface given an initial surface temperature and a mass flux and is also able to predict how the

surface reaches its steady state temperature. Furthermore, it was found that a dimensionless temperature could be defined such that time plots of both the calculated and experimental data in this form results in a collapsing of all the data. From this fact, the time constant, which describes the transient cooling of the surface, is determined to be of the mass flux and is found instead to depend on the properties of the solid.

Perhaps the greatest source of error expected in the code is the use of the closed-form solution in the near-field. Figures 15 and 16 in Chapter 4 show that relatively large discrepancies in temperature occur between the closed-form solution and the single droplet model. To evaluate the error caused by these discrepancies, an average difference in temperature of 10 °C is assumed. Underneath the droplet differences are usually from 5 °C to 15 °C. The contour plots in show that at steady state there are generally between 5 and 8 droplets existing on the surface. The difference expected in average temperatures is given by

$$\Delta T_{ave} = \frac{\Sigma (\Delta T A_d)}{A_t} \quad (45)$$

where A_d is the area underneath the a droplet ($2.77 \cdot 10^{-5} \text{ m}^2$), A_t is the total area of calculation ($1.5 \cdot 10^{-3} \text{ m}^2$), and ΔT is approximately 10 °C. Using (45) ΔT_{ave} is calculated to be 0.185 °C. Since the experimental infrared thermography itself produces errors that are ± 2 gray shade and thus ± 2 °C, the error in using the closed-form solution is negligible in the calculation of the average surface temperature.

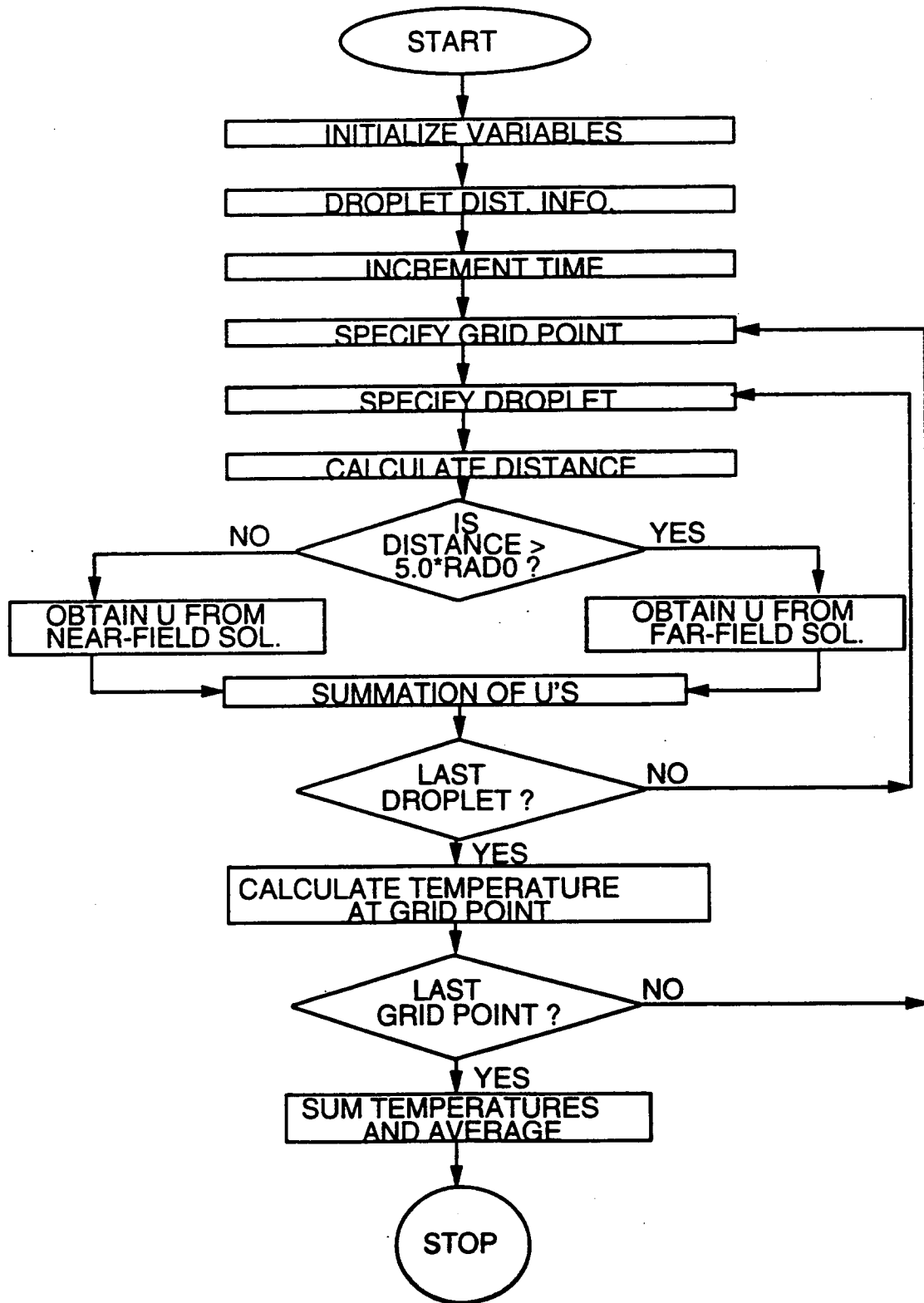


Figure 33 - Simplified Program Flow Chart

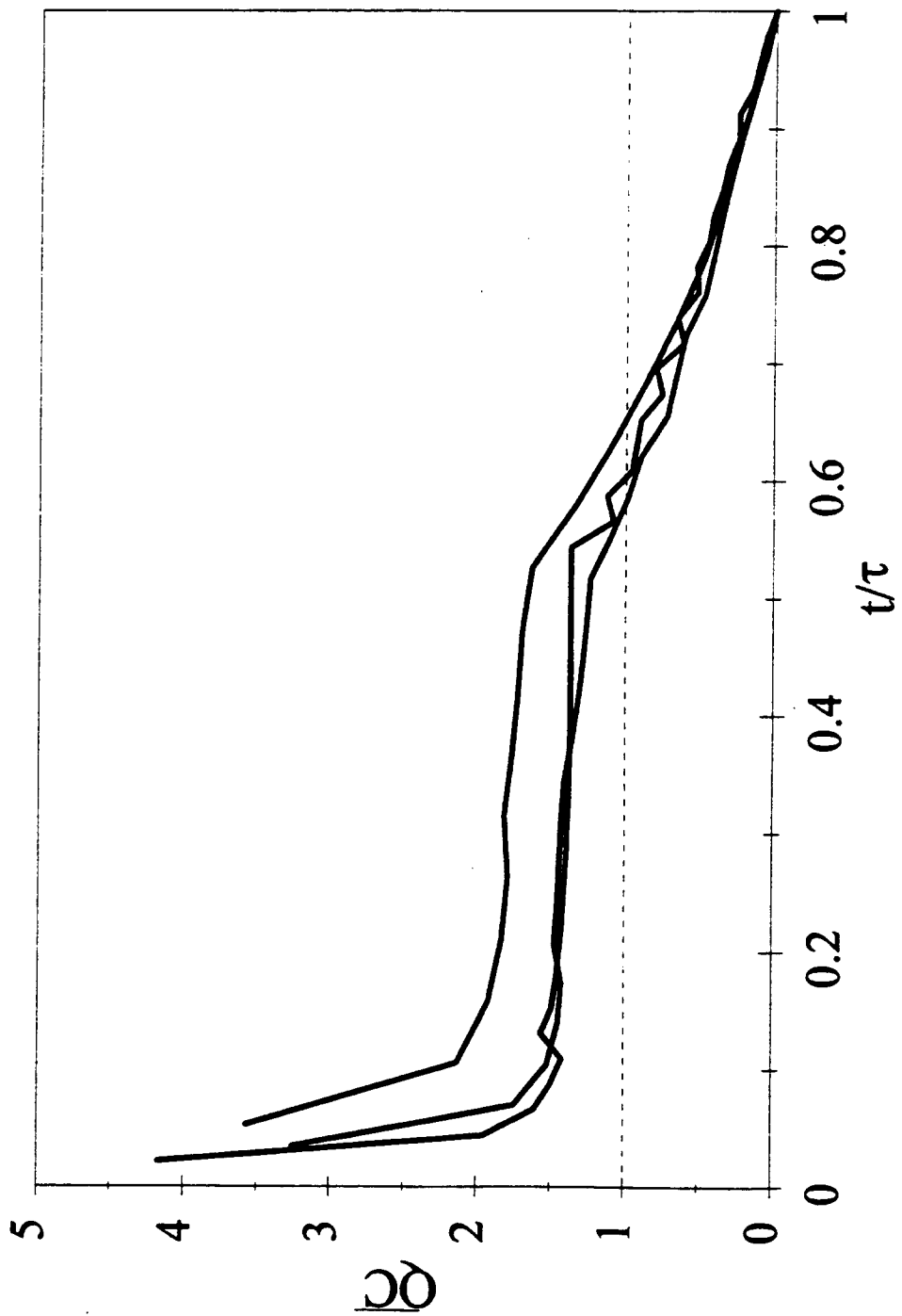


Figure 34 - Normalized Average Conductive Heat Removal

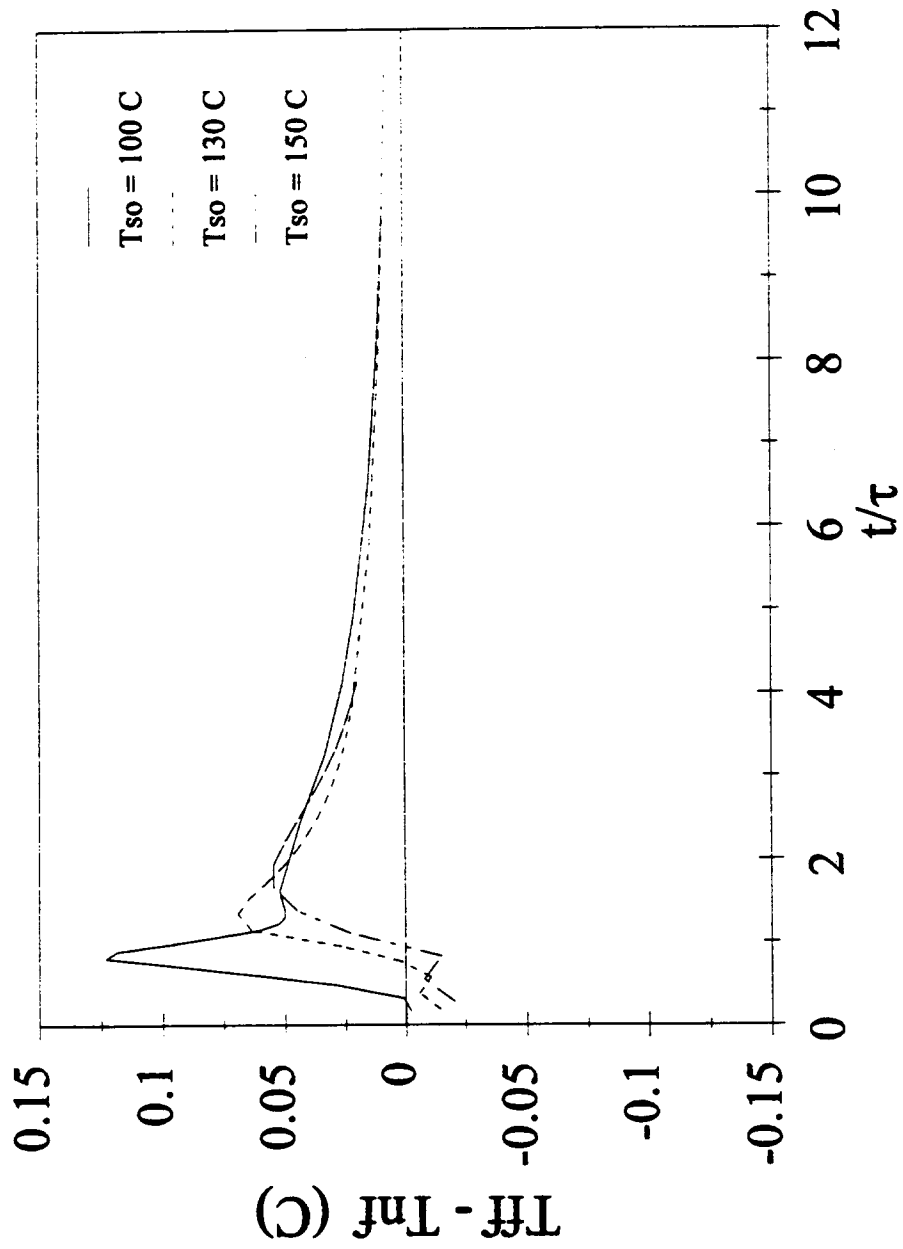


Figure 35 - Near and Far Field Solution Difference

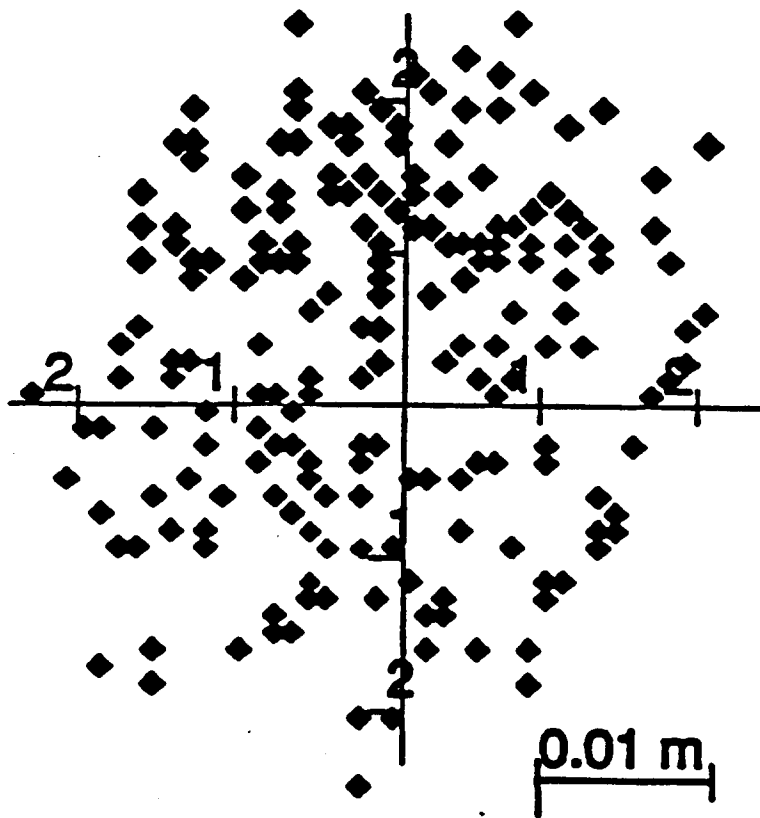


Figure 36 - Typical Experimental Droplet Distribution

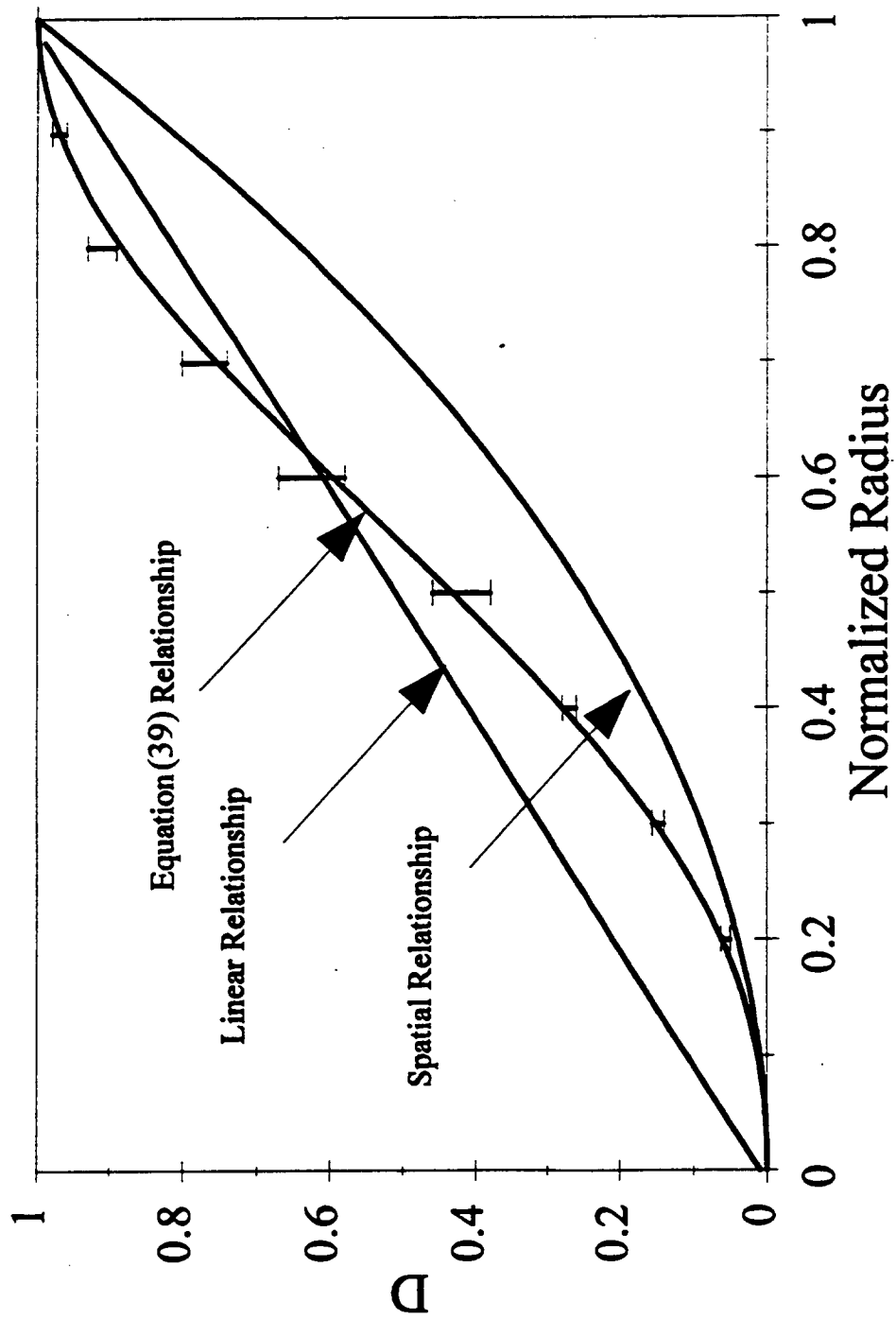


Figure 37 - Relationships Between D and Radial Position

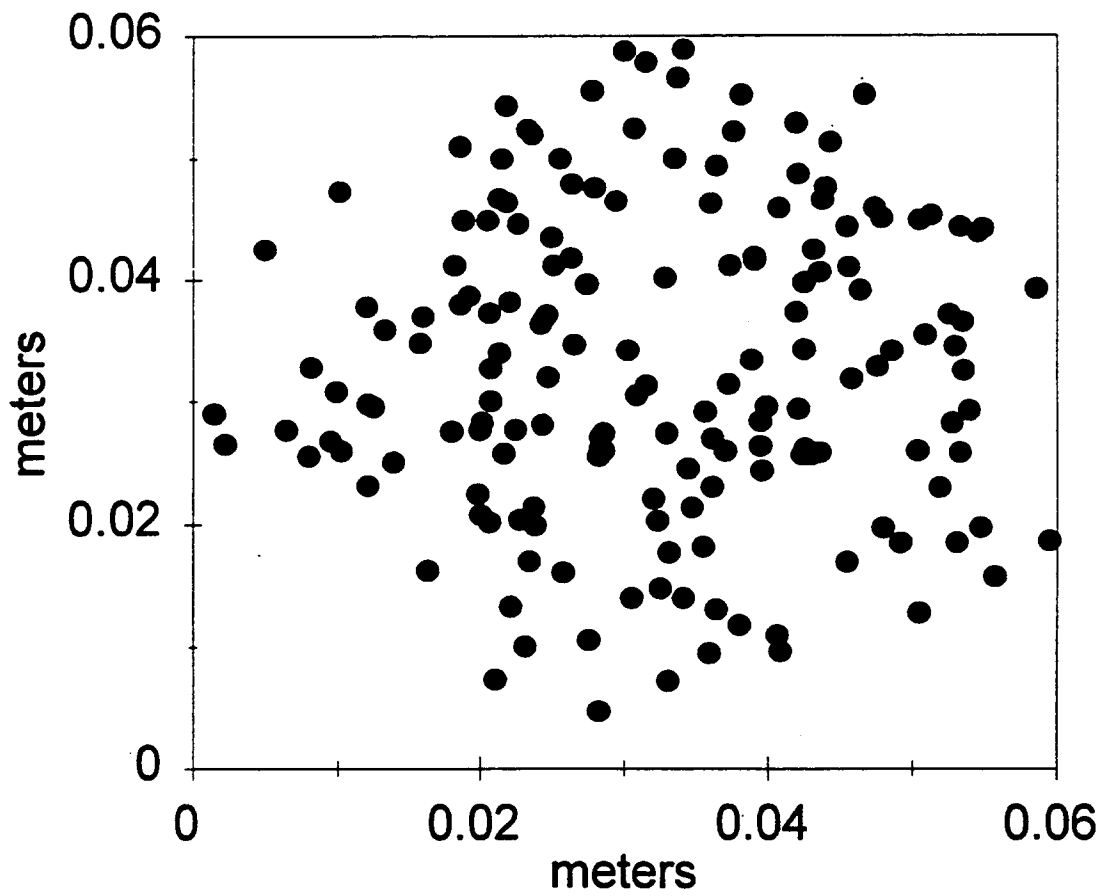


Figure 38 - Typical Calculated Droplet Distribution

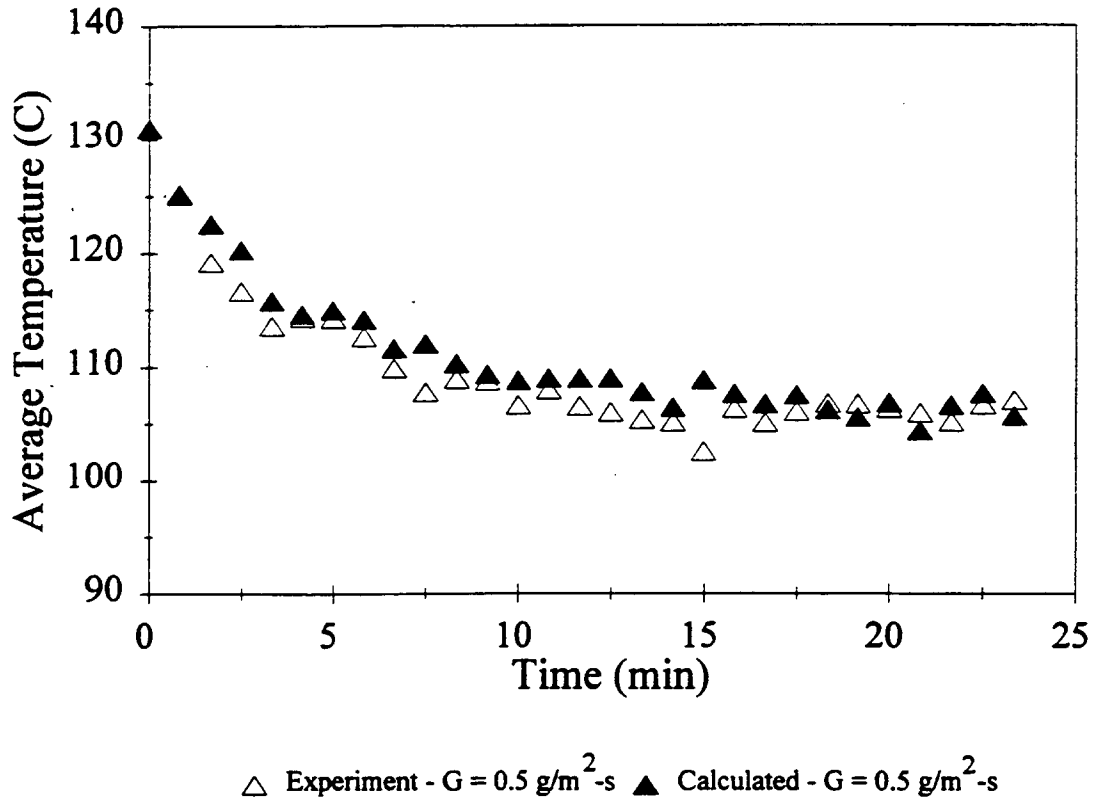
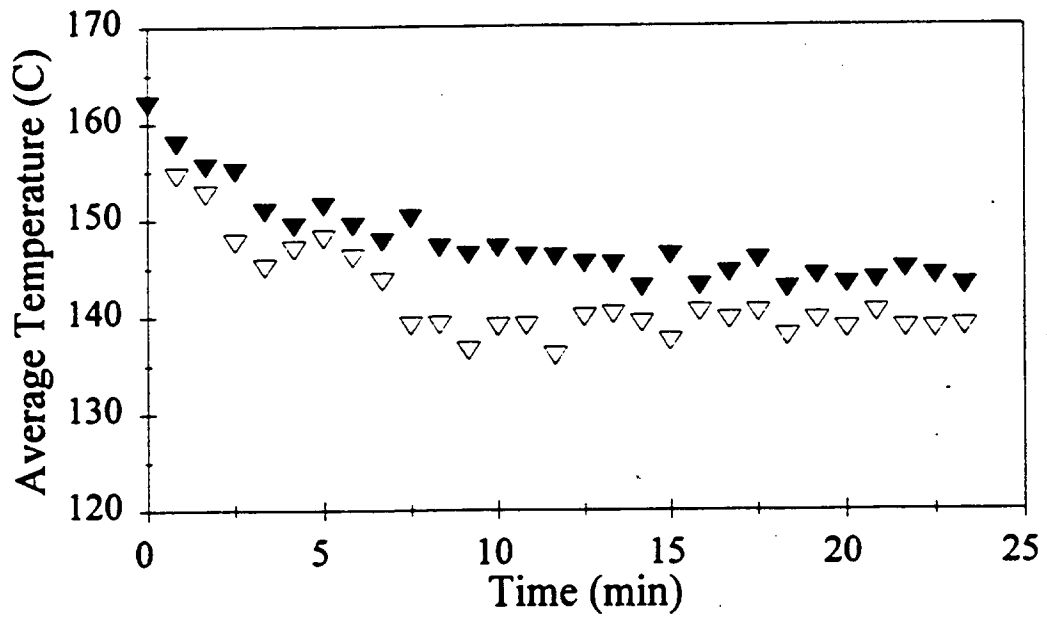
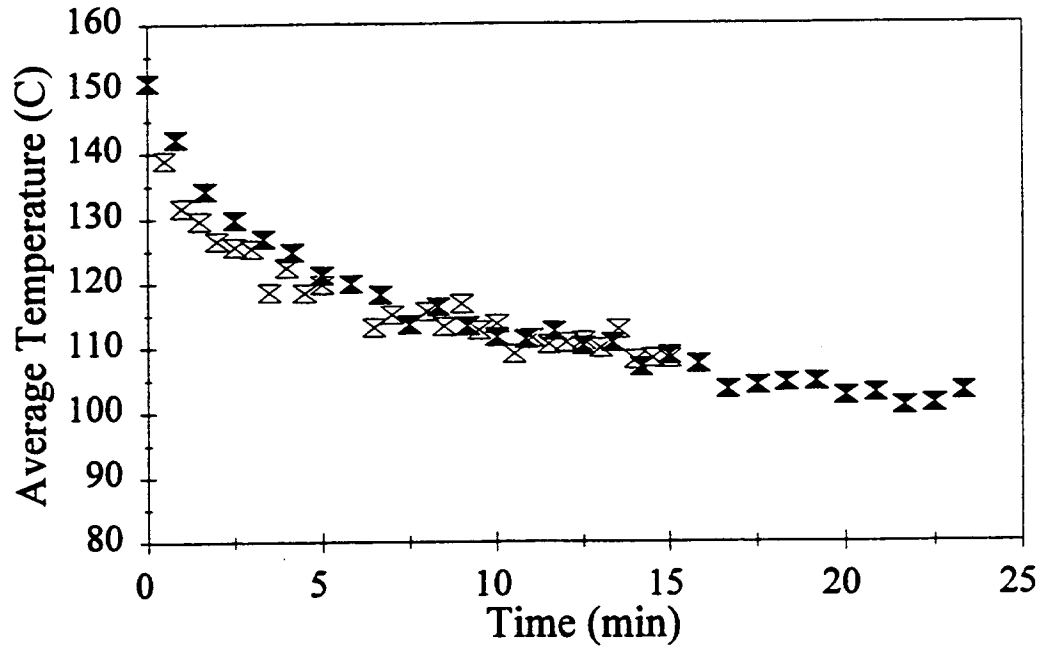


Figure 39 - Transient Temperature Plot: $T_{so} = 131 \text{ }^\circ\text{C}$



▽ Experiment - $G = 0.5 \text{ g/m}^2\text{-s}$ ▼ Calculated - $G = 0.5 \text{ g/m}^2\text{-s}$

Figure 40 - Transient Temperature Plot: $T_{so} = 162 \text{ }^\circ\text{C}$



⊗ Experiment - $G = 0.96 \text{ g/m}^2 \cdot \text{s}$ ⊗ Calculated - $G = 0.96 \text{ g/m}^2 \cdot \text{s}$

Figure 41 - Transient Temperature Plot: $T_{so} = 151 \text{ }^\circ\text{C}$

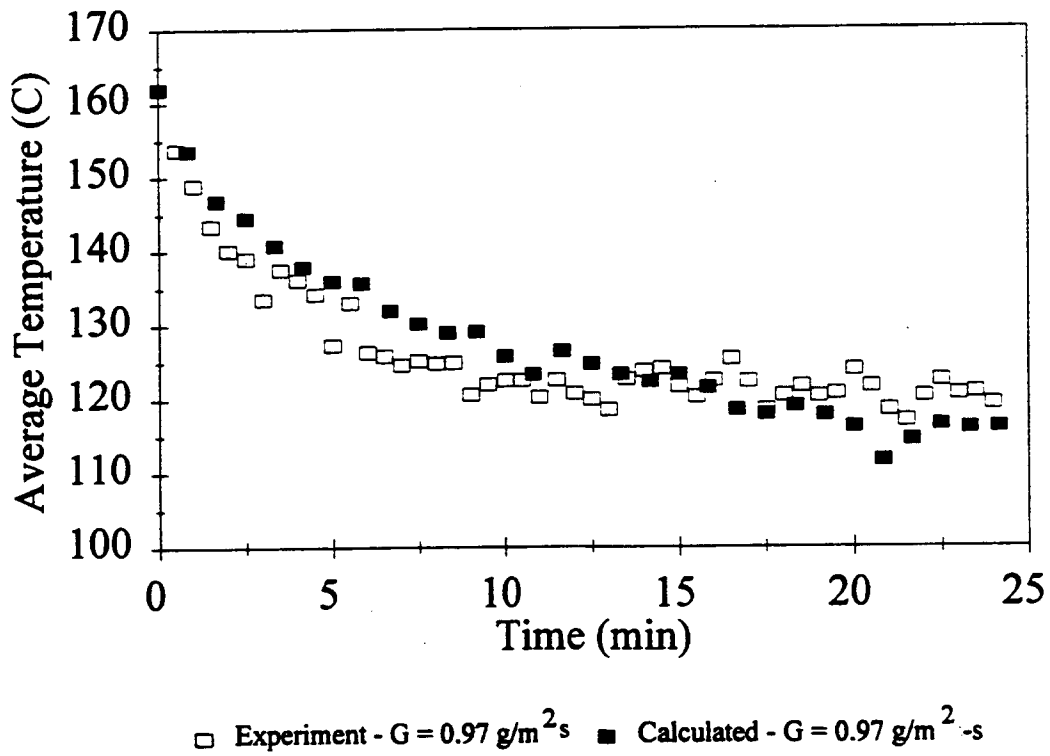


Figure 42 - Transient Temperature Plot: $T_{so} = 162 \text{ }^\circ\text{C}$

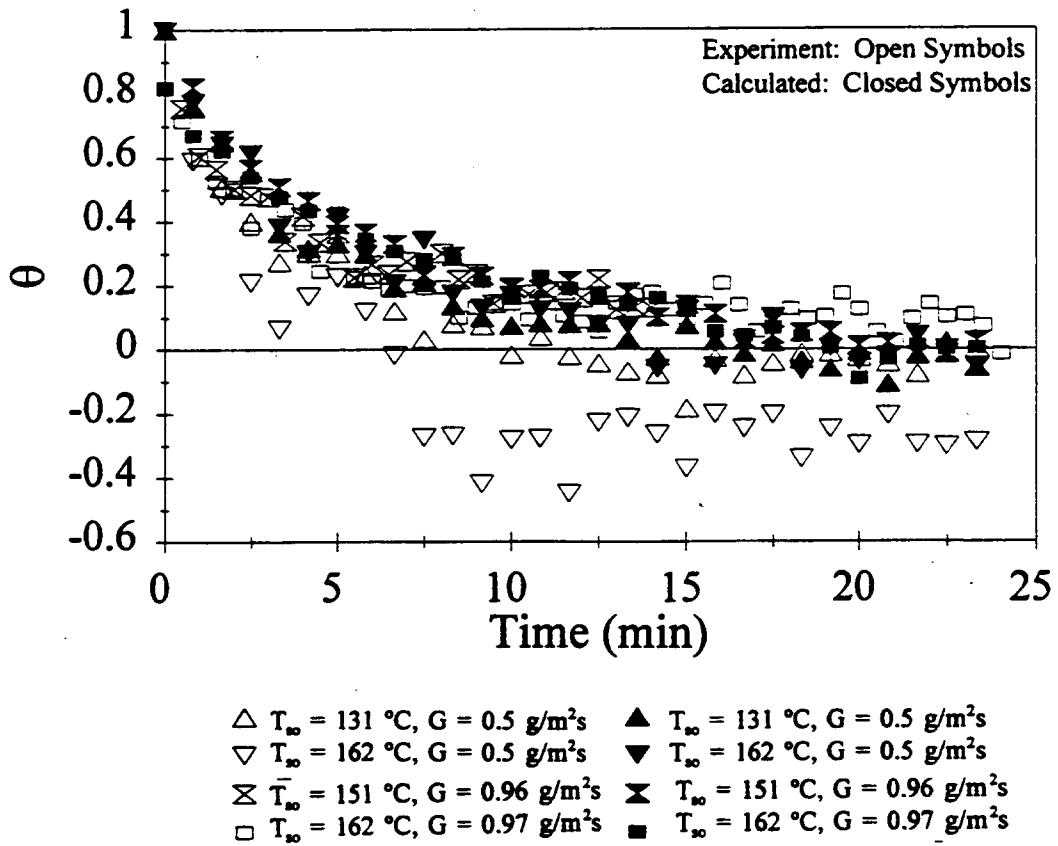


Figure 43 - Experimental and Calculated Transient Dimensionless Temperature Plot

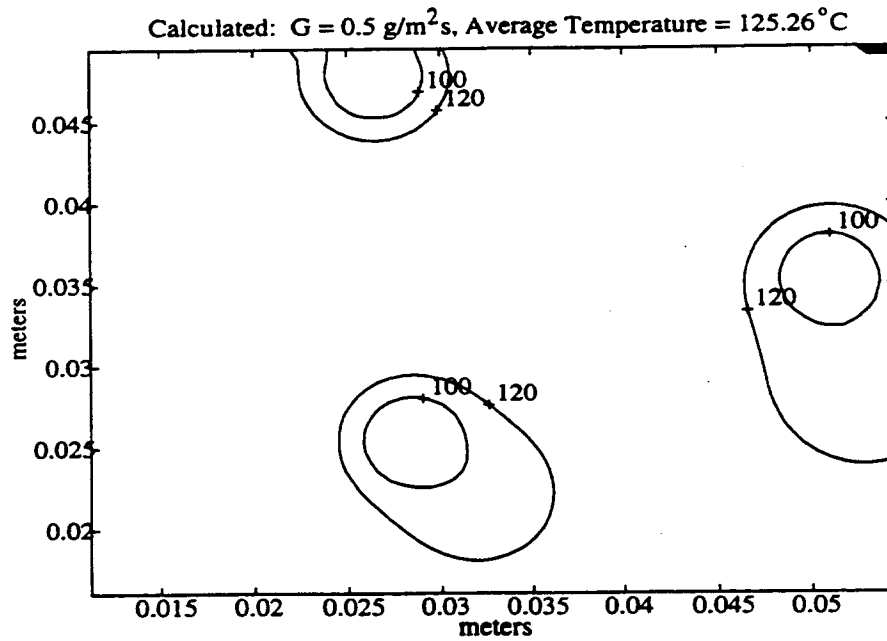
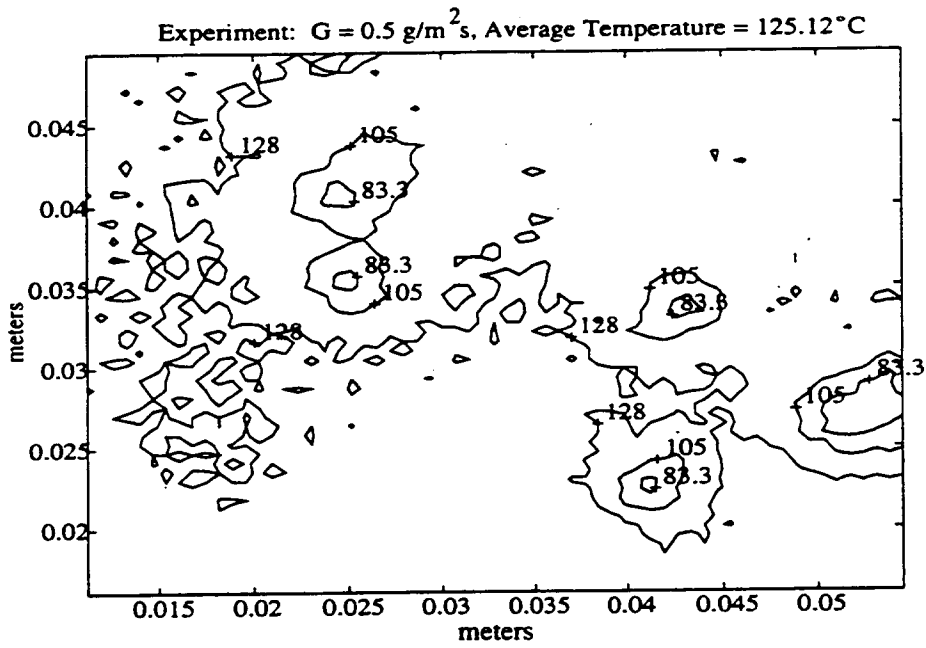


Figure 44 - Contour Plot: $T_{so} = 131^\circ\text{C}$, Time = 50 seconds

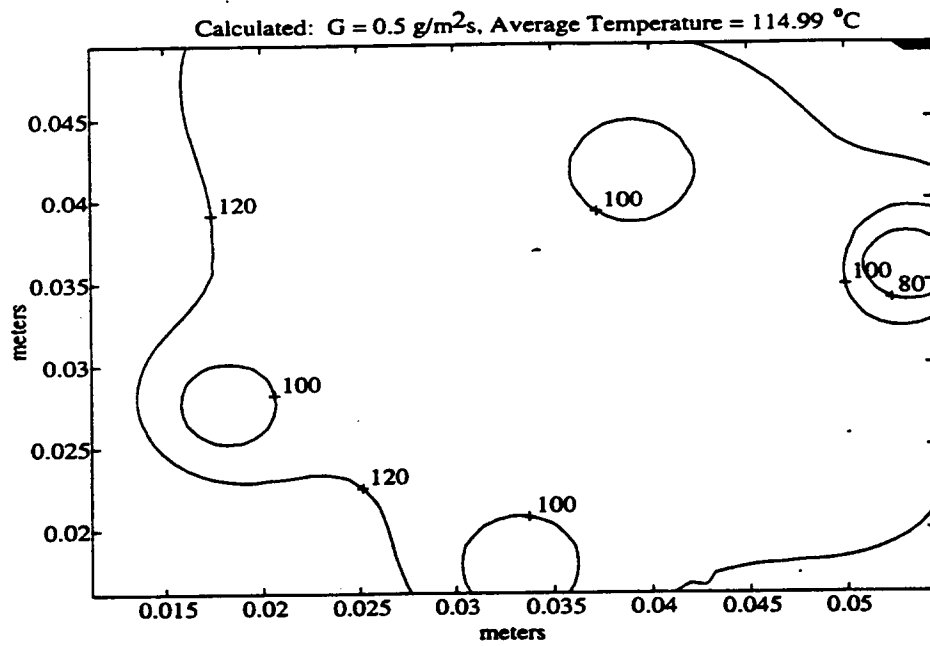
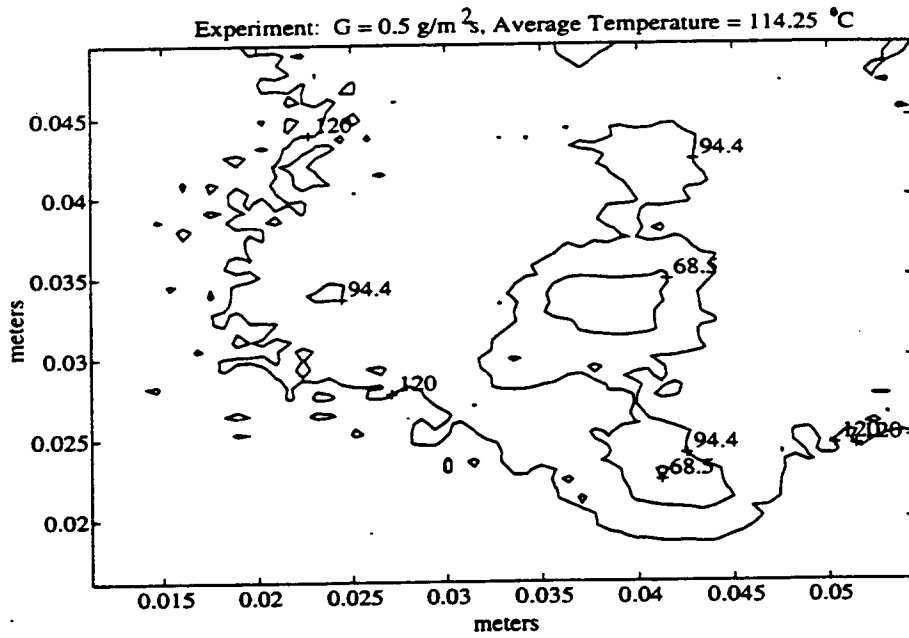


Figure 45 - Contour Plot: $T_{so} = 131 \text{ }^\circ\text{C}$, Time = 300 seconds

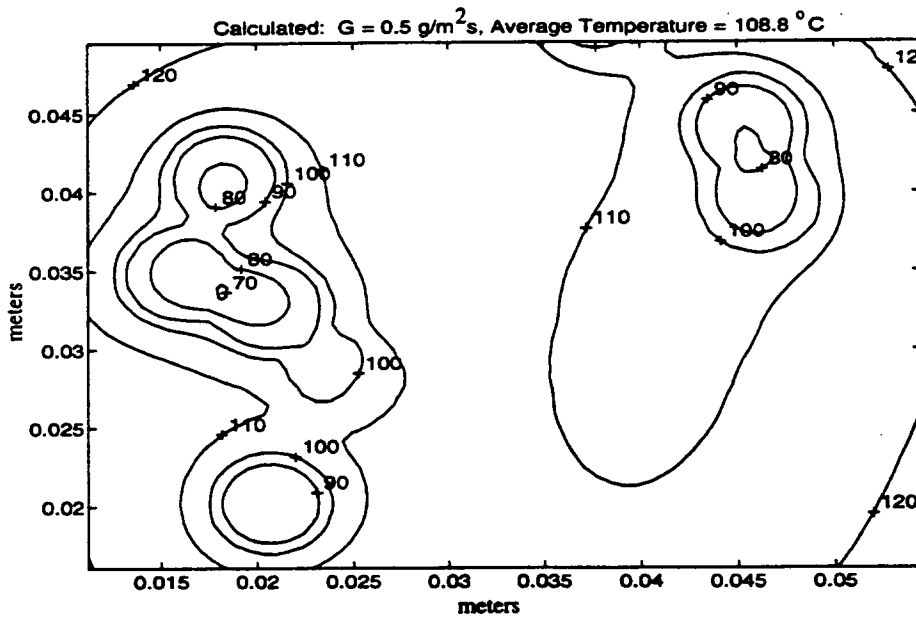
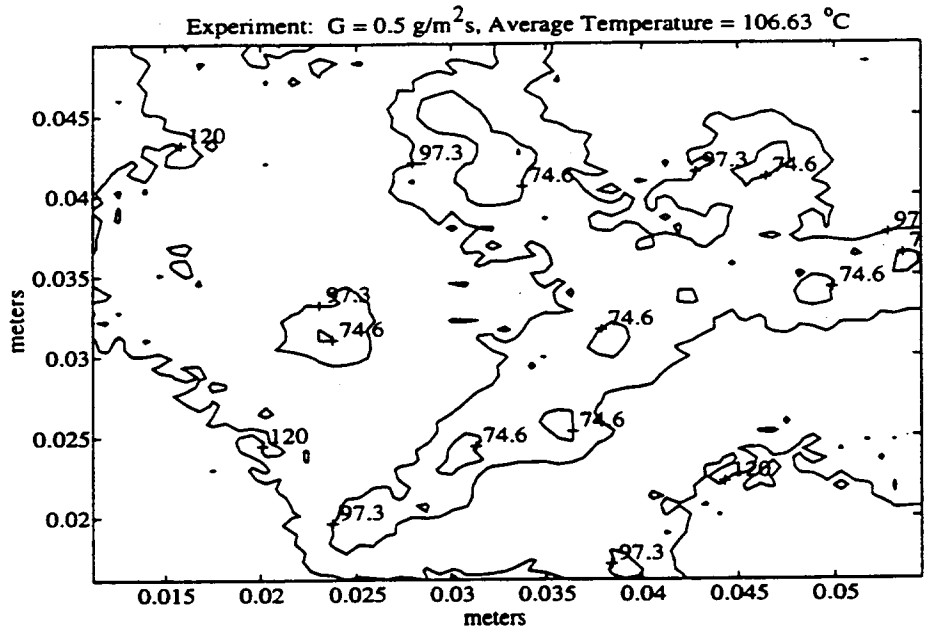


Figure 46 - Contour Plot: $T_{so} = 131 \text{ }^\circ\text{C}$, Time = 600 seconds

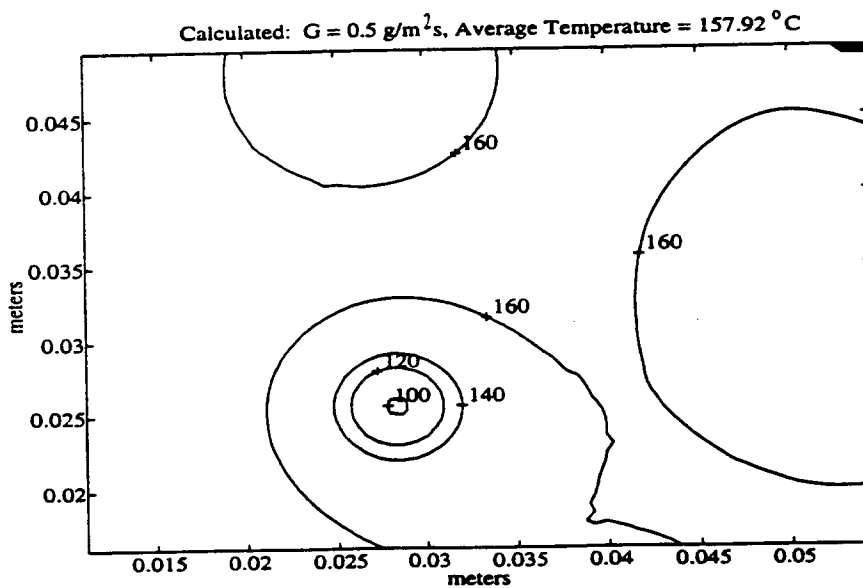
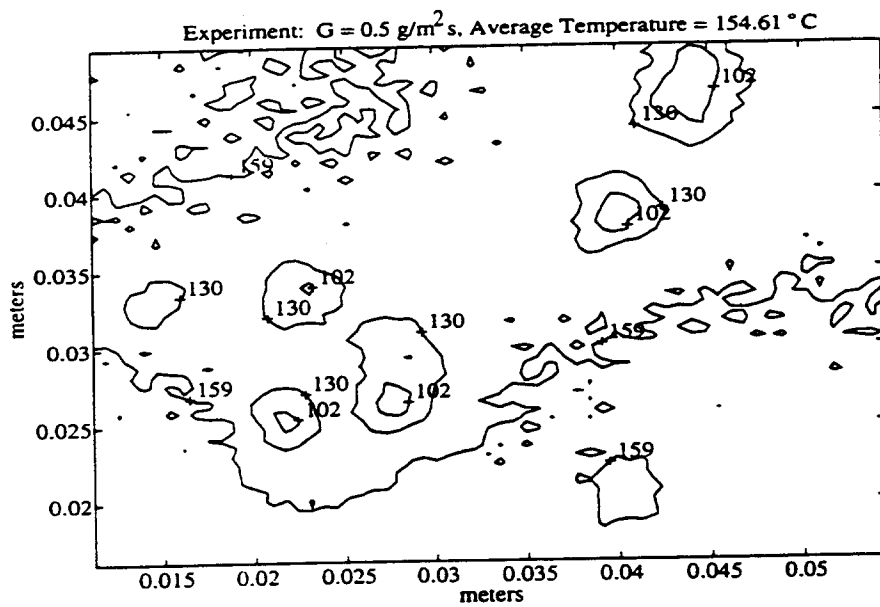


Figure 47 - Contour Plot: $T_{so} = 162 \text{ }^\circ\text{C}$, Time = 50 seconds

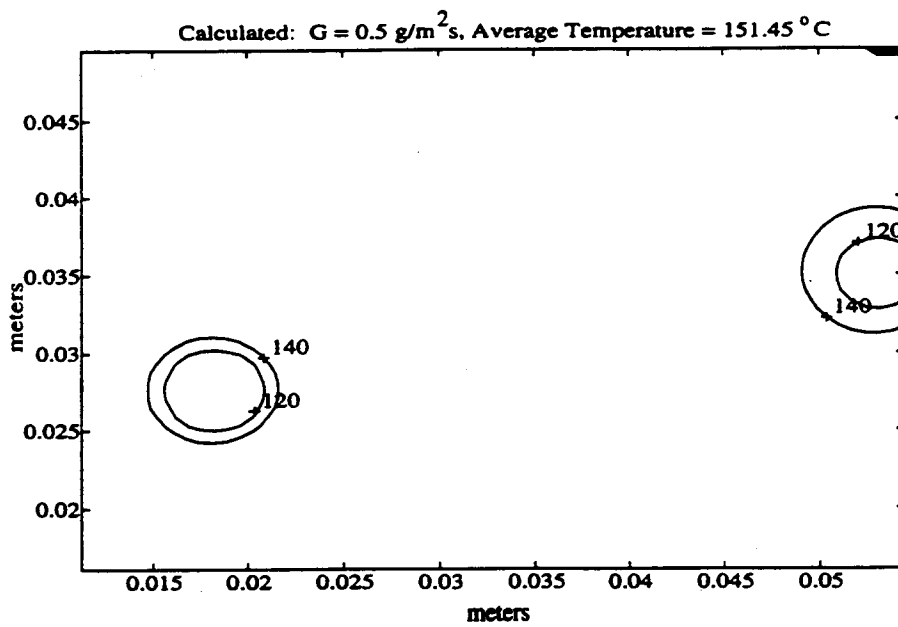
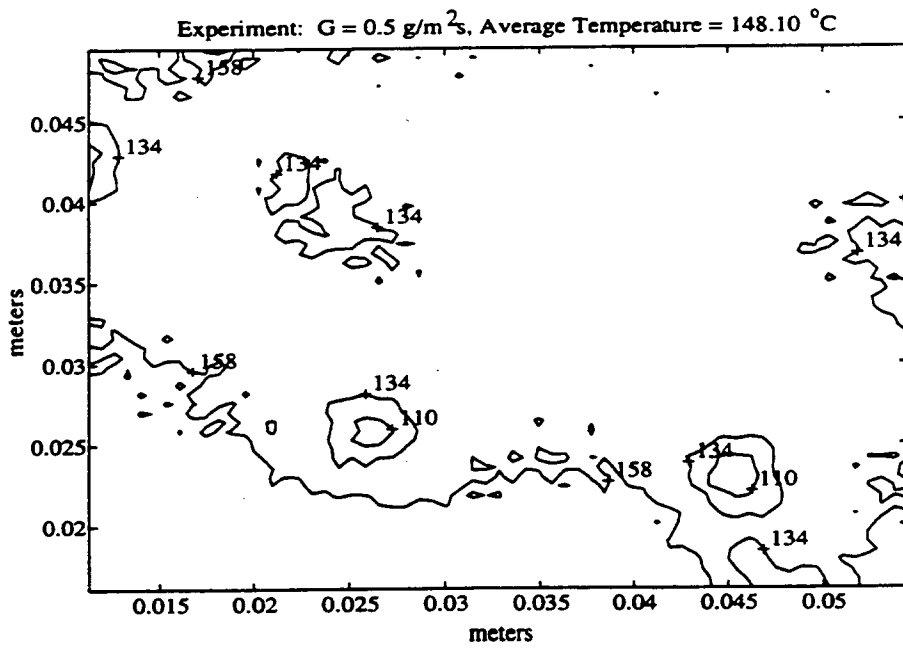


Figure 48 - Contour Plot: $T_{so} = 162 \text{ }^\circ\text{C}$, Time = 300 seconds

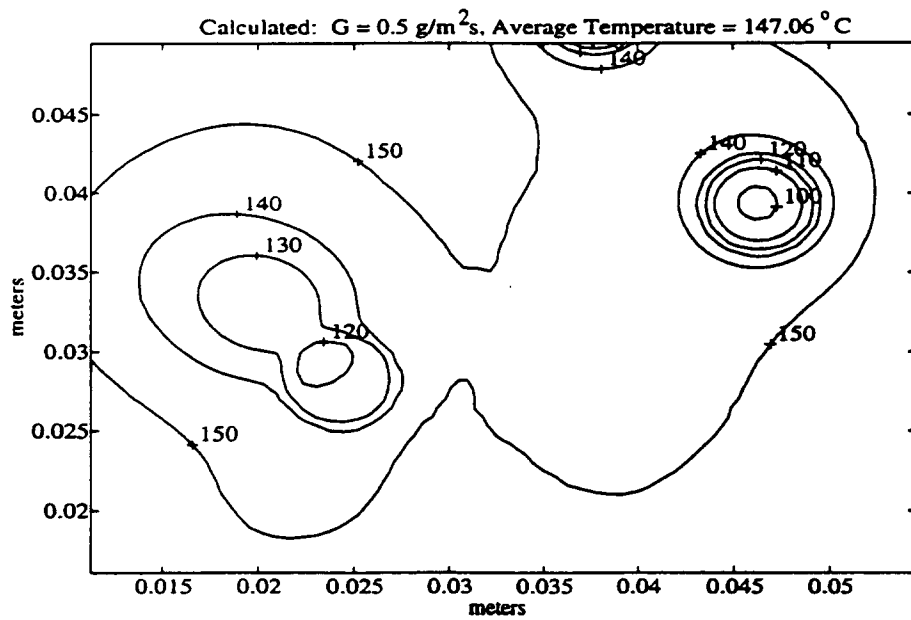
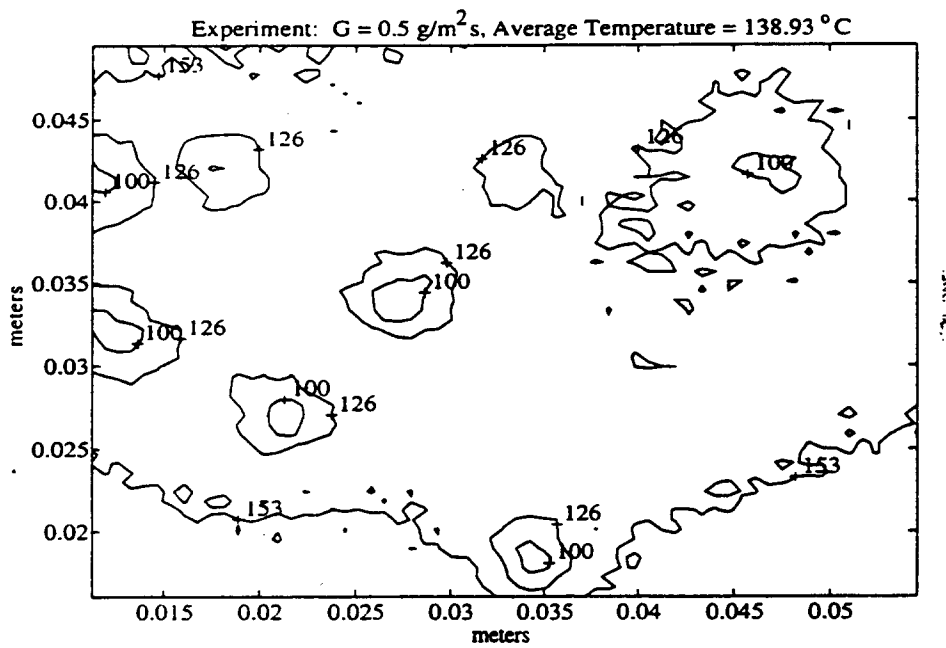


Figure 49 - Contour Plot: $T_{so} = 162 \text{ }^\circ\text{C}$, Time = 600 seconds

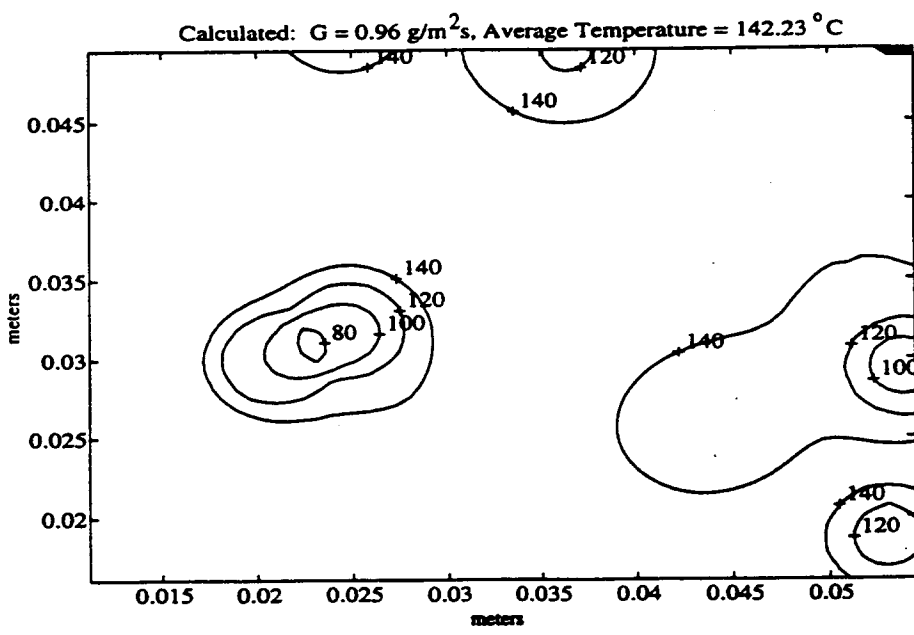
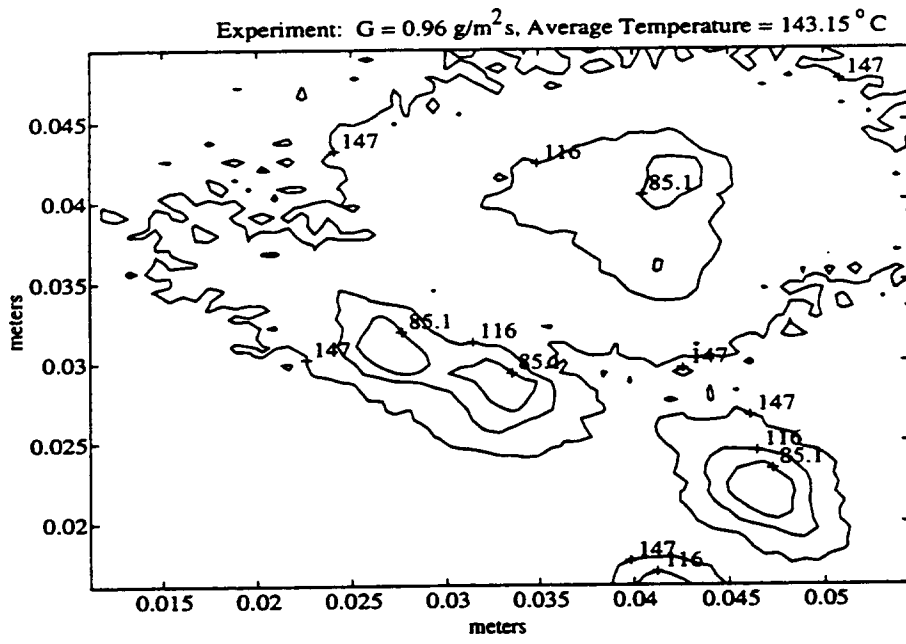


Figure 50 - Contour Plot: $T_{so} = 151 \text{ }^\circ\text{C}$, Time = 50 seconds

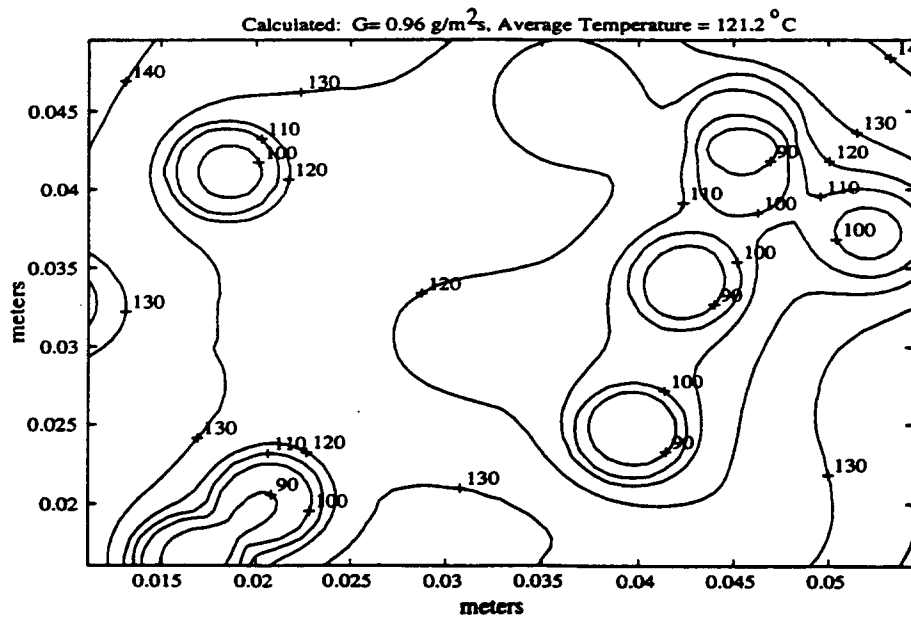
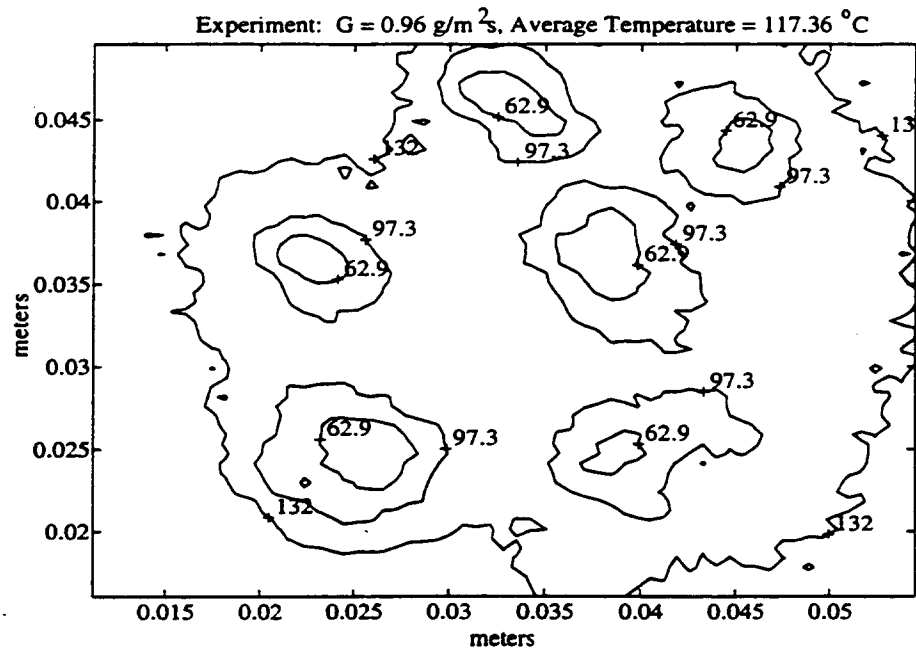


Figure 51 - Contour Plot: $T_{so} = 151 \text{ }^\circ\text{C}$, Time = 300 seconds

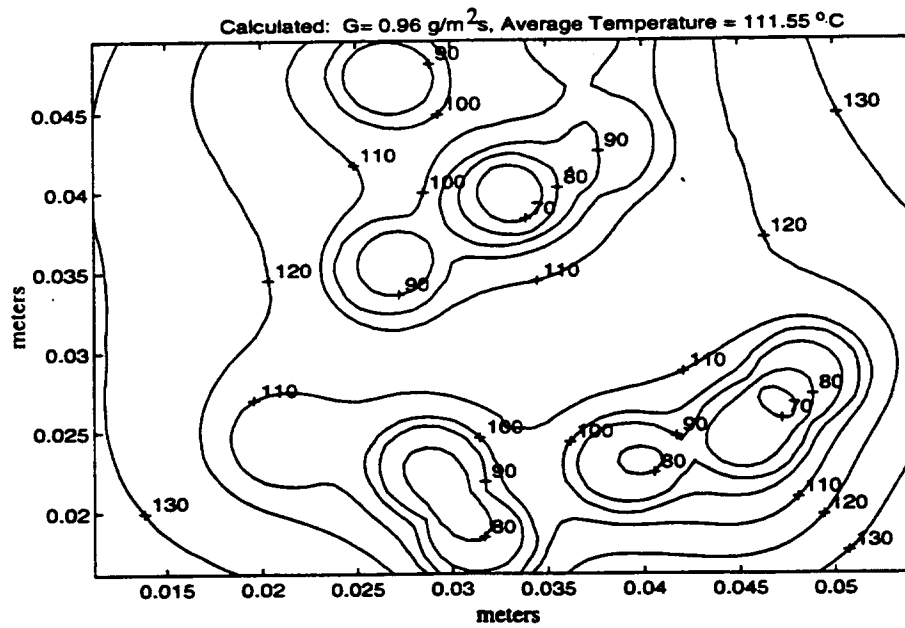
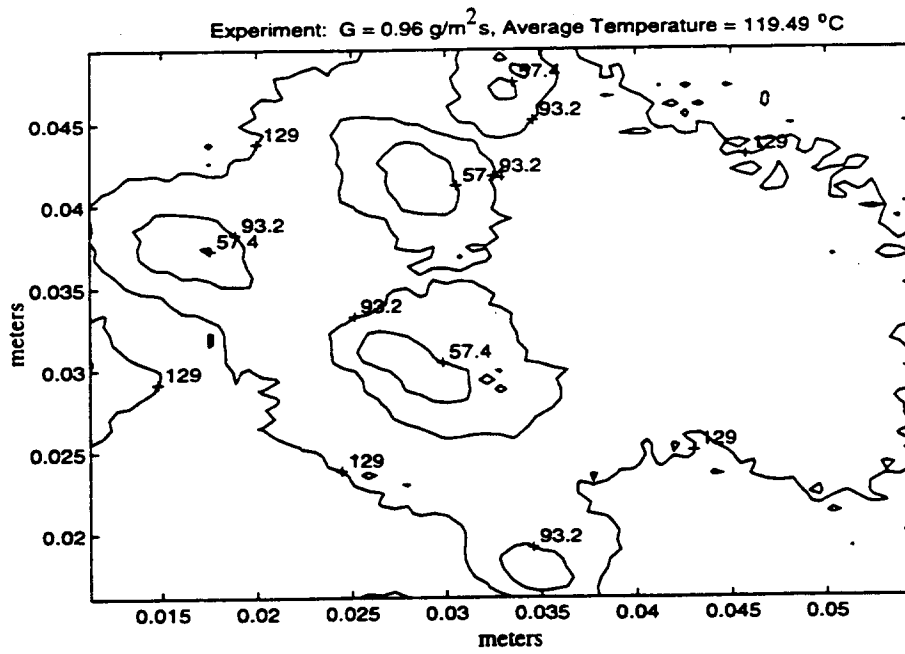


Figure 52 - Contour Plot: $T_{so} = 151 \text{ }^\circ\text{C}$, Time = 600 seconds

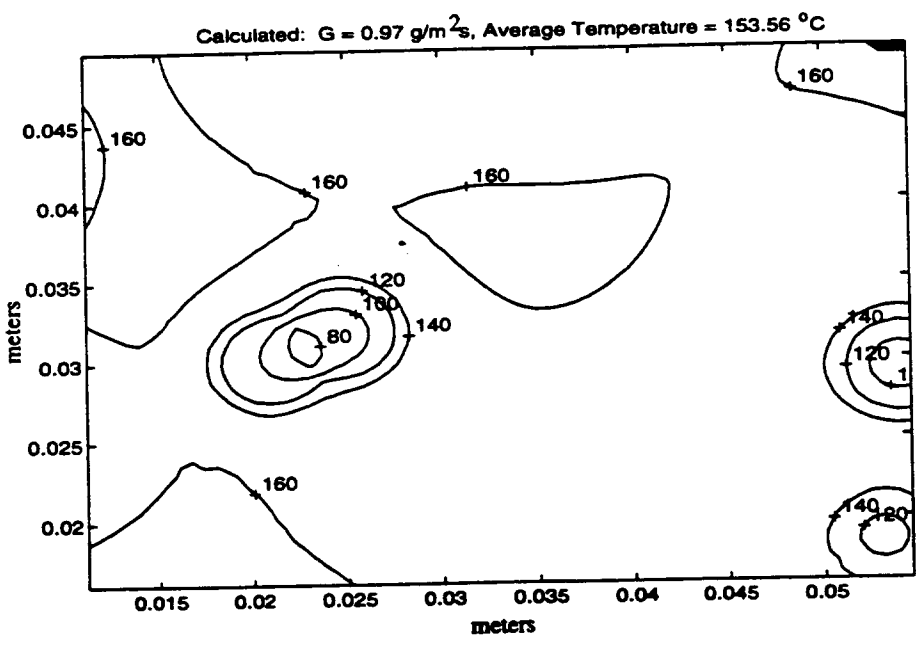
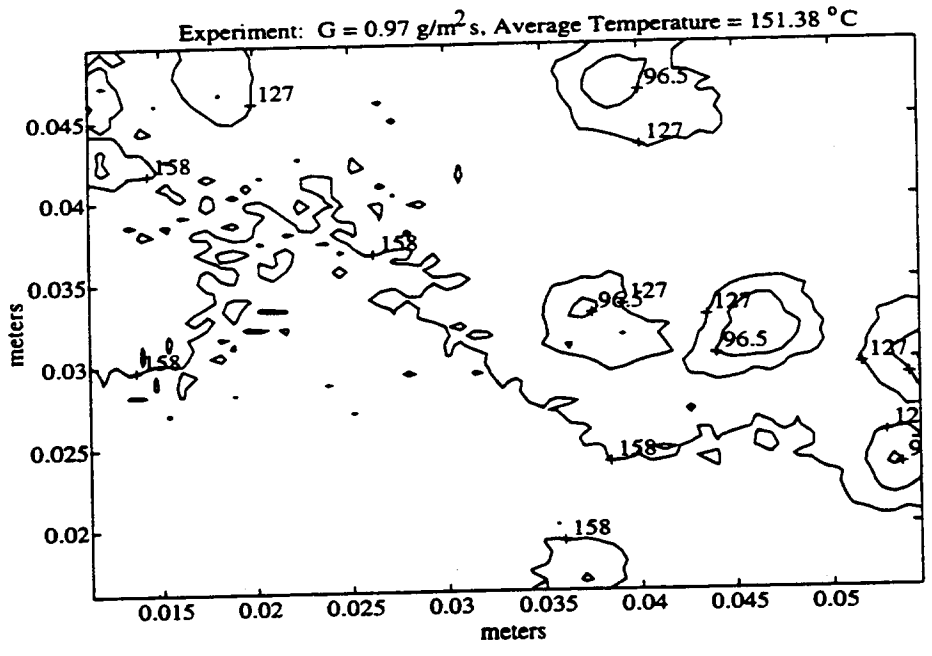


Figure 53 - Contour Plot: $T_{so} = 162 \text{ }^\circ\text{C}$, Time = 50 seconds

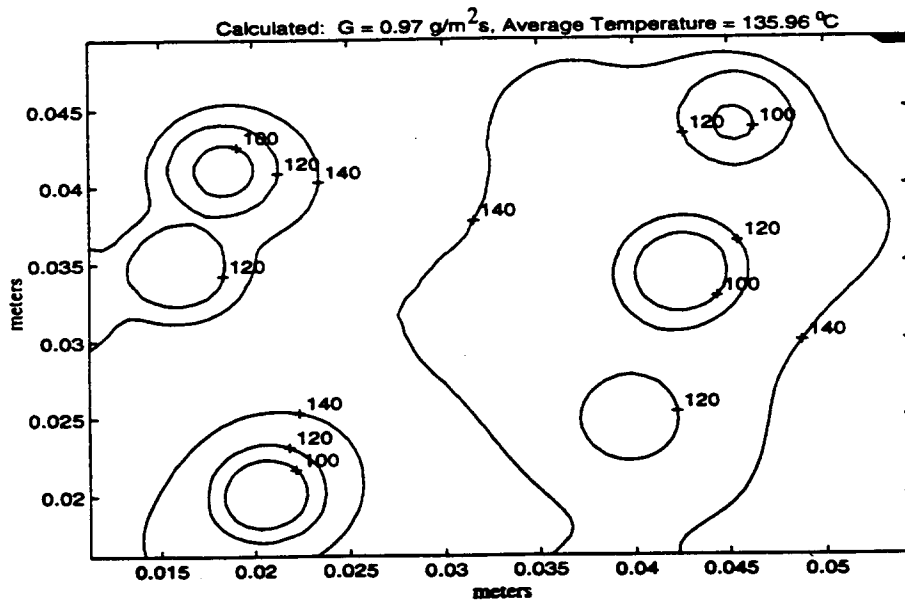
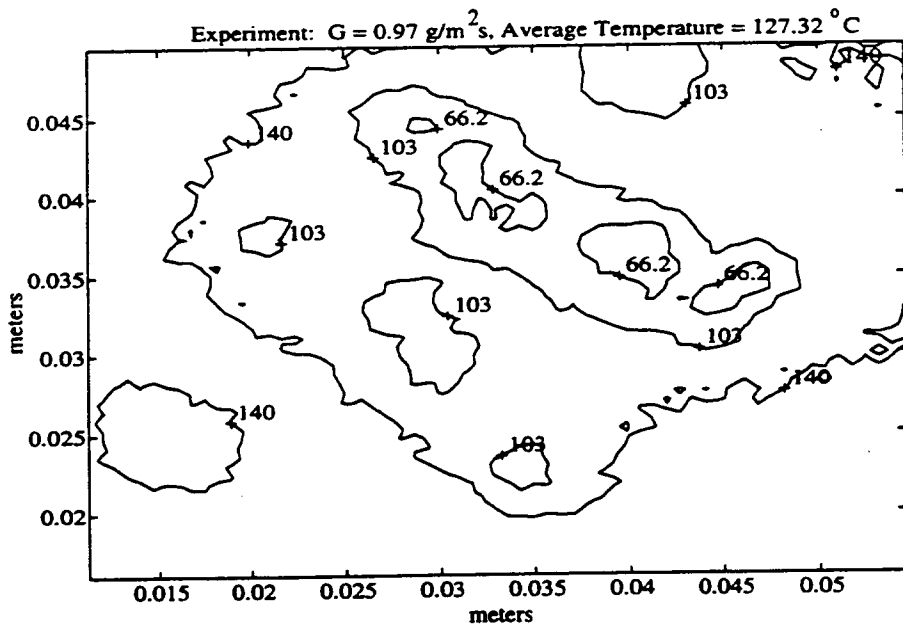


Figure 54 - Contour Plot: $T_{so} = 162 \text{ }^\circ\text{C}$, Time = 300 seconds

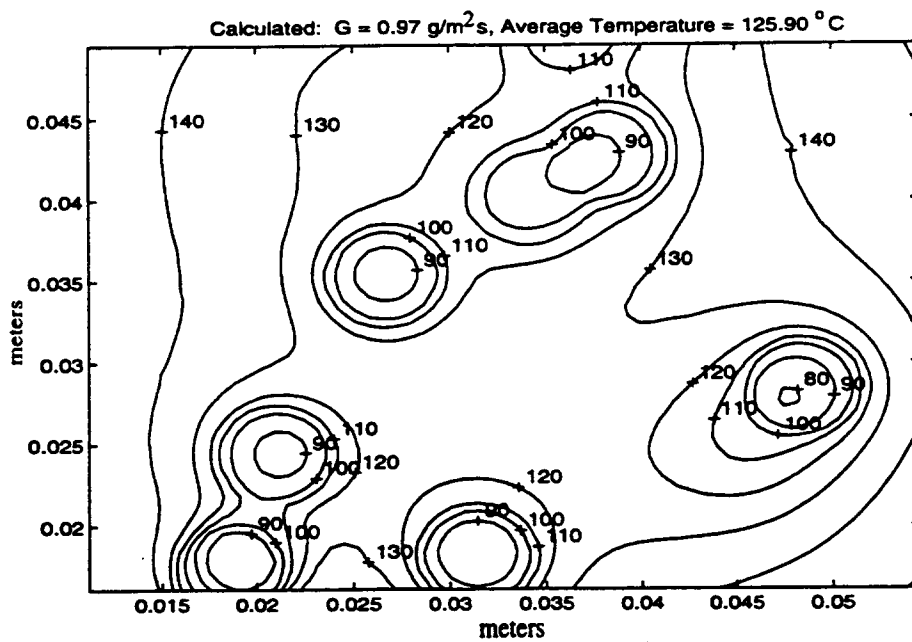
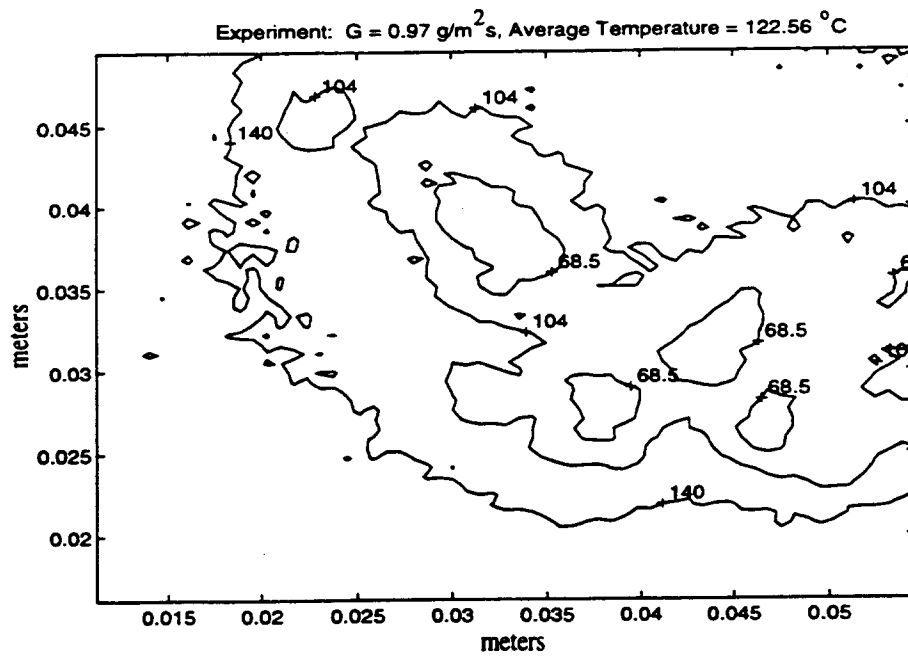


Figure 55 - Contour Plot: $T_{so} = 162 \text{ }^\circ\text{C}$, Time = 600 seconds

Time (min)	Expenment (C)	Calculated (C)
0.00	131.00	131.00
0.83	125.12	125.26
1.67	119.19	122.59
2.50	116.65	120.31
3.33	113.60	115.78
4.17	114.32	114.65
5.00	114.25	114.99
5.83	112.64	114.20
6.67	109.91	111.67
7.50	107.80	112.05
8.33	108.96	110.30
9.17	108.80	109.38
10.00	106.63	108.80
10.83	107.96	109.00
11.67	106.54	108.93
12.50	106.00	108.98
13.33	105.37	107.77
14.17	105.12	106.44
15.00	102.58	108.85
15.83	106.33	107.62
16.67	105.11	106.71
17.50	106.04	107.50
18.33	106.76	106.21
19.17	106.72	105.56
20.00	106.37	106.82
20.83	105.94	104.40
21.67	105.15	106.59
22.50	106.63	107.63
23.33	107.01	105.61

Table 13 - Raw Temperature Data: $G = 0.5 \text{ g/m}^2\text{s}$

Time (min)	Expenment (C)	Calculated (C)
0.00	162.00	162.00
0.83	154.61	157.92
1.67	152.70	155.55
2.50	147.77	155.03
3.33	145.15	150.93
4.17	147.01	149.39
5.00	148.10	151.45
5.83	146.14	149.38
6.67	143.67	147.76
7.50	139.08	150.17
8.33	139.16	147.12
9.17	136.47	146.35
10.00	138.93	147.06
10.83	139.02	146.24
11.67	135.95	146.14
12.50	139.89	145.43
13.33	140.16	145.35
14.17	139.24	142.94
15.00	137.35	146.25
15.83	140.38	143.04
16.67	139.57	144.40
17.50	140.32	145.80
18.33	137.87	142.79
19.17	139.54	144.08
20.00	138.64	143.25
20.83	140.27	143.62
21.67	138.68	144.78
22.50	138.57	144.02
23.33	138.82	143.05

Table 14 - Raw Temperature Data: $G = 0.5 \text{ g/m}^2\text{s}$

Time (min)	Experiment (C)	Time (min)	Calculated (C)
0.00	151.00	0.00	151.00
0.50	139.00	0.83	142.24
1.00	131.62	1.67	134.25
1.50	129.64	2.50	129.77
2.00	126.57	3.33	126.88
2.50	125.62	4.17	124.79
3.00	125.41	5.00	121.24
3.50	118.60	5.83	119.93
4.00	122.42	6.67	118.17
4.50	118.45	7.50	113.51
5.00	119.79	8.33	116.29
6.50	113.08	9.17	113.27
7.00	115.05	10.00	111.55
7.50	113.57	10.83	111.24
8.00	115.52	11.67	112.48
8.50	113.24	12.50	110.24
9.00	116.71	13.33	110.74
9.50	112.66	14.17	106.94
10.00	113.65	15.00	108.81
10.50	109.04	15.83	107.48
11.00	111.42	16.67	103.50
11.50	110.45	17.50	104.18
12.00	110.71	18.33	104.57
12.50	110.97	19.17	104.73
13.00	109.86	20.00	102.54
13.50	112.78	20.83	103.00
14.00	108.06	21.67	101.03
14.50	108.34	22.50	101.38
15.00	108.30	23.33	103.27

Table 15 - Raw Temperature Data: $G = 0.96 \text{ g/m}^2\text{s}$

Time (min)	Experiment (C)	Time (min)	Calculated (C)
0.00	162.00	0.00	162.00
0.50	153.74	0.83	153.57
1.00	148.92	1.67	146.80
1.50	143.44	2.50	144.53
2.00	140.18	3.33	140.78
2.50	139.07	4.17	137.91
3.00	133.52	5.00	135.98
3.50	137.56	5.83	135.69
4.00	136.15	6.67	131.90
4.50	134.22	7.50	130.17
5.00	127.32	8.33	128.96
5.50	132.99	9.17	129.07
6.00	126.38	10.00	125.81
6.50	125.85	10.83	123.36
7.00	124.64	11.67	126.46
7.50	125.19	12.50	124.76
8.00	124.86	13.33	123.38
8.50	125.00	14.17	122.41
9.00	120.65	15.00	123.35
9.50	122.04	15.83	121.56
10.00	122.56	16.67	118.59
10.50	122.57	17.50	117.99
11.00	120.33	18.33	119.11
11.50	122.63	19.17	117.88
12.00	120.84	20.00	116.27
12.50	120.01	20.83	111.76
13.00	118.60	21.67	114.52
13.50	122.72	22.50	116.55
14.00	123.84	23.33	116.09
14.50	124.19	24.17	116.22
15.00	121.72	25.00	112.74
15.50	120.36	25.83	112.66
16.00	122.58	26.67	110.12
16.50	125.46	27.50	114.80
17.00	122.43	28.33	110.02
17.50	118.63		
18.00	120.55		
18.50	121.83		
19.00	120.44		
19.50	120.83		
20.00	124.01		
20.50	121.76		
21.00	118.57		
21.50	117.10		
22.00	120.42		
22.50	122.58		
23.00	120.71		

Table 16 - Raw Temperature Data: $G = 0.97 \text{ g/m}^2\text{s}$

7. CONCLUSIONS

The development of the transient droplet geometry that is used in a model for the prediction of a single droplet evaporating on a low thermal-conductivity, semi-infinite solid subjected to radiant heat input was presented. Using the droplet configuration model, it was found that while the shape factor has a strong effect on evaporation time, the initial solid-liquid-vapor contact angle has virtually none.

With the model for the droplet geometry incorporated and a modification to the radiation terms to include the geometric effects of the droplet, an in-depth validation of the single droplet model against experiment was performed. Validation of the model showed that it is able to accurately predict transient surface temperature profiles caused by the evaporation of a droplet.

Experimental work using water containing dissolved gases was performed. The results were compared against previous experiments using degassed water. In general, there appeared to be no major differences in the transient cooling of the surface or the steady state temperature reached by the surface. Qualitative results showed differences, specifically with regards to the size of the wetted region underneath the droplet and temperature gradients near the droplet's edge.

A model for the prediction of surface temperatures of a hot, semi-infinite solid being cooled by a sparse spray of degassed water has also been presented. The validation of the single droplet evaporation model that includes the detailed descriptions of the transient droplet geometry and of the radiation effects led to the use of a simplified, closed-form solution in the sparse spray cooling model. This solution

decreases run times and memory usage by eliminating the need for a database.

The model is able to predict the transient thermal behavior of the solid surface over a range of initial surface temperatures. The surface temperatures of interest for fire protection applications are generally between 100 °C and 160 °C.

Using results obtained both experimentally and through the code, it was found that when plotting a dimensionless temperature versus time, all of the data collapses onto a single curve. In this way, the independence of the time constant that governs the transient cooling of the surface and the mass flux is established. Results support Dawson's hypothesis [9] that the properties of the solid are the factors which determine the time constant. Using the time constant to calculate the penetration depth yields a value equal to the radius of influence of a single droplet evaporating on the surface.

APPENDIX - PROGRAM MDEC

C.....SUSANNE C. TINKER
 C.....MASTER'S THESIS - 1992 - 94
 C.....ADVISOR: DIMARZO
 C.....UNIVERSITY OF MARYLAND
 C.....PROGRAM TO CALCULATE THE TRANSIENT SURFACE TEMPERATURE DISTRIBUTION
 C.....CAUSED BY SPRAY COOLING OF A SURFACE
 C234567
 PROGRAM MDEC
 C.....UNITS ARE KG-M-S

 COMMON TDROP, RAD0, TSO
 COMMON /CONST/ ALPHAS, CS, DELTA, KS, LAMDA, PI, RHOS, RHOW, TCP, V0

 REAL LTAU

 C.....SPECIFY VARIABLE TYPES
 REAL SAREA, V0, BETA0, RHOW, RHOS, CS, DELTA, TCP, ALPHAS, LAMDA, KS, PI
 REAL LDX, LDY, RDX, RDY
 REAL XWIDTH, YWIDTH
 REAL U, UTOT, DIST, TIME, TBEGIN, STEP, UCRIT
 INTEGER NX, NY, NDATTM, I, J, K, M, KLAST, LNDROP
 REAL FREQ, DELTIME, G, TEND, TTOT, TAVE
 INTEGER TDROP
 REAL RAD0, TSO

 C.....DIMENSION ARRAYS
 REAL XCALC(100), YCALC(100), T(100,100), DATTM(50)

 C.....DIMENSION ARRAYS CONTAINING DROPLET INFORMATION
 INTEGER NDROP(1000)
 REAL XD(1000), YD(1000), DEPTIME(1000), T0(1000), TAU(1000)
 CHARACTER*1 SCFLAG(1000)

 C.....THE AREA OF THE WETTED SURFACE AREA (TESTED AGAINST EXPERIMENT .0033 M²)
 PARAMETER (SAREA = 0.0033)
 C.....THE INITIAL SHAPE PARAMETER BETA0 (TESTED AGAINST EXPERIMENT FOR 2.3)
 PARAMETER (BETA0 = 2.3)

 C.....INITIALIZE UTOT
 UTOT = 0.0

 C.....DEFINE THE CALCULATION DOMAIN (ONLY A PORTION OF THE WETTED AREA)
 LDX = 0.0105
 LDY = 0.0155
 RDX = 0.0545
 RDY = 0.0495
 XWIDTH = RDX - LDX
 YWIDTH = RDY - LDY

 C.....DETERMINE THE MESH SIZE TO BE USED FOR THE CALCULATION DOMAIN
 C.....PRINT *, 'ENTER THE NUMBER OF GRID POINTS IN THE X-DIRECTION'
 C.....READ (6,*) NX
 C.....PRINT *, 'ENTER THE NUMBER OF GRID POINTS IN THE Y-DIRECTION'
 C.....READ (6,*) NY
 NX = 63
 NY = 59

 C.....MORE VARIABLES TO BE INPUT BY USER THROUGH KEYBOARD

```

C.....PRINT *, 'ENTER THE MASS FLUX (IN KG/M2-S) '
C.....READ (6,*) G
      G = 0.00097
C.....PRINT *, 'ENTER THE INITIAL SURFACE TEMPERATURE (IN CELSIUS) '
C.....READ (6,*) TSO
      TSO = 162.
C.....PRINT *, 'ENTER THE NUMBER OF TIMES TO OUTPUT DATA (INTEGER 50 max)'
C.....READ (6,*) NDATTM
      NDATTM = 13
C.....PRINT *, 'ENTER THE TIMES TO OUTPUT THE SPATIAL DATA (50 MAX)'
C.....DO 5 I = 1, NDATTM
C.....READ (6,*) DATTIM(I)
C.....DATTIM(I) = 100.
C.....PRINT *, 'ENTER TOTAL CALCULATION TIME'
C.....READ (6,*) TEND
      TEND = 1725.

C.....CALCULATE RAD0
      RAD0 = BETA0 * ((3.0 * V0)/(4*3.141592654))**(1/3.)

C.....CALCULATE THE TIME STEP AND THE FREQUENCY OF THE DROPLETS
      FREQ = (G * SAREA) / (V0 * RHOW)
      DELTIME = 1/FREQ
      TDROP = INT(FREQ*TEND)

      CALL DDIST(TEND, DELTIME)

C
C
C.....OPEN FILES
      OPEN(11, FILE = 'dropdat.dat', STATUS = 'OLD')
      OPEN(12, FILE = 'tempdat.dat', STATUS = 'NEW')
      OPEN(13, FILE = 'y.dat', STATUS = 'NEW')
      OPEN(14, FILE = 'x.dat', STATUS = 'NEW')
      OPEN(15, FILE = 'tempave.dat', STATUS = 'NEW')

C.....READ IN DROPLET DATA FROM DROPDAT.DAT AND INITIALIZE FLAG TO
C.....STOP CALCULATION IF TEMPERATURE OF CENTER OF DROPLET IS
C.....WITHIN .0001 OF T0
      DO 40 K = 1, TDROP
        READ(11,*) NDR0P(K), DEPTIME(K), T0(K), TAU(K), XD(K), YD(K)
        SCFLAG(K) = '0'
      40 CONTINUE

C.....CALCULATION OF TEMPERATURES AND AVERAGE SURFACE TEMPERATURES AT VARIOUS TIMES

      DO 80 TIME = 50., TEND, 50.
        WRITE(12,*) TIME
        IF(TIME .LT. TEND) THEN
          LNDROP = INT(FREQ*TIME)
        ELSE
          LNDROP = INT(FREQ*TEND)
        END IF

C.....TEST TO SEE IF DROPLET IS STILL AFFECTING SURFACE
      DO 60 M = 1, LNDROP
        DIST = 0.0
        CALL NEAR(TIME, M, DIST, DEPTIME, U, T0)
        IF (U .GT. 0.0) SCFLAG(M) = '1'

```

```

60     CONTINUE

C.....INITIALIZE ARRAYS AT EACH TIME
DO 75 J = 1, NY
    YCALC(J) = 0.0
DO 76 I = 1, NX
    XCALC(I) = 0.0
    T(L,J) = 0.0
76     CONTINUE
75     CONTINUE

    DO 50 J = 1, NY
        YCALC(J) = 0.0155 + (YWIDTH/NY)*(J)
    DO 55 I = 1, NX
        XCALC(I) = 0.0105 + (XWIDTH/NX)*(I)
        UTOT = 0.0
        IF (LNDROP .EQ. 0) THEN
            T(L,J) = TS0
        ELSE
            DO 70 K = 1, LNDROP
                IF (SCFLAG(K) .EQ. '1') GOTO 70
                IF (DEPTIME(K) .GT. TIME) GOTO 100

                DIST = SQRT((XCALC(I) - XD(K))**2 + (YCALC(J) - YD(K))**2)
                IF (DIST .GT. 5.0 * RADO) THEN
                    CALL FAR(TIME, K, DIST, DEPTIME, U, T0)

C             PRINT *, 'F ', DIST, K, U
                ELSE
                    CALL NEAR(TIME, K, DIST, DEPTIME, U, T0)
C             PRINT *, 'N ', DIST, K, U
                END IF
                IF (U .GT. 0.0) U = 0.0
                UTOT = UTOT + U
70         CONTINUE
            END IF
            T(L,J) = TS0 + UTOT
            TTOT = T(L,J) + TTOT
55     CONTINUE

C.....WRITE TO CONTOUR FILES ONLY FOR SPECIFIED TIMES

        IF (TIME .EQ. 50 .OR. TIME .EQ. 300 .OR. TIME .EQ. 600.) THEN
            WRITE(12,*) (T(L,J), I = 1, NX)
            END IF
        WRITE(13,*) YCALC(J)
50     CONTINUE
        WRITE(14,*) (XCALC(I), I = 1, NX)
100    TAVE = TTOT/((NX)*(NY))

C.....WRITE TRANSIENT AVERAGE SURFACE TEMPERATURE TO FILE

        WRITE(15,*) TIME, TAVE

C.....RESET TTOT, UTOT, AND TAVE
        TTOT = 0.0
        TAVE = 0.0
        UTOT = 0.0

80     CONTINUE

```

```

CLOSE (UNIT = 11)
CLOSE (UNIT = 12)
CLOSE (UNIT = 13)
CLOSE (UNIT = 14)
CLOSE (UNIT = 15)
END

```

```

SUBROUTINE DDIST(TEND, DELTIME)
C.....THIS SUBROUTINE CREATES A FILE CALLED DROPDAT.DAT WHICH CONTAINS ALL THE DROPLET
INFO
C.....TO BE USED IN THE MAIN PROGRAM THIS SUBROUTINE IS ONLY CALLED ONCE DURING THE
C.....EXECUTION OF THE MAIN PROGRAM

```

```

COMMON TDROP, RADO, TSO
COMMON /CONST/ ALPHAS, CS, DELTA, KS, LAMDA, PI, RHOS, RHOW, TCP, V0

REAL LTAU , RAND

REAL X(1000), Y(1000), DTIME(1000), TAU(1000)
REAL TEMP(1000), TIME, DIST, THETA, G, TSO, RADO, UTOT, RADHI
REAL TEND, DELTIME, R, U, UCRIT, RADLOC, RANDOM, RADLOW
REAL DELTA, KS, TCP, ALPHAS, CS, V0, RHOW, RHOS, LAMDA, PI
INTEGER NUM(1000), TDROP, K, I, J, COUNT
CHARACTER*1 SCFLAG(1000)

OPEN (UNIT = 11, FILE = 'dropdat.dat', STATUS = 'NEW')

C.....INITIALIZE RANDOM NUMBER GENERATOR SEED
R = 0.0

C.....INITIALIZE COUNT
COUNT = 0

C.....INITIALIZE TIME
TIME = 0.0

C.....INITIALIZE STOP CALCULATION FLAG
DO 15 I = 1, TDROP
  SCFLAG(I) = '0'
15 CONTINUE

DO 20 K = 1, TDROP
  TIME = TIME + DELTIME
  NUM(K) = K

C.....DETERMINE DROPLET LOCATION ON SURFACE USING ZETA = .56

  THETA = RAND(R)*PI*359/180.
  RANDOM = RAND(R)
  RADLOW = 0.0
  RADHI = 1.0
  RADLOC = (RADLOW+RADHI)/2.
25 G = 1.83*RADLOC**5-5.66*RADLOC**4+3.83*RADLOC**3+RADLOC**2
  IF ((G - RANDOM) .GT. 0.001) THEN
    RADHI = RADLOC
    RADLOC = (RADHI + RADLOW)/2.

```

```

      GOTO 25
    ELSEIF ((G - RANDOM) .LT. -0.001) THEN
      RADLOW = RADLOC
      RADLOC = (RADHI + RADLOW)/2.
      GOTO 25
    END IF
      X(K) = 0.0325*RADLOC*COS(THETA) + 0.0325
      Y(K) = 0.0325*RADLOC*SIN(THETA) + 0.0325

C.....CALCULATE DEPOSITION TIME OF DROPLET
      DTIME(K) = TIME

C.....CALCULATE SURFACE TEMPERATURE WHERE DROPLET HAS C.....LANDED

      IF (K .EQ. 1) THEN
        TEMP(K) = TS0
      ELSEIF (K .GT. 1) THEN

C.....CALCULATE TEMPERATURE OF SPOT AT WHICH NEW DROPLET LANDED TO DETERMINE T0 FOR ALL
C.....DROPLETS

        DO 35 J = 1, K-1
          IF (SCFLAG(J) .EQ. '1') THEN
            GOTO 35
          ELSE
            DIST = 0.0
            CALL NEAR(TIME, J, DIST, DTIME, U, TEMP)
            IF (U .GT. 0.0) SCFLAG(J) = '1'
          END IF
        C
          IF (SCFLAG(J) .EQ. '1') GOTO 35
          DIST = SQRT((X(K) - X(J))**2 + (Y(K) - Y(J))**2)

C.....USE FAR FIELD SOLUTION FOR DISTANCES GREATER THAN 5 RADII

          IF (DIST .GT. 5.0* RAD0) THEN
            C
              PRINT *, 'F ', K
              CALL FAR(TIME, J, DIST, DTIME, U, TEMP)
            C
              PRINT *, 'F ', K, J, U
          ELSE

C.....USE NEAR FIELD SOLUTION FOR DISTANCES LESS THAN 5 RADII

            C
              PRINT *, 'N ', K
              CALL NEAR(TIME, J, DIST, DTIME, U, TEMP)
            C
              PRINT *, 'N ', K, J, DIST/RAD0, U
          END IF
          IF (U .GT. 0.0) U = 0.0
          UTOT = UTOT + U
        C
          PRINT *, UTOT
        35
          CONTINUE
          TEMP(K) = TS0 + UTOT
        C.....RESET UTOT
          UTOT = 0.0
        END IF

C.....CALCULATE TIME AT WHICH DROPLET WILL EVAPORATE
      TAU(K) = LTAU(K,TEMP) + DTIME(K)
C.....DETERMINE IF STOP CALCULATION FLAG SHOULD BE USED

C.....WRITE TO DROPDAT FILE

```

```

WRITE (11,27) NUM(K), DTIME(K), TEMP(K), TAU(K), X(K), Y(K)
27 FORMAT (1X,I5, 1X, F15.6, 1X, F15.6, 1X, F10.3, 1X, 2E11.3)
20 CONTINUE
CLOSE (UNIT = 11)

RETURN
END

REAL FUNCTION LTAU(K,T)
REAL T(1000)
INTEGER K

C.....CURVE FIT TO EVAPORATION TIME DATA OBTAINED FROM GLENN WHITE'S CODE
LTAU = 1300. * EXP(-0.03 * T(K))

RETURN
END

REAL FUNCTION F(X)

COMMON /ARG/ ARG1, ARG2, ARG3
REAL X
REAL ARG1, ARG2, ARG3
REAL ERF, BESJ0E, BESJ0, BESJ1
F = BESJ0(ARG1 * X) * BESJ1(X) * (ERF(ARG2 * X)-ERF(ARG3 * X)) /X

RETURN
END

SUBROUTINE NEAR(TIME, K, DIST, DEPTIME, U, TEMP)
C.....THIS SUBROUTINE CALCULATES THE TEMPERATURE DEPRESSION AT A POINT
C.....DUE TO A DROPLET LOCATED
C.....LESS THAN 10 DROPLET RADII AWAY FROM THE POINT
C.....THE SOLUTION IS A CLOSED FORM SOLUTION FOR A DISK OF C.....CONSTANT STRENGTH
C.....GIVEN BY CARSLAW AND JAEGER AND MODIFIED BY GLENN WHITE

COMMON TDROP, RAD0, TS0
COMMON /ARG/ ARG1, ARG2, ARG3
COMMON /CONST/ ALPHAS, CS, DELTA, KS, LAMDA, PI, RHOS, RHOW, TCP, V0

EXTERNAL F

REAL RAD0, KS, ALPHAS, QI, QD, RAD, DELTA, TCP, CS, PI, RHOW
REAL RHOS, V0
REAL TIME, U, DIST, LTIME, TEMP(1000), DEPTIME(1000), TS0, C
REAL ARG1, ARG2, ARG3
INTEGER K, I, J, TDROP

C.....SPECIFY VARIABLES TO BE USED BY SUB QAGI
REAL EPSABS, EPSREL, RESULT, ABSERR, BOUND, WORK(5000), F

REAL LTAU

INTEGER INF, IER, LIMIT, LENW, IWORK(1000), NEVAL, LAST

C.....DEFINE VARIABLES NEEDED BY SUB QAGI (CMLIB LIBRARY) USED FOR CALCULATION OF SI
INTEGRAL
BOUND = .00001

```

```

INF = 1
EPSABS = .001
EPSREL = .001
LIMIT = 1000
LENW = 5000

C.....INITIALIZE U
U = 0.0

C.....DEFINE LOCAL EXISTENCE TIME OF DROPLET TO BE USED IN CLOSED FORM SOLUTION
LTIME = TIME - DEPTIME(K)

C.....CONDUCTIVE HEAT FLUX USING 2ND ORDER CURVE FIT TO RESULTS OBTAINED FROM GLENN
WHITE'S
C.....CODE EVAP.F

QD = 1.4*TEMP(K)**2 + 170.0*TEMP(K) - 21300
QI = KS*(TSO - TCP)/DELTA

ARG1 = DIST/RAD0
ARG2 = (ALPHAS*LTIME)**.5/RAD0
IF (LTIME .LE. LTAU(K,TEMP)) THEN
  ARG3 = 0.0
ELSE
  ARG3 = ((ALPHAS * (LTIME - LTAU(K,TEMP)))**.5) / RAD0
END IF
CALL QAGI (F, BOUND, INF, EPSABS, EPSREL, RESULT, ABSERR, NEVAL, IER, LIMIT, LENW, LAST,
IWORK,
      WORK)
U = -0.9 * (QD + QI) * RAD0 * RESULT / KS

RETURN
END

SUBROUTINE FAR(TIME, K, DIST, DEPTIME, U, TEMP)
C..... THIS SUBROUTINE CALCULATES THE TEMPERATURE DEPRESSION AT A POINT DUE TO A DROPLET
C..... LOCATED
C..... GREATER THAN 10 DROPLET RADII AWAY.
C..... THE SOLUTION IS THE CLOSED FORM SOLUTION GIVEN BY CARSLAW AND JAEGER FOR A POINT
HEAT
C..... SINK
COMMON TDROP, RAD0, TSO
COMMON /CONST/ ALPHAS, CS, DELTA, KS, LAMDA, PI, RHOS, RHOW, TCP, V0

REAL TIME, LTIME, DIST, U, DEPTIME(1000), TEMP(1000)
INTEGER K, TDROP
REAL V0, RHOW, RHOS, LAMDA, CS, ALPHAS, Q, QD, QI, DELTA, KS
REAL TCP, TSO
REAL A, B, PI, RAD0

REAL LTAU

C.....INITIALIZE U
U = 0.0

C.....CALCULATE LOCAL TIME

```

```

LTIME = TIME - DEPTIME(K)

IF (LTIME .LT. 0.6*LTAU(K,TEMP)) THEN
  U = 0.0
ELSE
  QI = KS * (TS0 - TCP)/DELTA
  QD = 1.4*TEMP(K)**2 + 170.0*TEMP(K) - 21300.0
  Q = (QD + QI) * PI * LTAU(K, TEMP) * (RADO)**2
  A = Q/(4*RHOS*CS*(PI * ALPHAS * (LTIME -.6*LTAU(K,TEMP)))**1.5)
  B = (DIST**2)/(4 * ALPHAS * (LTIME - .6*LTAU(K,TEMP)))
  U = -A * EXP(-B)
END IF
RETURN
END

```

```

BLOCK DATA
REAL ALPHAS, CS, DELTA, KS, LAMDA, PI, RHOS, RHOW, TCP, V0
COMMON /CONST/ ALPHAS, CS, DELTA, KS, LAMDA, PI, RHOS, RHOW, TCP, V0
DATA ALPHAS, CS, DELTA, KS, LAMDA, PI, RHOS, RHOW, TCP, V0 /5.79E-07, 888.9, 0.0254,
+1.297, 2225000., 3.141592654, 2520., 998.2, 35., 9e-09/

END

```

REFERENCES

1. Simon, F. and Hsu, Y., "Wetting Dynamics of Evaporating Drops on Various Surfaces," *NASA Technical Memo.*, NASA TM X-67913, 1971.
2. Toda, S., "A Study of Mist Cooling. First Report: Investigation of Mist Cooling," *Heat Transfer, Japanese Research*, 1:3, 39-50, 1972.
3. Bonacina, C., Del Giudice, S., and Comini, G., "Dropwise Evaporation," *Transactions ASME, Journal of Heat Transfer*, 101: 441-446, 1979.
4. Zhang, N. and Yang, WJ, "Natural Convection in Evaporating Minute Drops," *Transactions ASME, Journal of Heat Transfer*, 104: 656-662, 1982.
5. diMarzo, M., Trehan, A. and Evans, D., "The Cooling Effect of A Single Evaporating Droplet on A Hot Semi-Infinite Metal Body," *National Institute of Standards and Technology Report*, NBSIR 87-3517, 1987.
6. diMarzo, M., Kavooosi, F., and Klassen, M. "Transient Cooling of a Hot Surface by Droplets Evaporation," *National Institute of Standards and Technology Report*, NIST-GCR-89-559, 1989.
7. Liao, Y., "Dropwise Evaporative Cooling of Solid Surfaces," Doctoral Dissertation, University of Maryland at College Park, 1992.
8. diMarzo, M., Kidder, C., and Tartarini, P., "Infrared Thermography of Dropwise Evaporative Cooling of a Semi-Infinite Solid Subjected to Radiant Heat Input," *Experimental Heat Transfer*, 5: 101-114, 1992.
9. Dawson, H. and diMarzo, M., "An Experimental Study of Multiple Droplet Evaporative Cooling," *University of Maryland at College Park Mechanical Engineering Department Report*, No. 92-1, 1992.
10. White, G., Tinker, S., and diMarzo, M., "Transient Cooling of a Hot Surface by Droplets Evaporation," *University of Maryland at College Park Mechanical Engineering Department Final Report*, 1993.
11. Chandra, S. and Avedisian, C., "On the Collision of a Droplet with a Solid Surface," *Proceedings of the Royal Society*, 432: 13-41, 1991.
12. Viskanta, R. and Toor, J., "Absorption of Solar Radiation in Ponds," *Solar Energy*, 21: 17-25, 1978.

13. diMarzo, M., Tartarini, P., Liao, Y., Evans, D., and Baum, H., "Evaporative Cooling Due to a Gently Deposited Droplet," *International Journal of Heat and Mass Transfer*, in press, 1993.
14. Carslaw, H. and Jaeger, J., *Conduction of Heat in Solids*, Clarendon Press, Oxford, 1959.
15. Lavash, R.A., "Water Droplet Dispenser Control," Class Project Report, University of Maryland, 1990.
16. Kidder, C., "Dropwise Evaporative Cooling of a Ceramic Solid Surface Heated by Radiation," Master of Science, University of Maryland at College Park, 1990.
17. Personal Communication with M. diMarzo, 1994.

NIST-114 (REV. 6-93) ADMAN 4.09	U.S. DEPARTMENT OF COMMERCE NATIONAL INSTITUTE OF STANDARDS AND TECHNOLOGY	(ERB USE ONLY) ERB CONTROL NUMBER _____ DIVISION _____ PUBLICATION REPORT NUMBER _____ CATEGORY CODE _____ NIST-GCR-95-665
MANUSCRIPT REVIEW AND APPROVAL		PUBLICATION DATE: December 1994 NUMBER PRINTED PAGES: _____

INSTRUCTIONS: ATTACH ORIGINAL OF THIS FORM TO ONE (1) COPY OF MANUSCRIPT AND SEND TO THE SECRETARY, APPROPRIATE EDITORIAL REVIEW BOARD.

TITLE AND SUBTITLE (CITE IN FULL)

 Water Droplet Evaporation from Radiantly Heated Solids

CONTRACT OR GRANT NUMBER 7ONANB1H1173	TYPE OF REPORT AND/OR PERIOD COVERED Final Report Sept. 1992 - May 1994
--	--

AUTHOR(S) (LAST NAME, FIRST INITIAL, SECOND INITIAL) S. Tinker, and M. di Marzo University of Maryland College Park, MD 20742	PERFORMING ORGANIZATION (CHECK (X) ONE BOX) <input type="checkbox"/> NIST/GAITHERSBURG <input type="checkbox"/> NIST/BOULDER <input type="checkbox"/> JILA/BOULDER
--	---

LABORATORY AND DIVISION NAMES (FIRST NIST AUTHOR ONLY)
 BFRL/Fire Safety Engineering Division

SPONSORING ORGANIZATION NAME AND COMPLETE ADDRESS (STREET, CITY, STATE, ZIP)
 U.S. Department of Commerce
 National Institute of Standards and Technology
 Gaithersburg, MD 20899

<input type="checkbox"/> JOURNAL OF RESEARCH (NIST JRES) <input type="checkbox"/> J. PHYS. & CHEM. REF. DATA (JPCRD) <input type="checkbox"/> HANDBOOK (NIST HB) <input type="checkbox"/> SPECIAL PUBLICATION (NIST SP) <input type="checkbox"/> TECHNICAL NOTE (NIST TN)	<input type="checkbox"/> MONOGRAPH (NIST MN) <input type="checkbox"/> NATL. STD. REF. DATA SERIES (NIST NSRDS) <input type="checkbox"/> FEDERAL INF. PROCESS. STDS. (NIST FIPS) <input type="checkbox"/> LIST OF PUBLICATIONS (NIST LP) <input type="checkbox"/> NIST INTERAGENCY/INTERNAL REPORT (NISTIR)	<input type="checkbox"/> LETTER CIRCULAR <input type="checkbox"/> BUILDING SCIENCE SERIES <input type="checkbox"/> PRODUCT STANDARDS <input type="checkbox"/> OTHER _____
---	--	--

PROPOSED FOR NON-NIST PUBLICATION (CITE FULLY) _____	<input type="checkbox"/> U.S.	<input type="checkbox"/> FOREIGN	PUBLISHING MEDIUM <input type="checkbox"/> PAPER <input type="checkbox"/> DISKETTE (SPECIFY) _____ <input type="checkbox"/> OTHER (SPECIFY) _____
--	-------------------------------	----------------------------------	--

SUPPLEMENTARY NOTES

ABSTRACT (A 2000-CHARACTER OR LESS FACTUAL SUMMARY OF MOST SIGNIFICANT INFORMATION. IF DOCUMENT INCLUDES A SIGNIFICANT BIBLIOGRAPHY OR LITERATURE SURVEY, CITE IT HERE. SPELL OUT ACRONYMS ON FIRST REFERENCE.) (CONTINUE ON SEPARATE PAGE, IF NECESSARY.)

A model describing the configuration of a water droplet evaporating on the surface of a radiantly heated semi-infinite solid is developed. A shape factor and the solid-liquid-vapor contact angle describe the transient droplet shape, though the initial value of the latter parameter is found to have a negligible effect on the droplet's evaporation. The droplet shape model and a modified radiation heat term are incorporated into a previously-developed computer model to predict the evaporation of a single droplet on a semi-infinite solid subjected to radiant heat input. The code predicts transient temperature profiles that agree well with experiment. A simplified, closed-form solution for the prediction of surface temperatures in the vicinity of an evaporating droplet is used to fit the data produced by the single droplet model. This closed-form solution facilitates calculations used in a model for the cooling of a surface by the evaporation of a sparse spray of water. The previously collected data base for sparse spray cooling using degassed water is expanded with a new set of experiments using water containing dissolved gases.

KEY WORDS (MAXIMUM OF 9; 28 CHARACTERS AND SPACES EACH; SEPARATE WITH SEMICOLONS; ALPHABETIC ORDER; CAPITALIZE ONLY PROPER NAMES)

Cooling; drop sizes; droplets; evaporation; fire research; solid surfaces; sprinkler systems; water sprays

AVAILABILITY

<input checked="" type="checkbox"/> UNLIMITED	<input type="checkbox"/> FOR OFFICIAL DISTRIBUTION - DO NOT RELEASE TO NTIS
<input type="checkbox"/> ORDER FROM SUPERINTENDENT OF DOCUMENTS, U.S. GPO, WASHINGTON, DC 20402	
<input checked="" type="checkbox"/> ORDER FROM NTIS, SPRINGFIELD, VA 22161	

NOTE TO AUTHOR(S): IF YOU DO NOT WISH THIS MANUSCRIPT ANNOUNCED BEFORE PUBLICATION, PLEASE CHECK HERE.